THE PERKIN-ELMER CORPORATION
AEROSPACE DIVISION
2855 Metropolitan Place, Pomona, California 91767

# OPTIMIZATION STUDY

By L. G. Hall

March 1971



Contract NAS5-11185
SPO Number 30001



Prepared for
NATIONAL AERONAUTICS AND SPACE ADMINISTRATION
Goddard Space Flight Center
Greenbelt, Maryland

TABLE OF CONTENTS



LIST OF ILLUSTRATIONS

# INTRODUCTION

The purpose of this study is to establish techniques for obtaining the minimum weight and power (or occasionally size) for a mass spectrometer system which meets a given performance requirement. Often this optimization procedure is necessary in the opposite direction where weight and power are limited. The technique, however, usually proceeds equally well in either direction, once the independent and dependent variables are identified.

The type of mass spectrometer discussed in this study is the Quadrupole Mass Filter [1,2,3,4, and 5] which has been selected in several experiments for analysis of the earth's upper atmosphere and potentially for planetary atmospheres. For the above purposes, it is typically operated in one of three general modes, as follows:

a. Open Ion Source. Ambient particles are ionized with limited energy (temperature) equilibration to the ion source; ionizing chamber gas density limited to ambient density as modified by partial accommodation to ion source temperature and surface conditions.

b. Closed Ion Source, Close-Coupled to Ambient. Ambient particles are thermalized to ion source temperature; gas density established by transpiration flow to ambient atmosphere or to a thermalizing chamber.

c. Closed Ion Source, Excess Sample. Particles are thermalized to ion source temperature; gas density is established by flow through an inlet system from high pressure and is limited only by the leak rate as determined for the desired system operating conditions.

For the purpose of this report a generalized configuration of a Mode 2 ion source and the quadrupole is shown in Figure 1.

Each mode of operation requires a slightly different treatment and will arrive at a different optimum instrument. For example, analysis of energetic particles with an open ion source will generally require a larger system in order to accept the diverse paths of the particles. Conversely, high ambient pressure generally permits use of a smaller instrument when the ion source can operate at its linear limit of gas density. Other modes of operation can arise with a similar requirement for modification of the constraints. However, this discussion is limited to the three listed.

## METHOD OF OPTIMIZATION

Before an optimum instrument can be derived, a definition of the problem is typically given. For this study, since a range of applications was contemplated, attention was directed at maximizing the specific sensitivity of the mass spectrometer. Additional elements of the optimization procedure are required in order to arrive at a complete instrument.

Expressing this analytically, the performance to be achieved can be given as total sensitivity:

$$(S_T)_i \Big|_{i=1}^{n} = (e_o/n_o)_i \Big|_{i=1}^{n}$$

volts output/unit density, ambient; for $\eta$ species, readable in the density ranges

$$(n_o)_i \text{ (min)} < (n_o)_i < (n_o)_i \text{ (max)},$$

under a given set of operating conditions and in a given environment. The solution to the problem requires a consideration of interfering species at various density levels, both directly as ion fragment current and indirectly as "noise" (e.g., neutrals and secondary effects); the system linearity at high ambient densities; the system noise at low ambient densities as well as the implied design and operational parameters.

Assuming for each species a relationship between ambient and ion source gas density,

$$n_s = H_1 \, n_o, \tag{1}$$

where $H_1$ is generally a time varying function relating both to the sampling mode and vehicle orientation.

The current formed, $I_F^+$, by electron beam bombardment of the gas is substantially linear with density,

$$I_F^+ = K_a \, n_s. \tag{2}$$

The ion current collected $I_C^+$ can be expressed as,

$$I_C^+ = \Theta_S \, \Theta_A \, I_F^+ \tag{3}$$

where $\Theta_S$ = ion source transmission efficiency and $\Theta_A$ = mass analyzer transmission efficiency, each of which is in general a function of the mass spectrometer operating conditions.

For the purposes here, the output voltage, $e_o$, can be assumed proportional to collected current, or

$$e_o = K_b \, I_c^+ \tag{4}$$

combining (1) to (4),

$$S_T = e_o/n_o = K_a \, K_b \, \Theta_S \, \Theta_A \, H_1. \tag{5}$$

A knowledge of the variables under a given set of conditions, then allows determination of the unknown gas densities $(n_o)_i$ by observation of $e_{oi}$.

This study is then concerned with maximizing the product

$$K_a \, \Theta_S \, \Theta_A = S,$$

the specific mass spectrometer sensitivy, in amperes ion current/unit density in the ion source, i.e.,

$$S = I_c^+/n_s = K_a \, \Theta_S \, \Theta_A \tag{6}$$

In this approach, all of the performance parameters are analytically related and summarized in the one parameter S which then becomes a function of size, weight and power. The optimum instrument is then inferred by the least value of weight (as a summary parameter) that satisfies the sensitivity and signal-to-noise ratio required in the problem.

While $H_1$ is an important variable in the complete problem, it is only discussed to the extent that it impacts the mass spectrometer input condition in the mode of operation as described in the Introduction.

The method of optimizing S takes one of two approaches, depending upon whether the quadrupole analyzer is operated in the "flat-topped peak" or "pointed peak" condition, (these terms are more fully defined on the definition pages of Appendix 4).

The first case where the instrument is designed and tuned to produce flat-topped peaks requires that $\Theta_A = 1.0$; i.e., 100% of the ion current received by the analyzer is transmitted and collected. The great importance

of this characteristic is that minor variations of the analyzer operating conditions or the particle initial conditions do not influence the accuracy of the measurement. This, along with an ion source that is to first order independent of particle initial conditions (described later), is an essential factor in substantiating the measurements in certain space experiments.

It is found that optimization can be approximated when $\Theta_A = 1.0$. Analyzer entrance conditions of angle, position and energy of the particle will be solved in terms of desired resolution and peak shape. Secondly, this equation is substituted in an expression for $\Theta_S$. $\Theta_S$ is then differentiated for a maximum with respect to the remaining variables.

In the pointed-peak mode $\Theta_A$ (<1.0) becomes intimately a function of the electrical operating conditions of the quadrupole. Since there is as yet no closed, simple expression for transmission of the quadrupole as a function of the various conditions, optimization is a lengthly iterative procedure. In practice an open-ended solution of $\Theta_A$ for a given set of conditions is usually possible.

The quadrupole mass analyzer is first described in terms of its operating parameters in the next section. Subsequent sections, respectively, analyze the ion source parameters and combine the two equations.

## ANALYZER CHARACTERISTICS

By continuing the use of the optimization techniques of Reference 3 it is found that the quadrupole functions in a manner that appears similar in form to a double-focusing magnetic mass spectrometer with first order coefficients of angle and entry position equal to zero. It is thus an instrument of higher order. The equations can then be solved simultaneously with the ion source equations to optimize performance and establish sensitivity.

In general terms, all mass spectrometers operate within limits imposed by the solid angle of ion source emission, $\alpha^2$, the area, $A_e$, of ion emission and the upper and lower limits of an energy or velocity band, $\pm\beta$ where

$$\beta = \frac{dv}{v_o} \quad \text{and } v = \text{velocity.}$$

The quadrupole is no exception. It is the object of the optimization process to maximize this multi-dimensional "volume" to obtain the greatest current output. However, the quadrupole is different than most other mass spectrometers in the nature of imposition of penalties of weight and power in addition to it being unique in providing versatility.

Assume that the operation of the quadrupole analyzer is understood from prior work (c.f., References 1-5). Further, the analysis assumes that the quadrupole functions in a theoretical manner with respect to ion entrance conditions, i.e., the position, angle and energy of the ion as injected from the ion source arrive in a pure quadrupole field without end effects. Both quadrupole biasing[3] with nozzle injection and segmented rods[4] attempt to nullify or improve upon the effects of quadrupole rod termination; however, the full effects are not known.

### Scanning and Resolution

Following common usage, the coordinate system is oriented with the z axis along the axis of the rod structure, y is through the negative pair of rods and x through the positive pair (see Figure 1). Then from the quadrupole operating equations,

$$a = \frac{8\ e\ V_{dc}}{m r_o^2\ \omega^2} \quad \text{and } q = \frac{4\ e\ V_{ac}}{m r_o^2\ \omega^2} \tag{7}$$

where $a, q$ = dc and ac stability parameters,

$e$ = electronic charge (couloumbs),

$V_{dc}$ = applied dc rod voltage (volts),

$V_{ac}$ = applied ac rod voltage (volt-peak),

$m$ = ion mass (kg.),

$r_o$ = characteristic rod spacing from the axis (meters),

$\omega$ = angular frequency of applied ac voltage (radians/sec),

a technique of sweeping or scanning the spectrum can be described.

With reference to the stability diagram in Figure 2 (a and b), which show a very select portion of the overall stability characteristics, the region of interest is around $a = 0.23699$ and $q = 0.706$. Charged particles are stable when $\beta_y > o$ and $o < \beta_x < 1$, consequently within the triangular region. Scan lines 1, 2, 3, 4, and 5 depict lines of constant ratio:

$$a/q = 2\, V_{dc}/V_{ac} \tag{8}$$

which pass through the stability diagram when a given mass-to-charge ratio m/e is in the quadrupole field and as $V_{ac}$ or $\omega$ is varied. Higher resolution is achieved by increasing the scan line slope, a/q. Equation (7) can be used to establish parametric values which produce stability.

In order to define the normal scanning performance, it is desirable to relate the peak shape to the stability diagram. Figure 3 depicts the ion current transmitted through the quadrupole as a function of q, (and as implied by constant a/q) as the peak is scanned.

As a and q increase along scan line 3, for instance, ions of say $(m/e)_1$ are nominally stable in both x and y direction between A and D. However, a small, increasing current is transmitted and observed upon approaching A, which is due to ions of (m/e), unstable in the y direction which do not reach the rods for discharge within the limited length of the rod system. The longer the rods, the greater will be the fraction of unstable particles that reach amplitude $r_o$ and are eliminated. Brubaker[2] shows typical paths while the Quadrupole Ion Entrance Mask study of this final report shows the envelope of motion of unstable particles.

At the stability boundary at A, ions of (m/e), become y theoretically stable; however, they can also have a stable amplitude that is larger than

$r_o$ depending on their initial angle and position off-axis. As the scan line is followed from A to B, ions with successively larger y angles and offset have stable amplitudes less than $r_o$ and are transmitted. If the angle and offset are bounded at small value, they all have maximum amplitudes less than $r_o$ and 100% of the current is transmitted between B and C. The effects are approximately the same in reverse order upon crossing the x stability boundary from C to D and beyond. The correlation with peak shape is apparent from Figure 3.

Figure 3 also shows the peak width characteristics defined as the following:

$\Delta q_T$ = peak top width measured in q

$\Delta q$ = theoretical peak width between boundaries measured in q.

$\Delta q_B$ = peak base width to a defined fraction of peak height, measured in q (see definitions, Appendix 4).

$\Delta q_{x,y}$ = increments of q taken by peak sides

$\Delta q_{t\ x,y}$ = increments of q taken by tail.

These elements of peak shape will be used below.

Considering, then, the technique of scanning, it becomes apparent that sweeping voltage has certain advantages. While the spectrum could be scanned by holding $V_{ac}$ constant and varying $\omega$ especially if it is desired to continuously sweep a wide mass range, simple low power and precise methods of doing this have not yet been demonstrated. One advantage of the voltage scan is the simple time relationship that is easily produced.

From (7) if $\omega$ and $r_o$ are constant,

$$m = K V_{ac} \tag{9}$$

thus, if we let $V_{ac} = kt$ where t = time,

$$m = Kkt \tag{10}$$

and the peaks are equally spaced in time. Voltage scanning is assumed in the calculations of this report.

It is also possible to maintain constant resolution during the scan. Resolution is defined in Appendix 4, but can be more readily visualized from Figure 4a. Two adjacent, equal sized peaks are considered resolved if their contribution to the valley between them is equal or less than a specified fraction of the peak height. A stated resolution, $m/\Delta m$ is reached when the contributions are equal to the specified value.

Taking this limiting case, two mass peaks are resolved when from (7),

$$\left.\frac{\partial V_{ac}}{V_{ac}}\right|_{m = \text{constant}} = \left.\frac{\partial V_{ac}}{V_{ac}}\right|_{q = \text{constant}}$$

thus, $\frac{\partial q}{q} = \frac{\partial m}{m}$, or, for small increments, we assume

$$\frac{\Delta q_s}{q} = \Delta\, m/m, \text{ where } \Delta q_s \text{ is the peak separation} \qquad (12)$$

For the example in Figure 4a,

$$\Delta q_s = \Delta q_B = q\ \Delta\ m/m \qquad (13)$$

In the more general case, the peak separation expressed by $q\Delta m/m$ can be greater or less than $\Delta q_B$ for adjustment of peak overlap. thus we let

$$k_m\ \Delta q_B = \Delta q_s = q\ \Delta\ m/m \qquad (14)$$

For $k_m = 1$, the peaks are resolved at the base by the conventional definition. For $k_m = 1/2$, as shown in Figure 4b, the tail of adjacent peaks reach the measured peak center and the crosstalk becomes predominant. This we define by the tail fraction $\theta$ at the edge of the peak base. Other degrees of overlap can be achieved by $1/2 < k_m < 1$.

In order to establish the conditions where each peak is just resolved from its neighbor (unit resolution) let

$$\Delta\ m/m = m_u/m \text{ or } \Delta q_B \simeq 0.706\ m_u/k_m m \qquad (15)$$

where $m_u$ = unit mass.

From (8)

$$V_{dc} = \frac{a\ V_{ac}}{2q}, \qquad (16)$$

and letting $a = a_{pk} - \Delta a_{0.706}$,

where $a_{pk} = 0.23699$ = value of a at the peak of the stability diagram and

$\Delta a_{0.706}$ = increment of a between $a_{pk}$ and the intercept of the scan line with q = 0.706,

then,

$$V_{dc} = \frac{V_{ac}}{2q} \left(a_{pk} - \Delta a_{0.706}\right). \tag{17}$$

However, $\Delta a_{0.706} = 0.2524 \ \Delta q$ from the geometric relationship of the stability diagram and $\Delta q_B = \Delta_q + \Delta_{qt}$, (where $\Delta q_t = \Delta q_{tx} + \Delta q_{ty}$ by definition from Figure 3).

Experimentally it is found that $\Delta q_t$ remains constant if mass and $V_{ac}$ are constant as resolution is adjusted by increasing or decreasing $V_{dc}$. The peaks are seen to change in width in the central 100% transmission region without a marked change in shape or width of the tails. However, when scanning $V_{ac}$ and M, $\Delta q_t$ will change. From the Mask Study, Table I, $\Delta q_t$ appears to decrease with $\Delta$ m/m as m increases; i.e., approximately the same number of cycles are required for an ion to reach the rod at a given percentage of $\Delta q$ outside the boundary whether the scan line slope is set for resolution 100 or 200.

Thus, we assume

$$(\Delta q_t) = k_{t1} \ \Delta q, \tag{18}$$

where $(\Delta q_t)$ is a specific tail width giving the desired quality of resolution.

Also, for a given axial energy, the heavier ion will remain in the rod system for a greater number of cycles and thus have a higher probability of exclusion. Consequently, $\Delta q_t/\Delta q$ should even decrease at higher mass. Appendix 2 deals with the tail transmission probability and results in a relatively complex expression. For the purpose of describing the nature of unit resolution scanning we believe it is conservative albeit approximate, to use (18).

Thus, from (14), (17), and (18); $\Delta q_B = \Delta q\ (1 + k_{t1})$

and
$$V_{dc} = \frac{V_{ac}\ a_{pk}}{2q} - 0.2524\ \frac{V_{ac}}{2q}\ \frac{q\ m_u}{k_m\ (1 + k_{t1})} \tag{19}$$

Substituting from the quadrupole equation

$$q = \frac{4\ e\ V_{ac}}{m\ r_o^{\,2}\ \omega^2}\ , \tag{20}$$

for $V_{ac}$ in the second term, and from fixed values for $a_{pk}/2q$ in the first term;

$$V_{dc} = 0.16785\ V_{ac} - 0.1262\ \frac{q\ m_u\ r_o^{\,2}\ \omega^2}{4\ e\ k_m\ (1 + k_{t1})}\ . \tag{21}$$

The second term thus expresses a constant offset in $V_{dc}$ that is established relative to $V_{ac}$ at unity mass.

Summarizing this section, it is shown that a continuous scan of the spectrum can be adjusted for unit resolution throughout the spectrum and provide that the masses occur at a uniform rate in time by letting $V_{dc} = k_1\ V_{ac} - k_2$, and $V_{ac} = kt$. For obtaining maximum information from such a scan, adjustment of $k_m$ allows for overlap of peak sides and tails such that a minimum time is spent in measuring low utility information. $k_{t1}$ adjusts the base width allowance for the tails. The techniques of either stepping $V_{ac}$ from peak-to-peak or by compressed scanning are necessary to maximize the information content of a mass spectrometer. The quadrupole further exhibits the unique property among mass spectrometers of simple electrical adjustment to achieve both uniform pulse (peak) duration and repetition rate, as seen by the output measuring system, while maintaining a low ratio of lost time between peaks.

## Entrance Conditions for $\Theta_A = 1.0$

For 100% transmission through the quadrupole analyzer as considered here, it is necessary to limit the maximum entrance angles $\alpha_x$ and $\alpha_y$; the initial off-axis position of the ion,

$$\eta_x = \frac{x_e}{r_o} \text{ and } \eta_y = \frac{y_e}{r_o} \; ; \tag{22}$$

and the maximum injected energy from the ion source into the quadrupole. We establish these limits which govern sensitivity, through a tradeoff with resolution and peak shape.

From Figure 3 we establish the base width

$$\Delta q_B = \Delta q + \Delta q_{tx} + \Delta q_{ty}, \tag{23}$$

and the top width,

$$\Delta q_T = \Delta q - \Delta q_x - \Delta q_y, \tag{24}$$

where expressions for $\Delta q_x$, $\Delta q_y$, $\Delta q_{tx}$ and $\Delta q_{ty}$ are to be developed.

Thus the "scan space" taken up by the sides and tails of the peak is given by,

$$\Delta q_B - \Delta q_T = \Delta q + \Delta q_{tx} + \Delta q_{ty} - \Delta q + \Delta q_x + \Delta q_y$$

or
$$\Delta q_B \left(1 - \frac{\Delta q_T}{\Delta q_B}\right) = \Delta q_x + \Delta q_y + \Delta q_{tx} + \Delta q_{ty}. \tag{25}$$

However, from (14), $\Delta q_B = q\, \Delta m/k_m m$. Also, $\Delta q_T/\Delta q_B$ is the top-to-base ratio of the peak which we symbolize by T/B. Thus,

$$\frac{q\Delta m}{k_m m} \; (1 - T/B) = \Delta q_x + \Delta q_y + \Delta q_{tx} + \Delta q_{ty}. \tag{26}$$

Consequently, we see that an improved peak shape (large T/B ratio) and higher resolution can be achieved by minimizing the $\Delta q$ values on the right hand side of the equation. It is interesting to note that this is identical in form to a symmetrical magnetic sector instrument in which

$$r \frac{\Delta m}{m} \; (1 - T/B) = 2 \, S_I \tag{27}$$

where $S_I$ is the image or beam width and r the magnetic radius of curvature.

Thus, the sum of $\Delta q$ values of (26) is analogous to beam width. Comparison of the dependencies of $\Delta q$ upon entrance angle position and energy will disclose a further close resemblance of the quadrupole to the double-focusing magnetic mass spectrometer.

For evaluation of $\Delta q_y$ and $\Delta q_x$ in terms of initial conditions we turn to reference 3 (Appendix 1).[7] Their equation 14 restated here is

$$\frac{|y_{max}|}{y_o} = \frac{2.672}{\beta_y f_1} \left| \frac{0.505\, r_o\, \alpha_y}{y_o} + \frac{f_2}{f_1} \right| \tag{28}$$

where $y_{max}$ = maximum amplitude of y motion

$y_o$ = initial (entrance) y position

$\beta_y$ = stability parameter shown in Figure 12

$f_1$ = $(1.0 + 0.336 \cos \phi)$

$f_2$ = $0.336 \sin \phi$

$\gamma_y$ = $(V_I/V_{ac})^{1/2} \sin \alpha_y$; normalized transverse velocity

$\phi$ = phase of applied $V_{ac}$ at the time of ion entrance into the quadrupole field.

$V_1$ = voltage of ion injection into the quadrupole field

$\alpha_y$ = initial angle of entrance in the y-z plane

also $\gamma_x = (V_I/V_{ac})^{1/2} \sin \alpha_x$ .

This equation was derived directly from solutions to the Mathieu equations describing the ion motion; it involved dropping higher order terms. We will use this equation for form and check coefficient values against later work.

The largest value of $\beta_y$ attainable by given values of initial position $y_o$ and normalized velocity $\gamma_y$ can be found by first letting $|y_{max}| = r_o$ and solving for $\beta_y$, thus

$$\beta_y = 2.672 \left| \frac{0.595}{f_1} \gamma_y + \frac{f_2}{f_1^2} \eta_y \right|, \tag{29}$$

where $\eta_y = y_o/r_o$.

From Reference 3, the phase of $f_1$ and $f_2$ giving the largest value to (29) occur at

$$\phi \approx \frac{3\pi}{4}$$

with little variation for a wide range of relative values of $\eta_y$ and $\gamma_y$. Thus, for this value of $\phi$,

$$\beta_y \approx 2.07\ \alpha_y + 1.09\ \eta_y. \tag{30}$$

We now let the maximum values $(\eta_y)_{max}$ and $(\gamma_y)_{max}$ determine $(\beta_y)_{max}$, or to generalize,

$$(\beta_y)_{max} = F_1\ (\gamma_y)_{max} + F_2\ (\eta_y)_{max}. \tag{31}$$

From the stability diagram we also note that due to the slope of the scan line in passing through lines of equal $\beta$,

$$\Delta q_y = 2.55\ \beta_y^2 \tag{32a}$$

and

$$\Delta q_x = 1.30\ (1 - \beta_x)^2 \tag{32b}$$

From computer evaluation[6] of stable trajectories in the marginal transmission region ($\Delta q_x$ space) indicates that a function having similar proportionality to (31) exists for $(1 - \beta_x)$. Thus we assume

$$(1 - \beta_x)_{max} = F_3\ (\gamma_x)_{max} + F_4 (\eta_x)_{max} \tag{33}$$

Combining (26), (31), (32), and (33)

$$q\ \frac{\Delta m}{k_m m}\ (1 - T/B) = 2.55\ (\beta_y)^2_{max} + 1.30\ (1 - \beta_x)^2_{max} + \Delta qt_x + \Delta qt_y \tag{34}$$

Letting the brackets ( ) denote maximum values for $\eta$ and $\gamma$,

$$q\ \frac{\Delta m}{k_m m}\ (1 - T/B) = 2.55\ [(F_1\ (\gamma_y) + F_2\ (\eta_y)]^2 + 1.30\ [F_3\ (\gamma_x) + F_4\ (\eta_x]^2 + \Delta qt_x + \Delta qt_y \tag{35}$$

We would now like to simplify equation (35) and solve for the reduced coefficients in terms of some recent computer results[6]. This will allow us to update the coefficients to more reasonable results instead of using the theoretical values of (30). We assume a relationship will exist for maximum transmission whereby

$$(\gamma_x) = k_\gamma (\gamma_y) \text{ and } (\eta_x) = k_\eta (\eta_y) \text{ and where } k_\gamma$$

and $k_\eta$ will have an optimum. Expanding and collecting terms we find that

$$q \frac{\Delta m}{k_m m} (1 - T/B) = G_{11} (\gamma_y)^2 + 2 G_{12} (\gamma_y)(\eta_y) + G_{22} (\eta_y)^2 + \Delta q_{tx} + \Delta q_{ty} \tag{36}$$

where

$$G_{11} = 2.55 F_1^2 + 1.30 F_3^2 k_\gamma^2$$

$$G_{12} = 2.55 F_1 F_2 + 1.30 F_3 F_4 k_\gamma k_\eta$$

$$G_{22} = 2.55 F_2^2 + 1.30 F_4^2 k_\eta^2$$

In order to arrive at values for $G_{11}$, $G_{12}$, and $G_{22}$ which depend upon the density distribution of $\gamma$ and $\eta$ within their maximum values (among other factors) it is necessary at this point to rely upon the computer summation of a matrix of transmission probabilities in the stable region. For this comparison we have one value. In excess of $10^6$ trajectories were run[6] for a constant density distribution to $(\eta_x) = (\eta_y) = 0.08$, $(\gamma_x) = (\gamma_y) = 0.064$ and for each 0.1° of phase. Odd parity in the signs of $\eta$ and $\gamma$ give one transmission efficiency and even parity gives another efficiency. When averaged these values give the net efficiency. Sixteen values each of $\eta$ and $\gamma$ were run at the central value of each $\Delta\eta = 0.005$ and $\Delta\gamma = 0.004$. The quadrupole rods were assumed to be of infinite length so that no assumptions of transmission efficiency near the stability boundary or as a function of mass were necessary. Thus, $\Delta q_{tx} = \Delta q_{ty} = o$.

The resolution intercept of 21 for 100% transmission in Figure 5 represents the case of $T/B = 0$ while resolution now pertains to separation at the theoretical base of the peak ($k_m = 1$). Thus from (36),

$$\frac{q\Delta m}{m} = G_{11} (\gamma_y)^2 + 2 G_{12} (\gamma_y)(\eta_y) + G_{22} (\eta_y)^2 \tag{37}$$

We now note that this is the same result as if we had assumed from (35) that

$$2.55\ [F_1\ (\gamma_y) + F_2\ (\eta_y)]^2 = 1.30\ [F_3\ (\gamma_y) + F_4\ (\eta_y)]^2 \tag{38}$$

In fact we will find later, in Appendix 3, that this is a condition of maximum transmission for constant coefficients. It is logical that this would be so since the same q-space is taken up by the conditionally y-stable and x-stable sides of the peak.

From (37) we define a perfect square

$$G_{11}\ (\gamma_y)^2 + 2\ G_{12}\ (\gamma_y)(\eta_y) + G_{22}\ (\eta_y)^2 = [G_1(\gamma_y) + G_2\ (\eta_y)]^2 \tag{39}$$

and from (35) and (38),

$$\frac{q\Delta m}{m} = 2 \times 2.55\ [F_1\ (\gamma_y) + F_2\ (\eta_y)]^2, \tag{40}$$

when $T/B = \Delta q_{ty} = \Delta q_{tx} = o$ and $k_m = 1$

It is further shown in Appendix 3 that the transmission will be maximized when

$$(G_1)(\gamma_y) = (G_2)(\eta_y) \tag{41}$$

Consequently, from the computed intercept of $m/\Delta m = 21$ at $\gamma = 0.064$ and $\eta = 0.08$,

$$0.706/21 = \Big(G_1\ (0.064) + G_2\ (0.08)\Big)^2 = \Big(2\ G_1\ (0.064)\Big)^2,$$

and

$$G_1 = 1.43 = (G_{11})^{1/2} = 2.26\ F_1,$$

$$G_2 = 1.14 = (G_{22})^{1/2} = 2.26\ F_2,$$

$$G_{11} = 2.05,\ G_{12} = 1.64,\ G_{22} = 1.315,$$

$$F_1 = 0.634 \text{ and } F_2 = 0.508.$$

We could also have proceeded from (35) and (38) in the x-plane with

$$\frac{q\Delta m}{m} = 2 \times 1.30\ [F_3\ (\gamma_4) + F_4\ (\eta_x)]^2$$

to obtain

$$F_3 = 0.889 \text{ and } F_4 = 0.709.$$

The above argument of coefficient values rests upon the choices of $\gamma = 0.064$ and $\eta = 0.08$ and the resulting resolution of 21 in the computer run. This is probably not the optimum since the choices were based upon preliminary results that emphasized the y-plane. However, to optimize the transmission data versus phase angle and $\eta$ and $\gamma$ for other $\gamma/\eta$ ratios and $\gamma_x/\gamma_y$, $\eta_x/\eta_y$ ratios would require an extensive effort.

The choice, now, for an optimum could just as well have assumed $\gamma_x$ and $\eta_x$ were $(2.55/1.30)^{1/2}$ larger than $\gamma_y$ and $\eta_y$ since this is the extra capacity in the x-plane. As a result $F_3$ and $F_4$ would then be of the same order as $F_1$ and $F_2$. Since we have no logical basis for making this assumption we use the computer results with $F_3$ and $F_4$ values above.

Returning to the comparison of coefficients from (40) ff, we find that

$$\beta_y = 0.634\ (\gamma_y) + 0.508\ (\eta_y) \tag{42}$$

which yields substantially smaller coefficients than the theoretical values from Equation (30) where

$$\beta_y = 2.07\ (\gamma_y) + 1.09\ (\eta_y).$$

Smaller coefficients will lead to increased transmission since $\gamma$ and $\eta$ will be larger before limiting resolution is reached. It is important then to examine this difference. There appears to be two explanations, as follows:

(1) The G coefficients are in effect hybrid x and y plane coefficients, since the q space equations were made equal for the two planes. The scan line angle provided an advantage of 1.3/2.55 for the x plane, which when optimized reduced the effective y coefficients.

(2) The computer provided a distribution of density versus $\gamma$ and $\eta$. $\beta_y$ obtained from (30) is the largest value reached by any ion; whereas in reality, we are dealing with a number distribution associated with the function $F_1\ \gamma_y + F_2\ \eta_y$ which has the distribution shown below if ions are uniformly distributed in $\gamma$ and $\eta$.

Consequently, an apparently improved resolution is obtained at the 100% transmission intercept of Figure 5 because of the ion density at the limiting value.

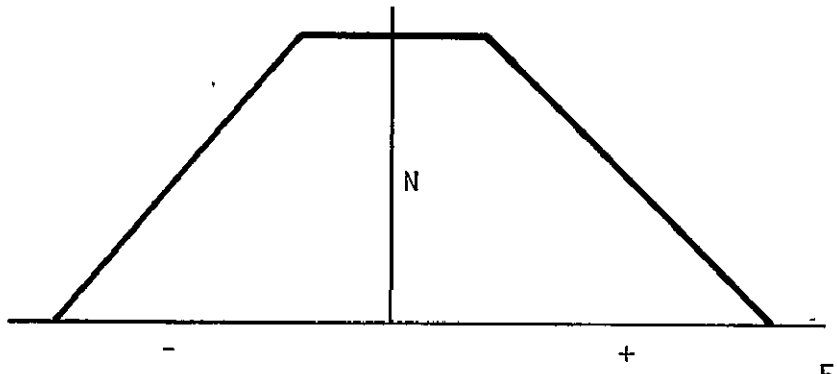


$F_1\gamma_y + F_2\eta_y$

$F_1$ = CONST.

$F_2$ = CONST.

$F_1(\gamma_y) \neq F_2(\eta_y)$

Consequently, we retain the more realistic values of (41) to describe the optimized (equalized x and y) 100% transmission edge.

We return to (35) where a satisfactory solution has been obtained for the stable portion of the equation and now draw upon the results of Appendix 2 to describe the width of the peak tail. From (A2-21) approximate expressions for the q-space occupied by the tail to a given transmission fraction $\Theta$ are

$$\Delta q_{ty} = \frac{0.0584}{n} \ell n \frac{0.0667}{\Theta_y} - 0.00250,$$

$$\Delta q_{tx} = \frac{0.0297}{n} \ell n \frac{0.0253}{\Theta_x} - 0.00128,$$

or if $\Theta_x = \Theta_y$,

$$\Delta q_t = \Delta q_{tx} + \Delta q_{ty} = \frac{0.088}{n} \ell n \frac{0.048}{\Theta} - 0.00378;$$

where n is the number of a-c cycles experienced by the ion and $\Theta_x$ = fractional transmission at $\Delta q_{tx}$ and $\Theta_y$ = fractional transmission at $\Delta q_{ty}$.

Letting $n = \frac{f\ell}{(v_z)}$ and combining with (42) yields

$$\frac{q\Delta m}{k_m m}\ (1 - T/B) = 2.55\ [F_1\ (\gamma_y) + F_2\ (\eta_y)]^2 + 1.30\ [F_3\ (\gamma_x) + F_4\ (\eta_y)]^2$$

$$+ \frac{0.88\ (v_z)}{f\ell}\ \ell n\ \frac{0.48}{\theta} - .00378, \qquad (43)$$

where $f$ = frequency, Hz

$\ell$ = rod length, meters

$(v_z)$ = maximum axial (z) ion velocity for the mass observed, meters/sec.

We now have an empirical equation defining resolution and peak shape as a function of initial position, angle and axial velocity. The top width is defined as the q-space taken up by the 100% transmission region of the peak and the base width as the q-space between equal x and y transmission fractions $\theta$. The equation appears to be useful when the tail width, $\Delta q_t \geq 0.000706$ or 10% of the theoretical peak width at a resolution of 100.

This mass analyzer function must now be matched to the ion source function, which can also be described in terms of the maximum (emitted) ion position angle and axial velocity.

## ION SOURCE CHARACTERISTICS

It is desirable to update the ion source function in terms of particle density and the mode of use.

The ion current formed in an ion source can be expressed as,

$$I_f^+ = Q_m \, I^- n_s \ell_e \text{ amps} \tag{44}$$

where

$Q_m$ = ionization cross section for ion of mass m (meter$^2$)

$I^-$ = ionizing electron current (amps)

$n_s$ = molecular density in the source (molecules/meter$^3$)

$\ell_e$ = useful ionization path length (meter)

If the electron beam has a useful width, w, for passage of the electron current $I^-$, then the ionization density formed is,

$$J_f^+ = \frac{Q_m \, I^- n_s \ell_e}{w \ell_e} = \frac{Q_m \, I^- n_s}{w} \quad \frac{\text{amps}}{\text{meter}^2} \tag{45}$$

which can be treated as an ion "cathode" with density proportional to electron current per unit width ($I^-/w$).

If magnification of this ion object takes place in the source independently in x and y, to form an image of the ion cathode at the final aperture as shown in Figure 14, then the illumination is,

$$J_e^+ = \frac{Q_m \, I^- n_s}{w \, M_x \, M_y} \quad \frac{\text{amps}}{\text{meters}^2}$$

where $M_x$ and $M_y$ are the respective magnifications. The dimensions of intervening apertures are assumed large enough so as not to remove current from the theoretical image.

The emitted current from the source is then,

$$I_s^+ = J_e^+ A_e = \frac{Q_m I^- n_s A_e}{w M_x M_y} \quad \text{amps} \tag{46}$$

where $A_e$ is the exit aperture area (meter$^2$).

When the pressure is limited only by instrument performance we use an approach based upon space charge effects in the ionizing region. This case (Mode 3, excess sample) is considered first.

Brubaker[7] has described the space charge conditions occurring in an ion source of infinite extent. His equations can be used to interpret the limits of pressure nonlinearity and therefore accuracy of the system. $I^-$ and n are then established by,

$$I^-/w = \frac{i_v V_R}{w} \quad \text{amps}, \tag{47}$$

and

$$n_s = \chi n_c = \chi \frac{3}{4 d Q_m} \left( \frac{V_r m_e}{a V_e m} \right)^{1/2} \quad (\text{meter})^{-3} \tag{48}$$

where

$i_v$ = parameter for normalizing electronic charge density (amps/volt)

$V_R$ = Repeller voltage (volts) with respect to accelerator voltage

$n_s$ = molecular density (molecules/meter$^3$) in the ion source

$\chi$ = fraction of critical density

$n_c$ = critical density (molecules/meter$^3$)

d = spacing of repeller to accelerator (meter)

$Q_m$ = cross section for ionization of ion mass m (meter$^2$)

$m_e$ = mass of the electron (kg)

$a$ = fraction of distance of electron beam from the accelerator to repeller

$V_e$ = electron voltage (volts)

$m$ = mass of ion (kg)

We redefine

$$Q_m\, m^{1/2} = \sum_{M=1}^{M_{max}} Q_m\, M^{1/2}\, m_u^{1/2} \quad \text{(with M in AMU)}$$

to sum all the charge present as intended, where $m_u$ = unit mass (kg).

Thus

$$I_s^+ = \frac{Q_m\, A_e}{M_x\, M_y\, w} (i_v\, V_R) \left( \chi \frac{3\, V_R^{1/2}}{4\, d \sum Q_m\, M^{1/2}} \left( \frac{m_e}{a\, V_e\, m_u} \right)^{1/2} \right) \text{amps} \qquad (49)$$

The equation now shows the strong dependency on $V_R$ reflecting that the rapid removal of ion charge provides a higher level of current for the source space charge conditions. For a nonlinearity (inaccuracy) the order of 5%, $i_{v/w} \simeq 4 \times 10^{-3}$ amps/volt meter and $x \simeq 0.6$ from experimental data. In terms of pressure, for $V_R = 20$ v and with $a = 0.5$, $V_e = 75$ v, $d = .0025$ meter, the critical pressure is $3.6 \times 10^{-4}$ torr. Thus when $x = 0.6$, the operating pressure can be $2.2 \times 10^{-4}$ torr while maintaining linear operation within approximately 5%.

Gathering terms,

$$I_s^+ = \frac{K_1\, A_e\, V_R^{3/2}}{M_x\, M_y\, d} \text{ amps}, \qquad (50)$$

where

$$K_1 = \frac{3\, i_v\, \chi\, Q_m}{4\, w \sum Q_m\, M^{1/2}} \left( \frac{m_e}{a\, V_e\, m_u} \right)^{1/2} \frac{\text{amps}}{(\text{volt})^{3/2}\ \text{meter}}$$

Assuming that the ion source will be used with a quadrupole mass analyzer it is desirable to express the strong dependence of (50) upon $V_R$ in terms of the axial velocity through the quadrupole, $v_z$. It is noted that there is a tradeoff between the added sensitivity to be gained by increasing repeller voltage and the loss in resolution from increased ion velocity spread and thus larger tails. In the limiting case, the quadrupole axis can be biased to the potential of the least energetic ion created in the electron beam without losing ions by reflection from the quadrupole

potentials. Thus the ion of maximum velocity (created at the most positive potential of the electron beam) will have an axial potential,

$$v_z = \frac{t}{d} V_R$$

where t is the thickness of the electron beam.

In practice it is often desirable to have a slightly larger $v_z$ than described by the real electron beam thickness. However, one may describe t as a pseudo-thickness which remains proportional to $V_R$. Thus,

$$t\, V_R/d = \frac{m\,(v_z)^2}{2e} \text{ volts},$$

or

$$V_R = \frac{d\, m\,(v_z)^2}{2et} \text{ volts}, \tag{51}$$

and (50) becomes

$$I_s^+ = \frac{K_1 A_e d^{1/2} (v_z)^3}{M_x M_y} \left(\frac{m}{2et}\right)^{3/2} \text{ amps}. \tag{52}$$

Further Abbes' Law[8] can be shown to describe $M_x$ and $M_y$ as follows:

$$\frac{1}{M_x} = \left(\frac{V_I}{V_o}\right)^{1/2} \sin(\alpha_x), \tag{53}$$

and

$$\frac{1}{M_y} = \left(\frac{V_I}{V_o}\right)^{1/2} \sin(\alpha_y).$$

where $V_o$ is the initial transverse ion energy per charge to be accepted by the ion source lens system and $(\alpha_x)$ and $(\alpha_y)$ the maximum emitted angles of the ion source for the value $V_o$.

Substituting in (51) and letting

$$K_2 = d^{1/2} \left(\frac{m}{2et}\right)^{3/2} \text{ volt}^{3/2}\ \text{sec}^3/\text{meter}^4,$$

$$I_s^+ = \frac{K_1 K_2 A_e V_I v_z^3}{V_o} \sin(\alpha_x) \sin(\alpha_y) \text{ amps} \tag{54}$$

Preparing for combination with the mass analyzer we let $A_e = 4(x_e)(y_e) = 4(\eta_x)(\eta_y)\ r_o^2$ from (22), and $V_I \sin(\alpha_x) \sin(\alpha_y) = V_{ac}(\gamma_x)(\gamma_y)$ from (28). Thus:

$$I_s^+ = \frac{4\ K_1 K_2\ V_{ac}\ r_o^2}{V_o} (v_z)^3 (\eta_x)(\eta_y)(\gamma_x)(\gamma_y) \text{ amps} \qquad (55)$$

where again ( ) denotes the maximum value of the included parameter.

Equation (55) now expresses the ion source emitted current as a function of variables common to the mass analyzer. It demonstrates that increased ion source current can be obtained by a larger and more powerful quadrupole or by increased ion velocity, angle or entrance area.

If we now consider the ion source equation when an excess of sample is not available we find that ion space charge is no longer a limit on performance. We retrace to Equations (47) and (48) and accept Equation (47) as valid since it describes the space charge depression due to the electron beam. The limiting ionizing current will be reached when space charge produces the same potential in the ionizing space as at the accelerator; i.e., zero field gradient in front of the electron beam. The potential then drops from $V_R$ at the repeller to zero at the electron beam creating a gradient,

$$E_Z = \frac{-V_R}{(1 - a)\ d}$$

in this space. From Poissons equation, $\nabla^2 V = -\rho/\varepsilon_o$ or

$$\frac{d^2 V_i}{d Z^2} = -\rho/\varepsilon_o$$

in the infinite planar model assumed.

$V_i$ = potential in the ionizing space (volts),

$\rho$ = spare charge density (coul/$m^3$)

$\varepsilon_o$ = permittivity of free space.

The gradient change through the electron beam is then

$$\frac{d\ E_Z}{dZ} = \rho/\varepsilon_o = J_e/v_e\ \varepsilon_o$$

where

$J_e$ = electron beam current density amps/meter$^2$,

and

$$v_e = \frac{2\ e\ V_e}{m_e}^{1/2} \quad \text{electron velocity meters/sec.}$$

The useful electron current passes through an area of wt where t is the electron beam thickness and w the useful width. Thus

$$\Delta E_z = \frac{\bar{I}\ \Delta z}{w\ t\ v_e\ \varepsilon_o} \quad . \tag{56}$$

But $\Delta z = t$. Consequently, $\Delta E_z = \bar{I}/w\ v_e\ \varepsilon_o$ or, for Modes 1 and 2,

$$(\bar{I}/w)_{1,2} = v_e\ \varepsilon_o\ \Delta E_z = \frac{v_e\ \varepsilon_o\ V_R}{(1 - a)d} = \left(\frac{2\ e\ V_e}{m_e}\right)^{1/2} \frac{\varepsilon_o\ V_R}{(1 - a)d} \quad \text{amps/meter} \tag{57}$$

Equation (48) does not apply since there is assumed to be negligible ion space charge. In practice, of course, either positive charge would build up or slightly less electron current would be injected to create a slight gradient toward the accelerator.

Substituting (57) into (46) gives

$$I_s^+ = \frac{Q_m\ \varepsilon_o\ V_R}{M_x\ M_y\ (1 - a)d}\left(\frac{2\ e\ V_e}{m_e}\right)^{1/2} n_s\ A_e \text{ amps} \tag{58}$$

Proceeding along previous lines and substituting (51), (53) and the equations following (54) into (58) we have

$$I_s^+ = \frac{4\ K_1' K_2'\ n_s\ V_{ac}\ r_o^2}{V_o}\ (v_z)^2\ (\eta_x)(\eta_y)(\gamma_x)(\gamma_y) \text{ amps} \tag{59}$$

where

$$K_1' = \frac{Q_m\ \varepsilon_o}{(1 - a)}\left(\frac{2\ e\ V_e}{m_e}\right)^{1/2} \text{ amp meter}^2/\text{volt}$$

and

$$K_2' = \frac{m}{2et} \text{ volt sec}^2/\text{meter}^3$$

In general, Equation (59) is used whenever the ambient density limits the ion source density, $n_s$ (either Mode 1 or 2), and Equation (55) when excess sample is available (Mode 3) and thus positive ion space charge limits the source pressure. Mode 1 then differs from Modes 2 and 3 in use of an imaging ion source as described in the above equations. Modes 2 and 3 could, in general, use a thermally imaging ion source since the initial energy of the ions is controlled by the ion source temperature and is not excessive. We do not go through the exercise here of describing the thermal-focus source because it gives substantially the same end result and requires a more emperical approach.

THIS PAGE INTENTIONALLY LEFT BLANK

## OPTIMIZED INSTRUMENT FUNCTION

The maximum exit conditions of the ion source from either (55), (Mode 3) or (59), (Modes 1 and 2) now provide the maximum acceptable input conditions for the mass analyzer as given in (43). Since we have predicated the development of the mass analyzer equation on 100% transmission, the current transmitted by the ion source becomes the collected current to the detector, i.e., $I_s^+ = I_c^+$. Thus,

$$I_{c_3}^+ = \frac{4\, K_1 K_2\, V_{ac}\, r_o^2}{V_o} (v_z)^3 (\eta_x)(\eta_y)(\gamma_x)(\gamma_y) \text{ amps}, \tag{60}$$

and

$$I_{c_{1,2}}^+ = \frac{4\, K_1' K_2'\, n_s\, V_{ac}\, r_o^2}{V_o} (v_z)^2 (\eta_x)(\eta_y)(\gamma_x)(\gamma_y) \text{ amps}, \tag{61}$$

where

$$K_1 = \frac{3\, i_v\, \chi\, Q_m}{4w \sum Q_m\, M^{1/2}} \left( \frac{m_e}{a\, V_e\, m_u} \right)^{1/2} \frac{\text{amps}}{\text{volt}^{3/2}\ \text{meter}}$$

$$K_2 = d^{1/2} \left( \frac{m}{2et} \right)^{3/2} \frac{\text{volt}^{3/2}\ \text{sec}^3}{\text{meter}^4} ,$$

$$K_1' = \frac{Q_m\, \varepsilon_o}{(1-a)} \left( \frac{2\, e\, V_e}{m_e} \right)^{1/2} \frac{\text{amp-meter}^2}{\text{volt}} ,$$

and

$$K_2' = \frac{m}{2et} \frac{\text{volt sec}^2}{\text{meter}^3} .$$

In Appendix 3, Equation (43) is combined with the above ion source equations by solving for $(\gamma_x)$, and substituting in (60) and (61) and then differentiating $I_c^+$ for a maximum as a function of $(\eta_x), (\eta_y), (\gamma_y)$ and $(v_z)$. In this process the optimized parameters are assumed to be independent of each other and that the coefficients are constant.

The resulting maximized Mode 3 (closed source) equation (A3-22), is,

$$I_c^+ (\max)_3 = \frac{0.957\ K_1 K_2\ V_{ac} (f\ell)^3\ r_o^2}{F_1 F_2 F_3 F_4\ V_o \left(\ell n\ \frac{.048}{\theta}\right)^3} \left( \frac{q\Delta m}{k_m m} \left(1 - \frac{T}{B}\right) + .00378 \right)^5 \text{ amps} \qquad (62)$$

where optimized values are,

$$(v_z)_3 = \frac{3}{5}\ \frac{(f\ell)(U + .00378)}{.088\ \ell n \left(\frac{.048}{\theta}\right)} \quad , \qquad (63)$$

$$(\eta_x)_3 = \frac{1}{2\ F_4} \left[ \frac{2\ (U + .00378)}{5\ (2.6)} \right]^{1/2} \quad ,$$

$$(\eta_y)_3 = \frac{1}{2\ F_2} \left[ \frac{2\ (U + .00378)}{5\ (5.1)} \right]^{1/2} \quad ,$$

$$(\gamma_x)_3 = \frac{1}{2\ F_3} \left[ \frac{2\ (U + .00378)}{5\ (2.6)} \right]^{1/2} \quad ,$$

$$(\gamma_y)_3 = \frac{1}{2\ F_1} \left[ \frac{2\ (U + .00378)}{5\ (5.1)} \right]^{1/2} \quad ,$$

and $$U = \frac{q\Delta m}{k_m m} \left(1 - \frac{T}{B}\right) .$$

For Modes 1 and 2 (open source) from (A3-26)

$$I_c^+ (\max)_{1,2} = \frac{0.152\ K_1' K_2'\ n_s\ V_{ac}\ (f\ell)^2\ r_o^2}{F_1 F_2 F_3 F_4\ V_o \left(\ell n\ \frac{.048}{\theta}\right)^2} \left( \frac{q\Delta m}{k_m m} \left(1 - \frac{T}{B}\right) + .00378 \right)^4 \text{ amps} \qquad (64)$$

The optimized values of the parameters are somewhat different due to the power of $(v_z)$. Thus,

$$(v_z)_{1,2} = \frac{1}{2}\ \frac{(f\ell)(U + .00378)}{.088\ \ell n\ \frac{.048}{\theta}} \quad , \qquad (65)$$

$$(\eta_x)_{1,2} = \frac{1}{2\,F_4}\left[\frac{(U + .00378)}{2\,(2.6)}\right]^{1/2},$$

$$(\eta_y)_{1,2} = \frac{1}{2\,F_2}\left[\frac{(U + .00378)}{2\,(5.1)}\right]^{1/2},$$

$$(\gamma_x)_{1,2} = \frac{1}{2\,F_3}\left[\frac{(U + .00378)}{2\,(2.6)}\right]^{1/2},$$

$$(\gamma_y)_{1,2} = \frac{1}{2\,F_1}\left[\frac{(U + .00378)}{2\,(5.1)}\right]^{1/2}.$$

## Discussion of Parameters

The important conclusions at maximum transmission are as follows:

a. The q-space taken by the $\eta$ and $\gamma$ functions are shared equally in a given plane, i.e., $F_1(\gamma_y) = F_2(\eta_y)$ and $F_3(\gamma_x) = F_4(\eta_x)$. This is so, regardless of future improvement in the optimum values found for the F functions.

b. The q-space taken by the x and y functions are equally shared, i.e., $2.55\,[F_1(\gamma_y) + F_2(\eta_y)]^2 = 1.3\,[F_3(\gamma_x) + F_4(\eta_x)]^2$. This results also in the conclusion that $2.55\,\beta_{y_E}^2 = 1.3\,(1 - \beta_x)_E^2$ at the edges of the 100% transmission band. Thus, $(1 - \beta_x)_E = 1.4\,\beta_{y_E}$ where the subscript E now refers to the resulting practical edge of the 100% transmission band.

   It is noted that as a result of Conclusions a and b, the q-space by each of the four functions, $F_1(\gamma_y)$, $F_2(\eta_y)$, $F_3(\gamma_x)$ and $F_4(\eta_x)$ are all equal.

c. The leverage in $v_z$ exerted by the "tail" function which is now included in the optimization equation is quite large. This effect is a result of being able to increase ion current for the same ionizing space charge when an increased repeller-accelerator voltage, and thus axial ion velocity, is allowed. There are several practical limitations to extending this advantage very far, However, one important influence is the election beam thickness which also governs the $\Delta V$ to be accepted by the analyzer. A well focused electron beam, such as from a line filament, can have the same importance as a considerable increase in rod length.

Conclusion c is only one of a series of parametric effects on the equation which can lead to practical improvements in transmission. We now reconstruct the equation in order to understand the physical effect of the various parameters.

We start with Equation (60) and recall that the area of the exit aperture of the ion source is $A_e = 4\, r_o^2\, \eta_x \eta_y$. Calculating from (63) for $(\eta_x)_3$ and $(\eta_y)_3$ we find from our choices of $F_4 = .709$ and $F_2 = .508$ that $\eta_x = \eta_y$ or that we have a square exit aperture. (It is also recalled that an alternative assumption would have made $F_2 \approx F_4$ and therefore $\eta_x \neq \eta_y$.) If, for example, we let $\Delta m/k_m m = 1/50$, $T/B = 0.5$ and with $q = 0.706$, $U = q\Delta m/k_m m\,(1 - T/B) = .00706$ then $(\eta_x)_3 = (\eta_y)_3 = 2.88 \times 10^{-2}$. Thus for an $r_o$ of 2.5 mm, the exit aperture is a square, 0.144 mm on a side.

Further, we recall that

$$\frac{V_{ac}}{V_o}\ \gamma_x \gamma_y = \frac{V_I}{V_o}\ \sin \alpha_x \sin \alpha_y = \frac{1}{M_x M_y}\ .$$

Calculating again from (63) and the above values $(\gamma_x)_3 = (\gamma_y)_3 = 2.3 \times 10^{-2}$. For $V_I = V_{ac} = 208$ V and $V_o = 0.208$ V, then $\sin \alpha_x = \sin \alpha_y = 2.3 \times 10^{-2}$ ($\alpha = 1.3°$) and

$$\frac{1}{M_x} = \frac{1}{M_y} = \frac{1}{M} = 0.727.$$

Thus a small magnification of 1.37 is required between the ion "cathode" (the ionizing region) and the source exit slit. If we demagnify the exit dimensions, we find that ions need only be drawn from an area

$$(A_o)_3 = \frac{A_e}{M^2} = (0.105\ \text{mm})^2 = 1.095 \times 10^{-8}\ M^2$$

in the ionizing region.

In fact, of course, the first ion source aperture is made larger to assure uniform focusing properties in the center of this lens. In addition the focusing model assumed an imaging ion source (see Appendix I). For the more commonly used thermal-imaging source a larger first aperture would be used to focus the center of the thermal image into the exit aperture.

We have, so far, found that

$$\frac{4\, V_{ac}\, r_o^2}{V_o}\ (\eta_x)(\eta_y)(\gamma_x)(\gamma_y) = A_o$$

where $A_o$ is defined as the area in the ionizing region from which ions are drawn to achieve the optimized transmission. But, by the same token, the

collected current is then the ion cathode density times the effective useful area or $I_c^+ = J_F^+ A_o$. Thus from (60), we must have that $K_1K_2 (v_z)^3 = (J_F^+)^3$ which could also have been shown by returning to the original equations. Likewise,

$$(J_F^+)_{1,2} = K_1'K_2' n_s (v_z)^2.$$

Consequently,

$$(I_c^+)_3 = [J_F^+]_3 [A_o]_3 = [K_1K_2 (v_z)^3]\left[\frac{4 V_{ac} r_o^2}{V_o} (\eta_x)(\eta_y)(\gamma_x)(\gamma_y)\right] \qquad (66)$$

and

$$(I_c^+)_{1,2} = [J_F^+]_{1,2}[A_o]_{1,2} = [K_1'K_2' n_s(v_z)^2]\left[\frac{4 V_{ac} r_o^2}{V_o} (\eta_x)(\eta_y)(\gamma_x)(\gamma_y)\right] \qquad (67)$$

(66) and (67) can be further expanded by the substitution of their respective optimized elements from (63) and (65). However, since the physical meaning is clear in (66) and (67) we retain them and turn to an examination of their first terms. Looking at the definitions ff (61) we see that none of the coefficients in $K_1$ can have much leverage or sensitivity. The $i_v\chi/w$ product sets the nonlinearity vs density to be accepted and cannot be increased greatly without reaching space-charge effected ion flow. Operation is also generally near maximum cross section, $Q_m$, by choice of $V_e$. a has only small leverage.

In $K_2$ now, we find that the election beam thickness, t, can have a substantial leverage on sensitivity. Further, the ion mass appears. The same is true on $K_2'$. We therefore isolate t and separate M and $m_u$ in the constants.

Since M appears in several places it is best to note their differences now. $\sum Q_m M^{1/2}$ appears in the denominator of $K_1$. This reflects the total ion space charge summed over the spectrum while $M^{1/2}$ reflects the velocity in moving toward the accelerator electrode. If we had traces of various gases, to say 100 AMU, in air the bulk of the charge could still reside in the low mass region and $\sum Q_m M^{1/2}$ would remain constant. This is the assumption that is carried through the remainder of the discussion. M also appears in Equation (51) for $V_R$ and in $K_2$ and $K_2'$. This pertains to the mass in view (being scanned) as it moves in the repeller-accelerator field. Later on we will substitute for $V_{ac}$ and find M describing the mass in view in the quadrupole. The latter two are thus the same.

$K_1'$ appears to have leverage by making a approach 1. While having the electron beam close to the repeller increases its capacity to the surroundings and thereby reduces the space charge depression, it also leads to practical problems of bombarding the repeller. It is felt that in practice, only limited improvement can be obtained here.

The constants are now calculated assuming the following values for illustration:

$$\left.\begin{aligned} i_v/w &= 4 \times 10^{-3} \text{ amps/volt meter} \\ \chi &= 0.6 \end{aligned}\right\} \quad \text{Approximately 5\% nonlinearity in } I^+ \text{ vs } \eta_s$$

That an $N_2$ sample is used having

$$Q_{28} \approx 1.8 \times 10^{-20} \text{ meter}^2$$

$$Q_{14} \approx 0.9 \times 10^{-20} \text{ meter}^2$$

$$\sum_{M=1}^{\infty} Q_m M^{1/2} \approx 1.8 \times 10^{-20} (28)^{1/2} + 0.9 \times 10^{-20} (14)^{1/2}$$
$$\approx 12.9 \times 10^{-20} \text{ meter}^2 \text{ (AMU)}^{1/2}$$

$$a = 0.5$$

$$V_e = 90 \text{ volts}$$

$$\left(\frac{m_e}{a\, V_e\, m_u}\right)^{1/2} = 3.49 \times 10^{-3} \text{ (volt)}^{-1/2}$$

$$d = 2.5 \times 10^{-3} \text{ meter}$$

$$m/e = 28 \times 1.035 \times 10^{-8} \text{ kg/coul.}$$

Thus, $K_1 = 8.8 \times 10^{-7} \text{ amp/volt}^{3/2} \text{ meter}$

$$K_2 = 1.87 \times 10^{-10}\, t^{-3/2}\, M^{3/2} \text{ volt}^{3/2} \text{ sec}^2/\text{meter}^4$$

$$K_1' = 1.8 \times 10^{-24} \text{ amp meter}^2/\text{volt}$$

$$K_2' = 5.19 \times 10^{-9}\, t^{-1}\, M \text{ volt sec}^2/\text{meter}^3$$

$$K_1 K_2 = 1.65 \times 10^{-20}\, t^{-3/2}\, M^{3/2} \text{ amp sec}^2/\text{meter}^5$$

$$K_1' K_2' = 9.28 \times 10^{-33}\, t^{-1}\, M \text{ amp sec}^2/\text{meter}$$

Letting f = 4.0 MHz, $\ell$ = 0.1 meter, $\theta = 10^{-4}$ and U = 0.00706 as above we can calculate the velocities from (63) and (65). Thus

$$(v_z)_3 = 4.79 \times 10^3 \text{ meter/sec (m/e 28 at 3.2 V)}$$

$$(v_z)_{1,2} = 3.99 \times 10^3 \text{ meter/sec (m/e 28 at 2.22 V)}$$

Also if we assume $n_s$ for Mode 1 and 2 to be $2.42 \times 10^{19}/m^3$ ($10^{-4}$ torr at 400°k) and t = $5 \times 10^{-4}$ meter, we find for M = 28 that;

$$(J_F^+)_3 = K_1 K_2 (v_z)_3^3 = 2.38 \times 10^{-2} \text{ amp/meter}^2,$$

and

$$(J_F^+)_{1,2} = K_1' K_2' n_s (v_z)_{1,2}^2 = 2.0 \times 10^{-2} \text{ amp/meter}^2.$$

It is interesting to note that the formed ion current densities are nearly the same, yet the imposed conditions were substantially different. We go on to evaluate $(A_o)_{1,2}$ for the same values as before and find

$$(A_o)_{1,2} = 1.713 \times 10^{-8} \text{ meter}^2.$$

Combining to find $I_c^+$ for the above conditions,

$$(I_c^+)_3 = (J_F^+)_3 (A_o)_3 = 2.38 \times 10^{-2} \times 1.095 \times 10^{-8} = 2.61 \times 10^{-10} \text{ amps} \quad (68)$$

$$(I_c^+)_{1,2} = (J_F^+)_{1,2} (A_o)_{1,2} = 2.0 \times 10^{-2} \times 1.713 \times 10^{-8} = 3.426 \times 10^{-10} \text{ amps} \quad (69)$$

Again, it is surprising to find the values so close. Looking for an explanation, it is apparent that the $A_o$ values will be nearly the same since their optimized components are about equal. However, the arbitrary choice of $n_s$ for the open source should have provided ample difference in $J_F^+$.

If we break $J_F^+$ into

$$J_F^+ = Q_m \left(\frac{I^-}{w}\right) n_s$$

we find that the distinguishing difference between the two modes is that the open source (Modes 1 and 2) has a high electron beam density but a low particle density. The reverse is true for the closed source.

From (57),

$$(\bar{I}/w)_{1,2} = 0.459 \text{ a/m} = 459 \text{ μa/mm}, \tag{70}$$

and by arbitrary choice above,

$$(n_s)_{1,2} = 2.42 \times 10^{18}/\text{meter}^3. \tag{71}$$

Whereas from (47), (51) and (63)

$$\left(\frac{\bar{I}}{w}\right)_3 = 0.0667 \text{ a/m} = 66.7 \text{ μa/mm} \tag{72}$$

and from (48, (51) and (63),

$$(n_s)_3 = 0.6\ n_c = 0.6 \times 3.32 \times 10^{19} = 2.0 \times 10^{19}/\text{m}^3 \tag{73}$$

So it appears that a trade off of extremes resulted from the choices made. If we examine the practical validity of these choices, the current density of (70) probably cannot be conducted[9] through a small isolating, rectangular slit if that is a requirement. Without setting up a whole new parametric system it is assumed that approximately 200 μa/mm could be used in practice if the passage length did not exceed 1 mm. Even this large value does point up that considerable sensitivity is to be gained by higher electron currents than the 10 - 40 μa range typically used. Sensitivities are therefore reduced by 200/459. Thus the revised values are:

$$(\bar{I}/w)_{1,2} = 0.200 \text{ a/m}, \tag{70R}$$

$$(I_c^+)_{12} = 1.5 \times 10^{-10} \text{ amps}, \tag{69R}$$

$$(J_F^+)_{1,2} = 8.8 \times 10^{-3} \text{ amp/meter}^2,$$

$$K_1'K_2' = 4.03 \times 10^{-33}\ t^{-1}\ M \text{ amp sec}^2/\text{meter}^{\ell},$$

and

$$K_1' = \frac{0.435\ Q_m\ \varepsilon_o}{(1 - a)} \left(\frac{2\ e\ V_e}{m_e}\right)^{1/2} \tag{61R}$$

The density in Modes 1 and 2 of $2.42 \times 10^{18}/\text{m}^3$ can probably be sustained without serious nonlinearity; however, it is not practical to say for sure without an actual test.

Now for the density in Mode 3. If a closed ion source is operated at the density of (73), corresponding to $8.3 \times 10^{-4}$ torr at 400°k, the gas flow from an ion source of 50 cc/sec speed would be $4.14 \times 10^{-2}$ torr cc/sec. This then, would produce a pressure of $4 \times 10^{-6}$ torr in a 10 liter/sec ion pump.

Without again optimizing an undefined task, it would seem that this sample flow and the resulting constraint is unrealistic for a small space-borne instrument. The limiting density is therefore arbitrarily reduced by a factor of 4.0 to

$$(n_s)_3 = 0.15\, n_c = 5 \times 10^{18}/m^3 \tag{73R}$$

by making $\chi = 0.15$ and thus

$$K_1 = 2.2 \times 10^{-7} \text{ amp}$$

$$K_1 K_2 = 4.12 \times 10^{-21}\, t^{-3/2}\, M^{3/2} \text{ amp sec}^2/\text{meter}^5$$

$$\left(I_c^+\right)_3 = 6.52 \times 10^{-11} \text{ amps} \tag{68R}$$

and

$$\left(J_F^+\right)_3 = 5.95 \times 10^{-3} \text{ amp/meter}^2$$

In principle it is possible to increase $i_v$ if $\chi$ is decreased in order to maintain the same space charge and nonlinearity. However this requires an experimental maneuver since the theory does not provide the means of making the translation from one to the other. In addition, other options of increasing electron current density from 66.7 μa/mm while maintaining low ion source pumping speed or of enclosing the filament are involved. Since this additional complexity is not warranted here, the revised values are used as attainable numbers for illustrative purposes.

The net result of these alternatives is to make the closed and open ion sources look more nearly alike in their operating levels. The fact remains, of course, that the size of the tube or leak to the environment is greatly different resulting in different source time constants. Because of the similarity of end results, however, only the open source modes are plotted; remembering also that for this source a larger electron density than typical is required to make the ion current values attainable.

## Parametric Performance Curves

Using the Mode 1 and 2 equations with the revisions discussed above, we proceed to plot the collectable ion current as a function of the various parameters.

Retaining the variable elements of (64) we recall that

$$I_c^+ (\max)_{1,2} \alpha \frac{M V_{ac} (f\ell)^2 r_o^2}{t V_o \left(\ell n \frac{.048}{\theta}\right)^2} \left(\frac{q\Delta m}{k_m m} (1 - T/B) + .00378\right)^4. \quad (74)$$

In order to reduce the number of variables we let $M = M_m$ and express the quadrupole equation as

$$V_{ac} = K_v M_m r_o^2 f^2 \quad (75)$$

where

$K_v = 7.2 \times 10^{-8}$

$M_m$ = maximum mass to be scanned (AMU)

$f$ = frequency (Hz)

and substitute in (74) to obtain

$$I_c^+ (\max)_{1,2} \alpha \frac{f^4 \ell^2 r_o^4 M_m^2}{t V_o \left(\ell n \frac{.048}{\theta}\right)^2} \left(\frac{q\Delta m}{k_m m} (1 - \frac{T}{B}) + .00378\right)^4 . \quad (76)$$

Since power is also an important function we let

$$P = \frac{2 V_{ac}^2 \omega C_q}{Q} = K_p' V_{ac}^2 f\ell \quad (77)$$

where $C_q$ is the quadrupole rod capacity (farads) which is assumed to scale linearly with $\ell$ by neglecting end and fixed capacities. Q is the circuit quality characteristic where it is assumed that by clever design Q can be held constant. While neither of these assumptions is valid in practice, the added complexity for a more complete description is beyond the scope of this discussion.

It is further an important simplification that we let $\ell$ be proportional to $r_o$ for most of the description. To do otherwise is to invite a lengthly chain reaction influencing the axial velocity and the repeller voltage where such is not necessary. The independent effect of $\ell$ will be shown later. Thus for this relationship we use

$$I_c^+ (\max)_{1,2} \alpha \frac{f^4 r_o^6 M_m^2}{t V_o \left(\ell n \frac{.048}{\theta}\right)^2} \left(\frac{q\Delta m}{k_m m}\left(1 - \frac{T}{B}\right) + .00378\right)^4 \quad (79)$$

and

$$P = K_p V_{ac}^2 f r_o \quad V_{ac} = K_v M f^2 r_o^2 \quad (80)$$

Scaling Size at constant power, $\theta$ as a parameter.- The simplest variation that can be found is by letting;

$$P = \text{const.}, \quad f r_o = 4 \times 10^6 \times .00254 = 1.016 \times 10^4 \text{ Hz, meter}$$

$$= \text{const.}, M_m = 50 = \text{const}, t = 5 \times 10^{-4} \text{ m} = \text{const},$$

$$V_o = 0.208 \text{ V} = \text{const}, \quad \Delta m/k_m m = 1/50 = \text{const},$$

$$k_m = 1, \quad T/B = 0.5 = \text{const and } V_{ac} = 208 \text{ V}.$$

Scaling ion current with size we have $I_c^+ \alpha r_o^2$. Figure 6 shows the collected current at $P_s = 10^{-4}$ torr (400°K) and sensitivity as a function of $r_o$ with $\theta$ as a parameter. Sensitivity as used throughout this section is considered to be the same as m/e 28 from $N_2$ even though mass is freely changed to describe the instrument performance.

It should also be noted that $V_o = 0.208$ V is the voltage of a 6 kT particle at 400°K. This is slightly more energy than required to encompass 99% of the one-directional velocities.

Scaling size, $M_m$ as a parameter.- Here we deal only with the maximum mass to be scanned, $M_m$, since this is generally the condition of maximum constraint. We further assume that to reach the maximum mass $V_{ac}$ and $V_{dc}$ are increased with a fixed offset in $V_{dc}$ to produce unity resolution, i.e.

$$\Delta m/m = 1/M_m \quad (81)$$

In order to set values for $k_m$ and $\theta$, we assume that the peaks sides overlap such that the tail transmission, $\theta$, is just reached at the top corner of the adjacent peak. Thus the valley between the peaks is essentially filled yet the full top width is available for value determination.

When this condition is reached, i.e., having an appearance lying between Figure 4a and 4b, then

$$\frac{q\Delta m}{m} = \frac{1}{2}\ \Delta q_B + \frac{1}{2}\ \Delta q_T = \frac{1}{2}\ \Delta q_B \left(1 + \frac{T}{B}\right) \text{, or since}$$

$$\Delta q_B = \frac{q\Delta m}{k_m m} \quad \text{from (14)},$$

$$k_m = \frac{1}{2}\left(1 + \frac{T}{B}\right), \tag{82}$$

and

$$U = \frac{q\Delta m \left(1 - \frac{T}{B}\right)}{0.5\ m \left(1 + \frac{T}{B}\right)}. \tag{83}$$

Substituting (81), (79) becomes

$$I_c^+ (\max) \alpha \frac{f^4\ r_o^6\ M_m^2}{t\ V_o \left(\ell n \frac{.048}{\theta}\right)^2} \left(\frac{2q\left(1 - \frac{T}{B}\right)}{M_m \left(1 + \frac{T}{B}\right)} + .00378\right)^4 \tag{84}$$

We now let:

$fr_o = 1.016 \times 10^4\ Hz_m = C$

$r_o =$ variable

$M_m =$ parameter $= 25, 50, 100, 200$ AMU

$t = 5 \times 10^{-4} = C$

$V_o = 0.208\ V = C$

$\theta = 10^{-5}$

$T/B = 0.5$

and $V_{ac} \alpha M_m$.

Thus power scales as $V_{ac}^2$ or $M_m^2$.

At $r_o$ = .00254 m and $M_m$ = 50, $V_{ac}$ = 208 V, P = $P_o$ and $\bar{I}/w$ = 200 μa/mm,

$$\left[I_c^+ \text{ (max)}\right] = 1.74 \times 10^{-10} \text{ amps}$$

Again sensitivities for both $\bar{I}/w$ = 200 μa/mm and 20 μa/mm are plotted vs $r_o$ in Figure 7.

It can be noted that the sensitivity does not fall off rapidly at $M_m$ = 100 and in fact recovers slightly in going to $M_m$ = 200. This is the effect of the constant .00378 (associated with U) in combination with increasing $V_{ac}$. This does not seem normal or logical and probably indicates that the narrowed peak width is within 0.1Δq of the theoretical boundary at a resolution of 100 and that the data in this range should not be used.

Additional study of the tail equation will have to be done before this can be clarified. The next curve shows this even more strongly.

Sensitivity vs Mass and Resolution.- This set of conditions is the same as in the preceding paragraphs; however, the role of $M_m$ and $r_o$ are reversed. Figure 8 shows $N_2$ sensitivity vs $M_m$ with $r_o$ as a parameter. $V_{ac}$ is scanned to cover the mass range to $M_m$ while holding unit resolution as defined above.

$r_o$ = 1.27, 2.54, 5.08 and 10.16 mm and $\bar{I}/w$ = 20 μa/mm.

It is apparent in looking at Figure 8 that the equations in their present form should be used at $M_m \leq 100$.

Constant Size, Constant Power Stepping.- If we now wish to cover a wide mass spectrum by stepping mass range on a given instrument, several approaches are possible. In each case $V_{ac}$ is scanned within the range and only the locus of sensitivity values at the top of the ranges ($V_{ac}$ (max)) is shown.

One approach yields constant power by letting $V_{ac}$ (max) = constant and adding external capacity to hold $f^2 M_m$ = constant. Thus with t, $V_o$, $r_o$ and θ constant

$$I_c^+ \text{ (max)} \propto \left(\frac{q\Delta m}{k_m m}\left(1 - \frac{T}{B}\right) + .00378\right)^4 \qquad (85)$$

and $$P = K_p^1 V_{ac}^2 \, fC = \text{constant}$$

Inductance $L = 1/w^2C = kC$.

Using $k_m = 1/2\ (1 + T/B)$, $\Delta m/m = 1/M_m$, and $T/B = 0.5$,

$$I_c^+ \text{ (max)} \ \alpha \left( \frac{q}{1.5\ M_m} + .00378 \right)^4 \tag{86}$$

with $r_o = .00254$, $I^-/w = 20\ \mu a/mm$, $t = 5 \times 10^{-4}$, $V_o = 0.208$ V, $\theta = 10^{-5}$ and $f = 4.0 \times 10^6$ Hz at $M_m = 50$, the sensitivity is plotted vs $M_m$ in Figure 9.

Another approach is to scale $V_{ac}$ upward as the maximum mass in the range is increased. This reduces somewhat the steep fall-off in sensitivity with mass. We let C = constant, $L \ \alpha \ N_2^2$, $V_{ac} \ \alpha \ N_2/N_1$, and $f \ \alpha \ (LC)^{1/2} \ \alpha \ 1/N_2$ where $N_2$ and $N_1$ are the secondary and primary turns of the r.f. transformer. Thus $P \ \alpha \ (N_2/N_1)^2 \ (N_1/N_2) = N_2/N_1 \ \alpha \ V_{ac}$; $M_m^2 \ f^4 \ \alpha \ V_{ac}^2 \ \alpha \ P^2 \ \alpha \ (N_2/N_1)^2$ and from (80), $M_m \ \alpha \ V_{ac}/f^2 \ \alpha \ (N_2/N_1) \ / \ (1/N_2)^2 = N_2^3/N_1$. Thus $N_2 \ \alpha \ N_1^{1/3} \ M_m^{1/3}$. If we hold $N_1$ constant and substitute $f^4 \ \alpha \ 1/(N_2)^4 \ \alpha \ 1/M_m^{4/3}$,

$$I_c^+ \text{ (max)} \ \alpha \ M_m^{2/3} \left( \frac{q}{1.5\ M_m} + .00378 \right)^4 \tag{87}$$

using the same values as for (86). The sensitivity is also plotted in Figure 9, using $S = 1.74 \times 10^{-7}$ a/torr at $M_m = 50$ and $I^-/w = 20\ \mu a/mm$. t, $V_o$ and $\theta$ are constant as above.

It is clear that without increasing size or by applying considerable power, sensitivity drops steeply with the maximum mass to be scanned in a given range (or conversely increasing with lower mass). Only by techniques such as scanning $V_{ac}$ directly with M for the full range can the sensitivity be maintained.

One thing that should be remembered is whenever resolution, $\Delta m/m$, is changed in $\left( \frac{q\Delta m}{k_m m} \left( 1 - \frac{T}{B} \right) + .00378 \right)^4$ that this implies a change in $\eta$, $\gamma$ and $v_z^2$ from the appropriate transforms. $\gamma$ automatically changes if $V_{ac}$ is the independent variable to cause $\Delta m/m$ to vary. $v_z$ is partially corrected

as the mass in view changes, since $v_z = \left(2et\ V_R/dm\right)^{1/2}$ and also

$$v_z = \frac{1}{2}\ \frac{(f\ell)\ (U + .00378)}{.088\ \ell n\ \frac{.048}{\theta}}\ .$$

Thus some compensation is made as m and U change but not by the same degree. This residual $v_z$, plus $\eta$ then must be changed by some electrical or mechanical alteration in the system in order to achieve the sensitivities shown. One possible means to automatically reach the resolutions called for is to decrease $V_R$ as mass increases.

Effect of Length and Electron Beam Thickness on Crosstalk.- If we look at the effect of length and electron beam thickness on crosstalk, the first step is to hold the sensitivity constant. By also letting f, $r_o$, $M_m$, $V_o$, $\Delta m/m$, $k_m$ and T/B be constant and reconstructing $\ell = kr_o$, which contributed $r_o^2$ to the equation,

then

$$\frac{\ell^2}{t\ \left(\ell n\ \frac{.048}{\theta}\right)^2} = \text{constant} \tag{88}$$

For values of $t = 5 \times 10^{-4}$ m, $\ell = 0.1$ m and $\theta = 10^{-5}$; k = 0.279 and

$$\theta = 0.048\ \exp - \left(\ell/(kt)^{1/2}\right)\ . \tag{89}$$

Figure 10 expresses $\theta$ as a function of $\ell$ with t as a parameter.

It is apparent that the effort to reduce t is well worth while if the length is an important physical constraint.

Open Ion Source, Mode 1.- For the focusing of energetic particles as is implied by the use of an open ion source it is necessary to accept energies $eV_o$ that are substantial. The scaling of a system to accommodate energies of the order of 10 ev can be readily done with the optimization equation expressed in its present form. The principle impact on design is not only that system will be larger but that an ion source having a different character of focusing is needed, i.e., a true imaging lens system as described in Appendix 1. The present equations describe this type of source.

Several scaling factors are simple to show if we plot $I_c^+$ vs $r_o$ with $V_o$ as a parameter. For instance, we can hold power constant (at $M_m$ constant) giving $I_c^+ \propto r_o^2/V_o$. Or we can let f = constant to yield $I_c^+ \propto r_o^6/V_o$ whereby $P \propto r_o^5 f$, greatly expanding the power consumption. A compromise might be

$f^2 = k/r_o$ in which $P \alpha r_o^3 f$ and $I_c^+ \alpha r_o^4/V_o$. We choose power constant (i.e., $f^2 r_o^2$ = constant) since it is quite a safe assumption although in practice one would probably shade this with some increase in power. Thus if we let $V_o = 1/2\ Mm_u\ v_v^2/e$ where $v_v$ is the vehicle velocity, and maintain $\Delta m/m = 1/M_m$, $T/B = .05$ and $k_m = 1/2\ (1 + T/B)$, then

$$I_c^+ (\max) \alpha \frac{r_o^2 M_m^2}{V_o} \left(\frac{q}{1.5\ M_m} + .00378\right)^4 \qquad (90)$$

$$\alpha \frac{r_o^2 M_m^2}{Mv_v^2} \left(\frac{q}{1.5\ M_m} + .00378\right)^4 .$$

Figure 10 shows $I_c^+$ plotted as a function of $r_o$ with $V_o$ as a parameter.

The interesting velocities are 2 km/sec for rockets, 4 km/sec for "an entry mass spectrometer" and 8 km/sec for earth satellites.

$I_c^+ (\max) = 8.43 \times 10^{-13}$ amps at $P_s = 10^{-4}$ torr and $T_s = 400°K$ when $M_m = 50$, $t = 5 \times 10^{-4}$m, $\theta = 10^{-5}$, $r_o = .00254$, $f = 4 \times 10^6$ Hz, and $V_o = 4.3$ V (M = 50 at 4 km/sec).

It is noted that relatively large instruments are required if the sensitivity is to be maintained. Alternative scaling factors would have required large powers to accomplish the same end.

## CONCLUSION

It has been shown that an approximate optimization scheme can be applied to a combined quadrupole mass analyzer and a generalized ion source to produce the framework for planning specific missions. While numerous assumptions and extrapolations have been used, the end results have been compared to the experimental data of several instruments and found to be in agreement within about a factor of two over a variety of operating conditions.

Additional effort is required to convert these results to a complete instrument for a defined purpose. Size, shape, weight and power considerations, as well as the nature of sampling and detection of ion current are all essential to successful performance. A variety of instrument characteristics can be shown when these additional factors are related to the optimized analyzer.

An interesting result has been obtained in that a double-focusing magnetic mass spectrometer has a very similar equation to the quadrupole analyzer having the form

$$I_c^+ = K \left(\frac{\beta}{t}\right)^{3/2} B^5 r_m^6 \left(k \frac{\Delta m}{m} \left(1 - \frac{T}{B}\right) - A_i\right)$$

where $\beta = \Delta v/v$, B = magnetic field $r_m$ = magnetic radius and $A_i$ = aberrations in $\alpha$ and $\beta$.

THIS PAGE INTENTIONALLY LEFT BLANK

APPENDIX 1

# QUADRUPOLE MASS SPECTROMETER FOR ENERGETIC PARTICLE MEASUREMENTS

L. G. Hall and M. R. Ruecker

SPACE SCIENCES LABORATORY

PERKIN-ELMER
Aerospace Division
2855 Metropolitan Place
Pomona, California 91767

ABSTRACT

Analytical expressions are developed which define the initial conditions for 100% transmission of a Quadrupole analyzer and which enable combination with equations for the focal properties of an ion source. The equation for the combined properties can be used to calculate the ion current intensity of the system as a function of the gas density, parameters of the mass spectrometer and upper limits of acceptance of initial energy and initial angle. It is shown that the measurement of density is, in principle, independent of the initial energy and initial angle at the time of ionization within the established upper limits. The equations are particularly useful in design of instruments for measurement in the upper atmosphere.

This work supported by the Jet Propulsion Laboratory and by Goddard Space Flight Center of the National Aeronautics and Space Administration.

# QUADRUPOLE MASS SPECTROMETER
# FOR ENERGETIC PARTICLE MEASUREMENTS

## INTRODUCTION

In terms of optimum performance, the design of any mass spectrometer considers the initial conditions under which the ions enter the analyzer. The initial condition of the ions, in turn, relates to the ion source properties. It is the purpose of this paper to present a means of analytically relating the quadrupole[1] analyzer with an ion source in one of two modes of focusing. For this purpose it is necessary to provide analytical expressions for both the analyzer and ion source operation.

## QUADRUPOLE ANALYZER

The discussion of the quadrupole analyzer is limited to operation of the quadrupole in conditions of 100% transmission. This choice is dictated by a desire to: 1) obtain a more accurate absolute value for the ion current as related to gas density in the ion source; and 2) obtain "flat-topped" ion intensity peaks which can be measured by stepping from peak-to-peak. This method of measurement may be useful in space applications, where time or information capacity is limited and where the peak intensity must be independent of small changes in voltage or frequency. The discussion that follows thus treats the top width of the peak and the top to base ratio as important parameters of the operation.

The functional characteristics of the quadrupole analyzer have been adequately described by Paul, Reinhard, V. Zahn[1*], and Brubaker[2]. Their work is not extensively reviewed here.

It has been shown[1] that the maximum amplitudes of motion are inversely proportional to the stability parameters $(1 - \beta_x)$ and $\beta_y$. Paul, Reinhard, and V Zahn have also computed the stability requirements as a function of entering phase angle under conditions 1) that the initial transverse velocity is zero or 2) that the initial position is zero. Since here we require an analytical expression with all initial conditions (i.e., position, $x_o$, $y_o$, transverse velocity, $\dot{x}_o$, $\dot{y}_o$,

*References 1 through 5 herein. See final page of this Appendix.

and phase angle, $\varphi$) as variables, by retaining only the first few and important terms, the following approximate expressions for x and y motion are derived.

$$x \approx A_x \left\{ c_o \sin\left(\frac{\beta_x \omega t}{2} + \delta_x\right) - \left(c_{-2}\right)_x \sin\left[\left(1 - \frac{\beta_x}{2}\right)\omega t - \delta_x\right]\right\} \qquad \text{A1 (1)}$$

and

$$y \approx A_y \sin\left(\frac{\beta_y \omega t}{2} + \delta_y\right)\left[c_o + 2\left(\overline{c_2}\right)_y \cos\left(\omega t + \phi\right)\right] \qquad \text{A1 (2)}$$

where

$$A_x,\ \delta_x = f\left(x_o,\ \dot{x}_o,\ \phi\right)$$

$$A_y,\ \delta_y = f\left(y_o,\ \dot{y}_o,\ \phi\right)$$

$\phi$ = Initial phase angle

$$c_o = 1,\ \left(\overline{c_2}\right)_y = \frac{c_2 + c_{-2}}{2} = 0.168 \neq f\left(\beta_y\right)$$

$$\left(c_{-2}\right)_x = f\left(\beta_x\right),\quad 0.8 < \left(c_{-2}\right)_x < 1.0$$

It is noted in Equation (1) that when $\beta_x$ is nearly 1 the arguments $\frac{\beta_x}{2}$ and $1 - \frac{\beta_x}{2}$ are nearly the same and since the coefficients[1] are of similar magnitude one obtains an amplitude modulated wave without carrier which is centered about the angular frequency $\frac{\omega}{2}$. On the other hand, when $\beta_y$ is small the y motion is the low frequency wave $\sin\frac{\beta_y \omega t}{2}$, with superimposed fine motion $(1 + 0.336 \cos \omega t)$ Brubaker has shown the trajectories for both motions computed with specific conditions and has also derived the elements of Equation (2) by the integration of incremental forces on the ion. We differ from his value for $2\left(c_2\right)_y$ only in obtaining 0.336 instead of 0.353.

From Equations (1) and (2) one can obtain values from the maximum amplitude of motion in each plane as a function of initial conditions. Since the y motion is simpler we use this for an example as follows:

From (2),

$$y = A_y \sin\left(\frac{\beta_y \omega t}{2} + \delta_y\right)\left[1 + 0.336 \cos(\omega t + \phi)\right] \qquad \text{A1 (3)}$$

and we first observe that $(y_{max}) = 1.336\, A_y$ . A1 (4)

Evaluation of (3) and its time derivative at $t = 0$ gives:

$$y_o = A_y f_1 \sin \delta_y \qquad \text{A1 (5)}$$

and

$$\dot{y}_o = A_y \left(f_1 \frac{\beta_y \omega}{2} \cos \delta_y - f_2\, \omega \sin \delta_y\right), \qquad \text{A1 (6)}$$

where

$$f_1 = (1 + 0.336 \cos \phi) \quad \text{and}$$

$$f_2 = 0.336 \sin \phi \ .$$

Solving for $A_y$:

$$A_y^2 = \frac{1}{f_1^2}\left\{y_o^2 + \frac{4}{\beta_y^2}\left(\frac{\dot{y}_o}{\omega} + y_o \frac{f_2}{f_1}\right)^2\right\} \ .$$

Substituting in (4) gives:

$$\left|y_{max}\right| = \frac{1.336}{f_1}\left\{y_o^2 + \frac{4}{\beta_y^2}\left(\frac{\dot{y}_o}{\omega} + y_o \frac{f_2}{f_1}\right)^2\right\}^{\frac{1}{2}} . \qquad \text{A1 (7)}$$

It can be easily shown that for resolution better than $\frac{m}{\Delta m} = 10$

The term $y_o^2$ can be neglected. Consequently,

$$\left|y_{max}\right| = \frac{2.672}{\beta_y f_1}\left|\frac{\dot{y}_o}{\omega} + y_o\frac{f_2}{f_1}\right| \qquad \text{A1 (8)}$$

where the absolute signs are obtained in the process of taking the square root.

By the method employed by Paul[1] an approximate equation for

$\left|x_{max}\right|$ evaluated at $\beta_x = 0.92$ is;

$$\left|x_{max}\right|_{\beta = 0.92} = 16.35\left(f_3 x_o^2 + f_4\frac{x_o\dot{x}_o}{\omega} + f_5\frac{\dot{x}_o^2}{\omega^2}\right)^{\frac{1}{2}} \qquad \text{A1 (9)}$$

where

$$f_3 = 0.40 - 0.20\cos\phi - 0.20\cos 2\phi,$$

$$f_4 = 0.93\sin\phi + 0.26\sin 2\phi, \text{ and}$$

$$f_5 = 1.63 + 1.86\cos\phi + 0.26\cos 2\phi .$$

The variable $\omega$ may be eliminated with the following substitutions:

$$\dot{y}_o = \left(\frac{2eV_I}{m}\right)^{\frac{1}{2}}\sin\alpha \qquad \text{A1 (10)}$$

where $eV_I$ is the injection energy and $\alpha$ the entrance half-angle. Using the quadrupole equation:

$$\frac{e}{m} = \frac{q\omega^2 r_o^2}{4V_{ac}} \qquad \text{A1 (11)}$$

and letting

$$\gamma = \left(\frac{V_I}{V_{ac}}\right)^{\frac{1}{2}} \quad \sin \alpha \,, \qquad \text{A1 (12)}$$

equation (10) becomes:

$$\frac{\dot{y}_o}{\omega} = \left(\frac{q}{2}\right)^{\frac{1}{2}} \quad r_o \gamma \qquad \text{A1 (13)}$$

In the region of the apex of the stability diagram q = 0.706.

Thus dividing $y_{max}$ by $y_o$ in Equation (8) and substituting Equation (13):

$$\frac{|y_{max}|}{y_o} = \frac{2.672}{\beta_y f_1} \left| \frac{0.595\, r_o \gamma}{y_o} + \frac{f_2}{f_1} \right| \qquad \text{A1 (14)}$$

Similar substitutions may be made for $|x_{max}|$.

From these equations we can now show examples of combined initial position and angle in Figure 12 where $(x_{max})$ and $(y_{max})$ are plotted as a function of initial phase angle, $\phi$, with $\gamma$ as a parameter. The value $\frac{r_o}{r_e} = 30$ is used where $r_e = x_o = y_o$ is the radius of a round entrance aperture.

Comparison with the curves which Paul has computed[3] for $x_o$, $y_o = 0$ or $\dot{x}_o$, $\dot{y}_o = 0$ indicate that the approximate solutions are in good agreement in the x - z plane where maxima are within 7% and the same shaped curve is obtained. In the y - z plane, ion motion reaches a maxima for a phase somewhat shifted from Paul's, however, maxima agree to better than 2%. It appears that one may use the approximate expressions with less error than 10% in the maxima of the curves.

By comparing the $\left|x_{max}\right|$ and $\left|y_{max}\right|$ curves it is seen that for equal values of $\gamma$, $\left|y_{max}\right| > \left|x_{max}\right|$.

It should be noted that the maximum amplitude in y - z plane occurs in the useful region between $127° > \phi > 142°$. A study was made over a variety of conditions where it was found that for equal initial conditions in the two planes, nominal worst case condition is at $\phi = \frac{3\pi}{4}$ in the y - z plane. At most, a small percentage error will occur, which is in a direction to reduce previous differences.

Consequently, the following generalizations are made:

For 100% transmission $\left|y_{max}\right|_{\phi = 3\pi/4} \leq r_o$,

thus

$$\frac{r_o}{y_o} = \frac{r_o}{r_e} \geq \frac{2.672}{\beta_y f_1} \left| 0.595 \frac{r_o \gamma}{r_e} + \frac{f_2}{f_1} \right|_{\phi = \frac{3\pi}{4}}$$

where

$$\left(f_1\right)_{3\pi/4} = 0.763 \text{ , } \left(f_2\right)_{3\pi/4} = 0.238 .$$

Thus letting $\frac{r_o}{y_o} = \frac{r_o}{r_e}$ and evaluating (14) at $\theta = \frac{3\pi}{4}$ gives

$$\frac{r_o}{r_e} \geq \frac{1.09}{\beta_y} \left| 1 + 1.9 \left| \gamma \right| \frac{r_o}{r_e} \right|$$

or solving explicitly for $\frac{r_o}{r_e}$ in the limiting case:

$$\frac{r_o}{r_e} = \frac{1.09}{\beta_y - 2.07 \left|\gamma\right|_{max}} \qquad \text{A1 (15)}$$

This equation asks: What is the largest value of $\gamma$ entering at any phase and for given $\beta_y$ which will just reach $r_o$, the position of the rod.

Referring to Figure 13, the interpretation is as follows: As the scan line passes through the stability diagram, $\beta_y$ is at first very small.

Consequently only low angle ions contained in low values of $\gamma = \left(\frac{V_I}{V_{ac}}\right)^{\frac{1}{2}} \sin \alpha$ are transmitted within a given $\frac{r_o}{r_e}$ ratio. As $\beta_y$ increases, larger angles are accepted and transmitted by the analyzer with consequent increase in collected current until one of two conditions become predominant. If, by some means, $\gamma$ is limited, a region of 100% transmission occurs with a resultant constant collected current or "flat-topped" peak. If $\gamma$ is unlimited the x stability takes over at a position where $\beta_y = 1-\beta_x$ and by the same mechanism ions are lost to the x poles as $\beta_x \longrightarrow 1$. In this condition, a pointed peak is produced.

While one could easily plot families of curves relating to specific values of $\frac{r_o}{r_e}$ and $\gamma$ and match these to an ion source, this relationship can be obtained more explicitly. Therefore, we proceed to examine ion sources.

ION SOURCES

When reduced to their elements, most ion sources can be typified as focusing in one of two modes. Figure 14 shows the most common method wherein the source ion current is peaked up by producing the smallest line or point "image" and thus the highest density. However, it is noted that given some thermal distribution in the gas being ionized, those with higher side velocity are not transmitted. If only a specific side velocity $\pm\dot{y}_1$ is present such as encountered in satellite motion the line spectra are not transmitted at all.

An alternative mode of focusing is shown in Figure 14b where an image of the ion object is produced. In this case each position in the image correlates with a position in the object. Also, up to a limit determined by the lens aperture sizes, the position in the image is independent of initial energies of the ions. It is noted then that the distribution of initial energies lies in the angular distribution.

Since this mode of focusing is more appropriate for energetic particle measurements, we may proceed to describe the ion density more analytically. For a magnification, M the ion density at the image plane is $\frac{J_o^+}{M^2}$ for $J_o^+$ current per unit area produced is the ionizing beam. Thus the source current is

$$I_s^+ = \pi r_e^2 \frac{J_o^+}{M^2} , \qquad \text{A1 (16)}$$

where $r_e$ is the radius of a round aperture.

From Abbe's law[4], the bundle of rays produced within an included angle $\theta_o$, at a point in the object plane, fall within an included angle $\theta_i$ at the image plane by the relationship;

$$y_o V_o^{\frac{1}{2}} \sin \theta_o = y_i V_i^{\frac{1}{2}} \sin \theta_i, \qquad \text{A1 (17)}$$

where $eV_o$ is the initial ion energy and $eV_i$ the total ion energy at the image plane.

Letting $\theta_o = \frac{\pi}{2}$ to include a worst case angle and since $\frac{y_i}{y_o} = M$ ,

$$\sin \theta_i = \left(\frac{V_o}{V_i}\right)^{\frac{1}{2}} \left(\frac{1}{M}\right) . \qquad \text{A1 (18)}$$

From (18), for a given value of $(V_o)_{max}$, we note that sin $\theta_i$ can be kept within some upper limit acceptable for transmission by the analyzer by adjusting the magnification and thus from (16) the ion source current becomes established. If the value chosen for $r_e$ is also sufficiently small for 100% transmission then the collected current for the mass spectrometer becomes,

$$I_c^+ = \pi r_e^2 \frac{J_o^+}{M^2} \qquad \text{A1 (19)}$$

Consequently for this mode of focusing we find that the measurement of partial density is, in principle, independent of initial conditions up to a maximum initial energy $(eV_o)_{max}$. It remains to establish $r_e$ and $\sin \theta_i$ such that the maximum ion current is collected under the restraints of 100% transmission and limited initial energy.

Combining ((19) and (20) yields

$$I_c^+ = \pi r_e^2 \, J_o^+ \left(\frac{V_I}{V_o}\right)_{max} \sin^2 \alpha_I \qquad \text{A1 (20)}$$

in which the injection voltage $V_I$ is used for the image plane energy $V_i$, and the maximum injection angle $\alpha_I$ is substituted for $\theta_i$. In Equation (20), M is an implicit variable used to limit $\sin^2 \alpha$ as $(V_o)_{max}$ is chosen. Since this equation contains $r_e$ and $\sin \alpha$ it may be solved simultaneously with the quadrupole equation.

Combined Quadrupole and Ion Source

By substituting for $y$ in (15) and solving for $V_I \sin^2 \alpha_{max}$, one obtains

$$V_I \sin^2 \alpha_{max} = 0.233 \, V_{ac} \left(\beta_y - 1.09 \frac{r_e}{r_o}\right)^2, \qquad \text{A1 (21)}$$

where $\alpha_{max}$ is the largest acceptable angle for given values of $\beta_y$ and $\frac{r_e}{r_o}$.

Angles less than this will be transmitted. Further, one may conclude for given $\alpha_I$ and $\frac{r_e}{r_o}$ that the collectable current, $I_c^+$, reaches a peak when $\alpha_{max} = \alpha_I$ and remain constant when $\alpha_{max} > \alpha_I$

Substituting in (20),

$$I_c^+ = \frac{0.233 \, V_{ac} \, \pi r_e^2 \, J_o^+}{(V_o)_{max}} \left(\beta_y - 1.09 \frac{r_e}{r_o}\right)^2, \qquad \text{A1 (22)}$$

where we note that $I_c^+ = o$ at $r_e = o$ and at $1.09 \frac{r_e}{r_o} = \beta_y$.

These conditions represent zero aperture and zero acceptable angle respectively. Zero angle in turn implies infinite magnification and thus zero current density.

By differentiating for a maximum, one finds that $a_I$ and $\frac{r_e}{r_o}$ contribute equally to the "beam width" when

$$\left(\frac{r_e}{r_o}\right)^2_{max} = 0.211 \ \beta_y{}^2 \qquad \text{A1 (23)}$$

and from (21)

$$V_I \sin^2 a_{max} = 0.0583 \ V_{ac} \beta_y{}^2. \qquad \text{A1 (24)}$$

With reference to Figure13, for "flat topped" peaks the ion current arrives at a maximum before the scan line reaches the $\beta_y = 1 - \beta_x$ intercept. If the base width, B, of the peak is defined to be that portion of the scan line within the stability diagram (i.e., the theoretical base width); and the top width, T, that portion lying between lines of $\beta_y = 1 - \beta_x$ (not at the intercept) and where the ion current is at its maximum value, then by calculation of the intercepts,

$$\left(\beta_y{}^2\right) = \left(1 - \beta_x\right)^2 = 0.164 \ \frac{dm}{m} \left(1 - \frac{T}{B}\right). \qquad \text{A1 (25)}$$

Equation (25) describes the $\beta_y$ and $\beta_x$ intercepts with the scan line which are required to produce the resolution $\frac{dm}{m}$ for a top to base ratio, $\frac{T}{B}$. Iso - $\frac{T}{B}$ lines may be constructed by inspection.

We now require that the ion current reach maximum value at the above $\beta_y$ - scan line intercept. This consequently defines the values of $\left(\frac{r_e}{r_o}\right)$ and $\sin^2 a_{max}$ for

maximum ion current as:

$$\left(\frac{r_e}{r_o}\right)^2_{max} = 0.0346 \frac{dm}{m}\left(1 - \frac{T}{B}\right) \qquad \text{A1 (26)}$$

and

$$V_I \sin^2 \alpha_{max} = 0.00955\, V_{ac} \frac{dm}{m}\left(1 - \frac{T}{B}\right) \qquad \text{A1 (27)}$$

From (22), (23) and (26),

$$I_c^+{}_{max} = 3.15 \times 10^{-4} \frac{V_{ac}}{(V_o)_{max}} \pi r_o^2 J_o^+ \left(\frac{dm}{m}\right)^2 \left(1 - \frac{T}{B}\right)^2. \qquad \text{A1 (28)}$$

Throughout the T region then $I_c^+{}_{max}$ is constant at this value since

$$\alpha_{max} > \alpha_I.$$

Thus, with given limits on the initial conditions and choice of the quadrupole parameters one may calculate the expected current of mass peaks meeting criteria of shape and resolution. The interesting result is that, for this mode of ion source focusing, the collected current is, in principle, a measure of partial density in the ionizing region independent of the initial energies up to $(V_o)_{max}$.

An instrument for atmospheric studies has been constructed along these lines having $r_o$ = 7.5 mm, $r_e$ = 0.25 mm and length $\ell$ = 22 cm. While the ion current exceeds that expected, an accurate confirmation of Equation (28) has not been made. This is partially due to the difficulty of obtaining a rectangular energy distribution and partially as discussed later to a method of biasing the quadrupole rods.

A check on Equation (27) was made however, to determine the validity of injection angle versus resolution and $\frac{T}{B}$ ratio. Figure 15 shows two partial spectra typical

of those used to calculate the apparent injection angle, given measurements for the other variables. $V_{ac}$ was the independent variable while $\frac{T}{B}$ was the primary dependent variable. The theoretical base width was used (i.e., without tails) measured by extending the peak sides. Figure 16 gives the apparent angle vs $V_{ac}$ where the inset shows the directly measured angular distribution. The apparent angle is approximately constant over the range of $V_{ac}$ however, with the density distribution less than the measured angle by a factor of $\sim 1.5$. This contraction in apparent angle is believed to be due to the effect of quadrupole biasing.

Quadrupole Biasing

The length of the quadrupole rods is required to have a certain minimum value which depends upon the values of several parameters. von Zahn[5] stated this relationship in the simple form:

$$n \geq 3.5 \sqrt{\frac{m}{\Delta m}} \qquad \text{A1 (29)}$$

where $n$ = number of cycles of the r.f. voltage which occur while the ion is in the quadrupole field. This equation implies that if a half height resolution of $\frac{m}{\Delta m}$ is required then $n$ cycles must occur in order that the peak tails do not make an appreciable contribution to the width of the peak. By relating $n$ to the axial ion energy, $V_z$, and using the quadrupole equation one obtains:

$$\frac{\ell}{r_o} = K \sqrt{\frac{13.9\ V_z}{V_{ac}} \frac{\Delta m}{m}} \qquad \text{A1 (30)}$$

where $\ell$ is the length of the quadrupole rods, and $K$ is a constant which depends upon the exact criterion used to measure the resolution and the contribution of the tails to the peak base width. If von Zahn's criterion is used, $K = 3.5$. For one percent peak height resolution $K \approx 7$.

In normal quadrupole operation the ion source injection voltage is equal to the axial kinetic energy of the ions in the quadrupole, i.e., $V_I = V_z$. When an ion source is required to capture and focus energetic particles which have an

appreciable angle of incidence, the injection voltage, $V_I$, must be large. This implies that the length of the quadrupole rods will be excessive. It was found, however, that by placing a bias voltage $V_B$ between the ion source and the quadrupole rods the mass spectrometer may be successfully operated in a mode where:

$$V_z = V_I - V_B \qquad \text{A1 (31)}$$

A schematic representation of this technique, along with an approximate axial potential distribution, is shown in Figure 17 . The effect of the quadrupole bias voltage is shown in Figure 18 . As the bias voltage is raised the peak tails are diminished. There is no observable decrease in sensitivity as $V_B$ is increased until the point at which the injection energy of the least energetic ions is exceeded in which case they are cut off. Even though the reduction in the size of the tails is not considered, the $\frac{T}{B}$ ratio apparently improves as the bias is applied. This may indicate that the field around the entrance nozzle is causing a contraction of the effective angle of injection.

## APPENDIX 1 REFERENCES


1. W. Paul, H. P. Reinhard and V. von Zahn; Z. Physik 152, 143 (1958).
2. W. M. Brubaker; Neuvieme Colloq. Spectroscopicum Intern., Lyon, France, 1961.
3. Reference 1, Fig. 4.
4. c.f.: Klemperer; Electron Optics, Cambridge University Press, 1953, p 14.
5. U. v. Zahn: Diplomarbeit Bonn, 1956 (unpublished).

THIS PAGE INTENTIONALLY LEFT BLANK

# APPENDIX 2

## PEAK TAIL EQUATIONS

In order to obtain a relevant mass peak-width for the quadrupole it it necessary to describe the "tail" distribution as a function of a $\Delta q$ from the center or edge of the theoretical peak. For the 100% transmission portion of the peak, it was sufficient to describe the extreme particle as defining the top edge of the peak. Since the tail has been shown to be a function that continues to infinity, it is necessary to define the tail function before a selection of a reasonable cut-off point can be made.

The purpose here is to obtain a relatively simple analytical expression for the tail as a function of $\Delta q_t$ away from the peak in order to handle this function in the optimization procedure. Computed data is used to elucidate a function that is then matched to experimentally measured peak tails. Rather than following a rigorous and ambiguous mathematical derivation, it is further the purpose to gain some physical insight into the unstable particle behavior.

We start by replotting a limited amount of computed data from the Mask Study. Figures 19 and 20 show the log of normalized particle amplitude, $A = y/r_o$ as a function of number of cycles of travel in the quadrupole. Only the envelope of motion is shown. Phase of particle entry, $\phi_o$, and fractional distance, $\Delta q_t/\Delta q$ from the theoretical peak edge are used as parameters as well as $\eta_y$ and $\gamma_y$. The data available allow the plotting of y-axis motion.

An interesting result is found in that after sufficient travel, motion approximates exponential growth versus the number of cycles, n. It is seen that near entry the motion envelope is non-exponential. It is also observed that as $\Delta q_t/\Delta q$ approaches zero (near the theoretical boundary) the motion falls away from the positive exponential growth. This, of course, is to be expected since a continuous function must describe the transition from unstable growth to stable, bounded motion. The end function used here will then be limited in its applicability to $\Delta q_t/\Delta q = 0.1$, i.e., 10% outside of the theoretical boundary.

We are basically interested in the number of cycles taken for the particle to reach the characteristic radius, $r_o$, as a function of the initial conditions. For the purposes here the details of motion at small radius or near entry are of no interest if we can properly describe the motion as the particle assumes a final function.



2 Ø

Consequently, we note from Figure 19 and 20 that:

a. The slope of the positive exponential depends upon $\Delta q_t/\Delta q$.

b. The intercept with n = o depends upon $\phi_o$ and $\eta$ and $\gamma$.

c. Amplitude is proportional to $\eta$ and $\gamma$ when taken separately (see Mask Study).

Placing the observations of the steady-state function in mathemetical notation

$$\ell n\ A = an + f'(\eta,\gamma,\phi_o) + f(\Delta q_t/\Delta q)$$

We can either leave $f'(\eta,\gamma,\phi_o)$ in its present position or combine it with A. Since we wish to separate the variables and $\eta$ and $\gamma$ control A linearly, we choose to place it in the form

$$\ell n \frac{A}{f(\eta,\gamma,\phi_o)} = an + f(\Delta q_t/\Delta q)$$

Fitted empirically to the group of curves of $\eta$ = .0025, we find,

$$A = f(\eta,\gamma,\phi_o)\ \exp\left[\left(.043 + .121\ (\Delta q_t/\Delta q)\right) n - 1.1\ (\Delta q_t/\Delta q)\right] \qquad \text{(A2-1)}$$

Thus $\Delta q_t/\Delta q$ not only controls the slope versus n but also the intercept and the interesting crossover.

Since the function of $\eta$, $\gamma$, and $\phi_o$ appears to be of similar form to stable particles, we let

$$f(\eta,\gamma,\phi_o) = (F_1'\gamma_y + F_2'\eta_y), \qquad \text{(A2-2)}$$

or

$$A = (F_1'\gamma_y + F_2'\eta_y)\ \exp\left[\left(.043 + .121\ (\Delta q_t/\Delta q)\right) n - 1.1\ \Delta q_t/\Delta q\right] \qquad \text{(A2-3)}$$

where $F_1'$ and $F_2'$ are assumed to be functions of $\phi_o$ alone. We now have an approximate expression for normalized amplitude that provides linearity as a function of $\eta$ and $\gamma$ individually, and contains a positive exponential slope proportional to n. When A = 1 and particles strike the rods, the "position", n, is controlled by the initial conditions of $\eta$, $\gamma$ and $\phi_o$.

Since we are interested only in the position at which the particle reaches $r_o$, we let A = 1 so that the relationship between position and initial condition becomes,

$$(F_1'\gamma_y + F_2'\eta_y) = \exp\left[-\left(.043 + .121\ (\Delta q_t/\Delta q)\right)n + 1.1\ \Delta q_t/\Delta q\right] \qquad \text{(A2-4)}$$

Turning now to particle density, for each $\eta$, $\gamma$ and $\phi_o$ particle injected into the quadrupole there will be a position n of particle loss (either to the rods or transmitted to the collector) for each $\Delta q_t/\Delta q$ assumed. Since we do not know the functions $F_1'$ and $F_2'$ we must assume a variety of independent values. We further assume they may be negative but have bounded negative and positive values. We now let $\eta$ and $\gamma$ have uniform density distribution to $\pm(\eta_y)$ and $\pm(\gamma_y)$ where the brackets ( ) indicate maximum values. Thus:

$$\frac{\partial N}{\partial \eta}\Bigg|_{-(\eta_y)}^{+(\eta_y)} = \text{constant and } \frac{\partial N}{\partial \gamma}\Bigg|_{-(\gamma_y)}^{+(\gamma_y)} = \text{constant}$$

If we integrate the distribution over all $\eta$ and $\gamma$ values for a given $\phi_o$ we can show in general the form to be as follows;

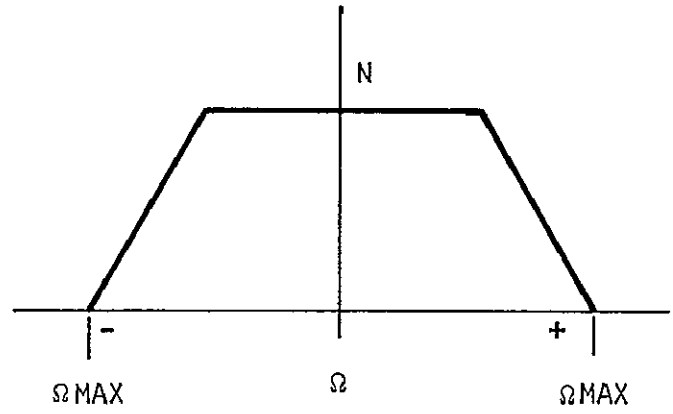


where we let $\Omega$ be an amplitude function such that,

$$\Omega\left(\phi_{o_a}\right) = \left(F_{1_a}'\gamma_y + F_{2_b}'\eta_y\right) , \qquad \text{(A2-5)}$$

when $F_{1_a}'$ and $F_{2_b}'$ have specific constant values at $\phi_o = \phi_{o_a}$ as $\eta$ and $\gamma$ vary to change $\Omega$.

As initial phase changes, now, we expect $F_1$ and $F_2$ to assume a variety of values which are small. Consequently, if we assume

$$\left.\frac{\partial N}{\partial \phi_o}\right|_{0}^{2\pi} = \text{constant};$$

when the value of $\Omega$ is small, the constant injection rate creates a high particle density within the small band of $\Omega$ values. Likewise with large $F_1'$, $F_2'$, and thus $\Omega$, the density is low. These various conditions are symbolized below.

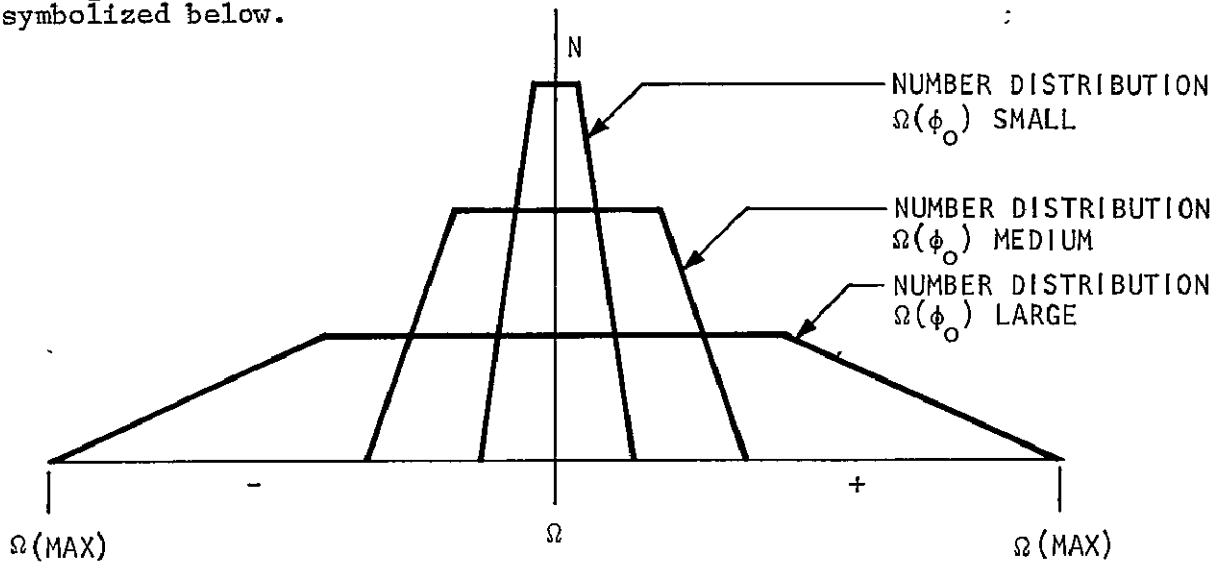


It is apparent also that as the relative values of $F_1'$ and $F_2'$ vary, the individual distributions can change from

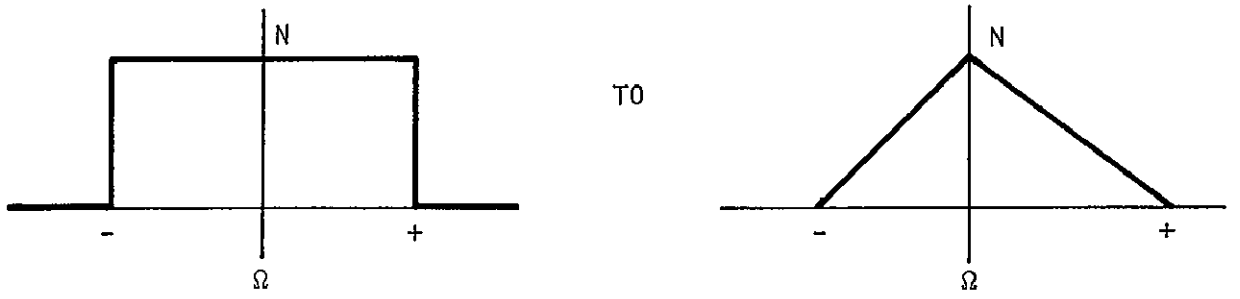


However, with the assumptions made, there will be a limit $\pm\Omega$ (max) in amplitude which describes the maximum values attained by $\Omega$ under large-value combination of the variables.

We further assume that, as in describing the amplitude of stable particles (see Appendix 1), the negative and positive values of $\Omega$ create envelopes of motion on negative and positive sides of the x-axis (in the y plane). Since it makes no difference which side of the axis is involved, we combine the negative and positive distribution by letting

$$\Omega = \left| \left(F_1'\gamma_y + F_2'\eta_y\right) \right| \tag{A2-6}$$

We also now use absolute values in (A2-3) and (A2-4). Now let us mentally sum all of the combinations envisioned above and assume the following distribution:

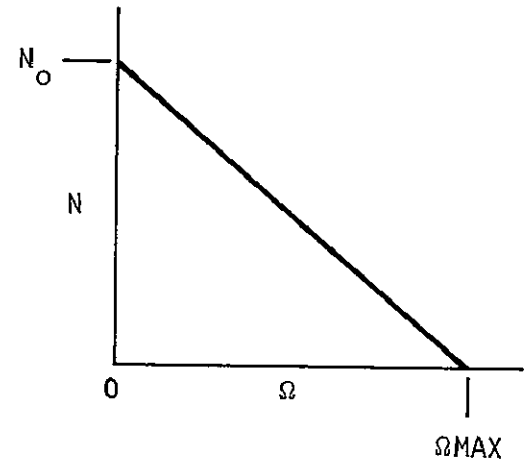


$$\text{i.e.} \qquad N(\Omega) = N_o - k\Omega \Big|_{o}^{\Omega_{max}} \tag{A2-7}$$

This function now represents

$$N(\Omega) = N(\gamma_y, \eta_y, \phi_o) = \int_o^{2\Pi} \int_{-(\eta_y)}^{+(\eta_y)} \int_{-(\gamma_y)}^{+(\gamma_y)} N(\Omega)\, d\gamma d\eta d\phi_o \tag{A2-8}$$

While the result assumed is not a rigorous solution, it provides necessary simplicity until a more exact function can be established. It further may be a conservative viewpoint since the highest density occurs at low values of amplitude where the particles are more freely transmitted by the quadrupole. This will give rise to an assumption of larger tails if the true function has a lower relative distribution at low $\Omega$.

Combining (A2-6) and (A2-4)

$$\Omega \Big|_{o}^{\Omega_{max}} = \exp\left[-\left(.043 + .121\ (\Delta q_t/\Delta q)\right) n + 1.1\ \Delta q_t/\Delta q\right] \qquad \text{(A2-9)}$$

Also in (A2-7) we let N = o at $\Omega = \Omega_{max}$ or so that $k = N_o/\Omega_{max}$.

$$N(\Omega) = N_o\left(1 - \frac{\Omega}{\Omega_{max}}\right)\Big|_{o}^{\Omega_{max}} \qquad \text{(A2-10)}$$

Combining (A2-8) and (A2-9) we have an alternate equation,

$$N(n) = N_o\left\{1 - \frac{1}{\Omega_{max}}\ \exp\left[-\left(.043 + .121\ (\Delta q_t/\Delta q)\right) n + 1.1\ \Delta q_t/\Delta q\right]\right\} \qquad \text{(A2-11)}$$

useful between $n = f(\Omega_{max})$ and $n = \infty$.

We can obtain a picture of the relative location of particles by superimposing the distribution versus Ω on a scale of the exponential of -an as follows:

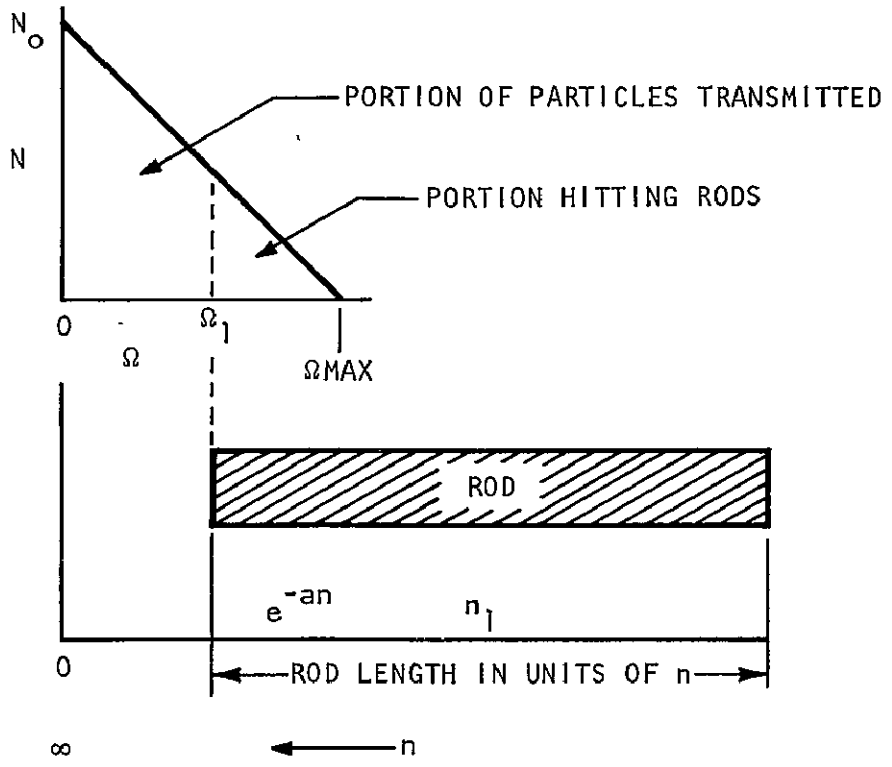

It is now simple to express the number transmitted per cycle $N_t$ as

$$N_t = \int_o^{\Omega} N(\Omega)\, d\Omega = \int_{\infty}^{n} N(n)\, dn \qquad \text{(A2-12)}$$

and the total number of particles per cycle as

$$N_T = \int_o^{\Omega_{max}} N(\Omega)\, d\Omega \qquad \text{(A2-13)}$$

Consequently,

$$N_t = N_o\, \Omega \left(1 - \frac{\Omega}{2\,\Omega_{max}}\right), \qquad \text{(A2-14)}$$

$$N_T = 1/2\, N_o\, \Omega_{max}, \qquad \text{(A2-15)}$$

and the tail fraction transmitted,

$$\Theta = N_t/N_T = \frac{\Omega}{\Omega_{max}} \left(2 - \frac{\Omega}{\Omega_{max}}\right) \qquad \text{(A2-16)}$$

Solving for $\Omega/\Omega_{max}$ we obtain

$$\Omega/\Omega_{max} \approx (2 - \Theta/2),\ \Theta/2 \qquad \text{(A2-17)}$$

for $\Theta >> \Theta^2/4$. Since we are interested in $\Theta << 10^{-2}$ this assumption appears valid.

The second solution provides a physical solution since $\Theta \to 0$ as $\Omega = f(n) \to 0$ when $n \to \infty$.

Eliminating $\Omega$ from (A2-9) and (A2-17) and solving for $\Delta q_t$ gives,

$$\Delta q_t = \frac{\Delta q}{.121\, n - 1.1}\, \ell n \left(\frac{2}{\Theta\, \Omega_{max}}\right) - \frac{.043\, \Delta q}{.121\, n - 1.1} \qquad \text{(A2-18)}$$

Since the basis of the values in Figures 19 and 20 for $\Delta q_t/\Delta q$ was at a resolution of 100 where $\Delta q = q\Delta m/m = .00706$ we substitute this value. We also drop the 1.1 from the denominator for simplification because our greatest interest is for $n > 35$ cycles. We further let $2/\Omega_{max} = k_\theta$. Thus

$$\Delta q_t = \frac{.0582}{n}\, \ell n \frac{k_\theta}{\theta} - .00251 \qquad \text{(A2-19)}$$

or in generalized form

$$\Delta q_t = \frac{a}{n} \ell n \frac{k_\theta}{\theta} - b \qquad \text{(A2-20)}$$

We now treat this as a simplified general form of the tail function. Because of the similarity of shape (except for magnitude) between x and y tails we assume the same form of equation for both.

At this point, we would normally integrate and average over a range of n in order to obtain the effect of the various z velocities from the ion source. However, this leads to a more complex expression and becomes unwieldly in optimizing the instrument performance. The net result of this exercise is to demonstrate that nearly all of the transmitted particles are strongly weighted to come from the highest velocity group. We therefore assume that the ions arise from a thin plane in the ionizing region that is located very close to the position giving maximum velocity ($v_z$). The simplified equation (A2-20) then applies.

We further ignore the mild dependence of $\Omega_{max}$ on ($\eta$) and ($\gamma$) because of the very small leverage exerted on the equation compared to the many orders of magnitude in a range that we will consider for $\theta$. This would otherwise lead only to a very complex result with $\eta$ and $\gamma$ in both proportional and logarithmic form.

We thus take the equation of (A2-20) and fit it to the experimental peak shape shown in Figure 21. This peak on a logarithmic recording appears to demonstrate a classical form of the quadrupole peak shape with the relative magnitudes of x and y tail clearly shown. The fitted lines of (A2-20) are shown in Figure 21.

From this procedure we obtain;

$$\Delta q_{tx} = \frac{0.0297}{n} \ell n \frac{0.0258}{\theta_x} - 0.00128, \qquad \text{(A2-21)}$$

and

$$\Delta q_{ty} = \frac{0.0584}{n} \ell n \frac{0.0667}{\theta_y} - 0.00250.$$

If we let $\theta_x = \theta_y$ to define the peak base-width to equal transmission on either side we find the combined contributions to base-width to be:

$$\Delta q_t = \Delta q_{tx} + \Delta q_{ty} = \frac{0.088}{n} \ell n \frac{0.048}{\theta} - .00378. \qquad \text{(A2-22)}$$

It remains now to combine this contribution to the peak width with the stable portions of the equation in order to optimize the transmission.

## APPENDIX 3

### OPTIMIZATION

We proceed to optimize the collected current by combining ion source and mass analyzer equations. In (60) where

$$I_c^+ = \frac{4\,K_1\,K_2\,V_{ac}\,r_o^2}{V_o}\,(V_z)^3\,(\eta_x)(\eta_y)(\gamma_x)(\gamma_y)\ \text{amps}, \tag{60}$$

and (43) where

$$\frac{q\Delta m}{k_m m}\,(1 - T/B) = 2.55\,[F_1(\gamma_y) + F_2(\eta_y)]^2 + 1.3\,[F_3(\gamma_x) + F_4(\eta_x)]^2 + \left(\frac{.088}{f\ell}\,\ell n\,\frac{.048}{\theta}\right) v_z - .00378, \tag{43}$$

we temporarily assign the following letter symbols to simplify tracking the operations:

$$U = \frac{q\Delta m}{k_m m}\,(1 - T/B),$$

$$P = \left(\frac{.088}{f\ell}\,\ell n\,\frac{.048}{\theta}\right) v_z - .00378,$$

$$A = 2.55\,[F_1(\gamma_y) + F_2\,(\eta_4)]^2,$$

$$B = 1.3\,[F_3(\gamma_x) + F_4(\eta_x)]^2,$$

$$C = \frac{4\,K_1\,K_2\,V_{ac}\,r_o^2}{V_o}\,.$$

Thus

$$U = A + B + P, \text{ or}$$

$$B = 1.3\,[F_3\,(\gamma_x) + F_4\,(\eta_x)]^2 = U - P - A,$$

and

$$\gamma_x = \frac{1}{F_3}\left[\left(\frac{U - P - A}{1.3}\right)\right]^{1/2} - F_4(\eta_x).$$

Substituting in (60),

$$I_c^+ = C\,(v_z)^3(\eta_x)(\eta_y)(\gamma_y)\,\frac{1}{F_3}\left[\left(\frac{U - P - A}{1.3}\right)^{1/2} - F_4(\eta_x)\right]. \qquad \text{(A3-1)}$$

Treating each variable as independent in an equation of constant coefficients and differentiating $I_c^+$ for a maximum in $\eta_x$,

$$\frac{dI_c^+}{d(\eta_x)} = 0 = -F_4(\eta_x) + \left(\frac{U - P - A}{1.3}\right)^{1/2} - F_4(\eta_x),$$

or

$$F_4(\eta_x) = \frac{1}{2}\left(\frac{U - P - A}{1.3}\right)^{1/2}. \qquad \text{(A3-2)}$$

Therefore, at maximum $(\eta_x)$,

$$I_c^+ = C\,(v_z)^3\,(\eta_y)(\gamma_y)\,\frac{1}{2\,F_3F_4}\left(\frac{U - P - A}{1.3}\right)^{1/2} \times \frac{1}{2}\left(\frac{U - P - A}{1.3}\right)^{1/2},$$

or

$$I_c^+ = C\,(v_z)^3\,(\eta_y)(\gamma_y)\,\frac{1}{4 \times 1.3\,F_3F_4}\,(U - P - A). \qquad \text{(A3-3)}$$

One could now proceed to expand A and maximize $I_c^+$ as a function of $\eta_y$ and $\gamma_y$. However, the complexity tends to cloud an important conclusion. We can visualize the result more easily if we note that the optimization process could have started with a substitution of $\eta_x$ into (60). In that case we would have found that

$$F_3(\gamma_x) = \frac{1}{2}\left(\frac{U - P - A}{1.3}\right)^{1/2}, \qquad \text{(A3-4)}$$

or thus that

$$F_3(\gamma_x) = F_4(\eta_x). \qquad \text{(A3-5)}$$

This first important result discloses that at maximum collected current, the contributions of angle $(\gamma)$ and position $(\eta)$ functions to q-space are equal. This is true regardless of the eventual values of $F_3$, $F_4$, $(\gamma)$ and $(\eta)$ which produce an optimum or whether they are mildly coupled functions or not.

We likewise could have shown

$$F_1(\gamma_y) = F_2(\eta_y) = \frac{1}{2}\left(\frac{U - P - B}{2.55}\right)^{1/2} \tag{A3-6}$$

demonstrating that the same is true in the y-plane.

We now back up to simplify visualizing the result and from (A3-5) and (A3-6) find that

$$(\eta_x) = \frac{F_3}{F_4}\ (\gamma_x) \text{ and } (\eta_y) = \frac{F_1}{F_2}\ (\gamma_y) \tag{A3-7}$$

Substituting in (60),

$$I_c^+ = C\ (v_z)^3\ (\gamma_x)^2\ (\gamma_y)^2\ \frac{F_3}{F_4}\ \frac{F_1}{F_2} \tag{A3-8}$$

From (43) and the latter substitutions, as well as (A3-5) and (A3-6),

$$U - P = 2.55\ [2\ F_1(\gamma_y)]^2 + 1.3\ [2\ F_3\ (\gamma_x)]^2 \tag{A3-9}$$

Solving for

$$(\gamma_x)^2 = \frac{U - P - 2.55\ [2\ F_1(\gamma_y)]^2}{1.3 \times 4\ F_3^{\,2}} \tag{A3-10}$$

and inserting in (A3-8),

$$I_c^+ = C\ (v_z)^3\ (\gamma_y)^2\ \frac{F_1\left(U - P - 2.55\ [2\ F_1(\gamma_y)]^2\right)}{1.3 \times 4\ F_2F_3F_4} \tag{A3-11}$$

Differentiating $I_c^+$ for a maximum in $(\gamma_y)$,

$$\frac{dI_c^+}{d(\gamma_y)} = 0 = (\gamma_y)^2\left(-2 \times 2.55\ F_1[2\ F_1(\gamma_y)]\right) + 2(\gamma_y)\left(U - P - 2.55\ [2\ F_1(\gamma_y)]\right)^2 \tag{A3-12}$$

$$U - P = 2.55\ [2\ F_1(\gamma_y)]^2 + 2.55\ F_1(\gamma_y)\ [2\ F_1(\gamma_y)]$$

$$= 2 \times 2.55\ [2\ F_1(\gamma_y)]^2;$$

$$2.55\ [2\ F_1(\gamma_y)]^2 = \frac{U - P}{2} \tag{A3-13}$$

or

$$(\gamma_y)^2 = \frac{(U - P)}{2 \times 2.55 \times 4\ F_1^2} \tag{A3-14}$$

Inserting this result in (A3-11) yields,

$$I_c^+ = C\ (v_z)^3\ \frac{(U - P)^2/2}{1.3 \times 2.55 \times 4 \times 8\ F_1F_2F_3F_4}$$

or

$$I_c^+ = \frac{C(v_z)^3(U - P)^2}{1.3 \times 2.55 \times 64\ F_1F_2F_3F_4} \tag{A3-15}$$

The second important result can now be noted. (A3-10) could have been a solution for $(\gamma_y)^2$. In which case we would have found that

$$1.3\ [2\ F_3(\gamma_x)]^2 = \frac{(U - P)}{2}, \tag{A3-16}$$

or thus that

$$2.55\ [2\ F_1(\gamma_y)]^2 = 1.3\ [2\ F_3(\gamma_x)]^2. \tag{A3-17}$$

Expanding (A3-17) into the original terms,

$$2.55\ [F_1(\gamma_y) + F_2(\eta_y)]^2 = 1.3\ [F_3(\gamma_x) + F_4(\eta_x)]^2 \tag{A3-18}$$

This is the result which was presumed in Equation (38) and was the substance of the solutions in that section. It demonstrates that the collected current is maximized when the q-space taken in the x and y planes are equal.

Again it is noted that this is true regardless of the individual optimum values of coefficients and variables and that future work can be conducted to optimize the choices of ($\eta$) and ($\gamma$) without revising these results.

Summarizing the results, so far, we have found that at maximum collected current,

$$F_3(\gamma_x) = F_4(\eta_x) = \frac{1}{2}\left(\frac{U - P}{2.6}\right)^{1/2} \tag{A3-19}$$

and

$$F_1(\gamma_y) = F_2(\eta_y) = \frac{1}{2}\left(\frac{U - P}{5.1}\right)^{1/2}$$

It is also apparent from ff (41), that since $G_1 = 2.26\ F_1$ and $G_2 = 2.26\ F_2$, (41) is true, i.e.,

$$G_1)(\gamma_y) = (G_2)(\eta_y) \ . \qquad (41)$$

Expanding P in (A3-15), we have now,

$$I_c^+ = \frac{C(v_z)^3}{212\ F_1F_2F_3F_4}\left(U - (\frac{.088}{f\ell}\ \ell n\ \frac{.048}{\theta})\ v_z + .00378\right)^2 \qquad (A3\text{-}20)$$

Differentiating $I_c^+$ as a function of $v_z$

$$\frac{dI_c^+}{dv_z} = 0 = 2(v_z)^3\left(-\frac{.088}{f\ell}\ \ell n\ \frac{.048}{\theta}\right)\left(U - (\frac{.088}{f\ell}\ \ell n\ \frac{.048}{\theta})\ v_z + .00378\right)$$

$$+ 3(v_z)^2\left(U - \left(\frac{.088}{f\ell}\ \ell n\ \frac{.048}{\theta}\right)\ v_z + .00378\right)^2$$

$$(2 + 3)\left(\frac{.088}{f\ell}\ \ell n\ \frac{.048}{\theta}\right)\ v_z = 3(U + .00378)$$

$$(v_z) = \frac{3}{5}\ \frac{(U + .00378)}{\left(\frac{.088}{f\ell}\ \ell n\ \frac{.048}{\theta}\right)} \qquad (A3\text{-}21)$$

and

$$I_c^+ = \frac{C\left(\frac{3}{5}\right)^3 (U + .00378)^3 \left(\frac{2}{5}\right)^2 (U + .00378)^2}{212\ F_1F_2F_3F_4\left(\frac{.088}{f\ell}\ \ell n\ \frac{.048}{\theta}\right)^3}$$

Letting

$$P' = \frac{.088}{f\ell}\ \ell n\ \frac{.048}{\theta}$$

$$I_c^+ = \frac{27 \times 4\ C(U + .00378)^5}{212 \times (5)^5\ F_1F_2F_3F_4\ (P')^3}$$

Inserting the values for C, U and P and combining the numerical constants,

$$I_c^+ (max)_3 = \frac{0.957\ K_1 K_2\ V_{ac}\ (f\ell)^3\ r_o^2}{F_1 F_2 F_3 F_4\ V_o \left(\ell n\ \frac{.048}{\theta}\right)^3} \left(\frac{q\Delta m}{k_m m}\ (1\text{-}T/B) + .00378\right)^5 \quad \text{amps} \qquad \text{(A3-22)}$$

The dimensions are the same as (60) since $(f\ell)^3$ has the dimensions (meter/sec)$^3$. (A3-22) relates to Mode 3 operation.

It is desirable to express the component parts of (A3-22) both for later calculations and to visualize the relative importance of the parameters. Thus substituting P into (A3-19) and referring to (60) for the general framework,

$$(v_z)^3 = \left(\frac{3}{5}\right)^3 \frac{(f\ell)^3 (U + .00378)^3}{(.088)^3 \left(\ell n\ \frac{.048}{\theta}\right)^3} \quad m^3\ sec^{-3} \qquad \text{(A3-23)}$$

$$(\eta_x) = \frac{1}{2\ F_4} \left[\frac{2(U + .00378)}{5\ (2.6)}\right]^{1/2}$$

$$(\eta_y) = \frac{1}{2\ F_2} \left[\frac{2(U + .00378)}{5\ (5.1)}\right]^{1/2}$$

$$(\gamma_x) = \frac{1}{2\ F_3} \left[\frac{2(U + .00378)}{5\ (2.6)}\right]^{1/2}$$

$$(\gamma_y) = \frac{1}{2\ F_1} \left[\frac{2(U + .00378)}{5\ (5.1)}\right]^{1/2}$$

where

$$U = \frac{q\Delta m}{k_m m}\ (1 - T/B).$$

The third important result which becomes evident after having broadened the optimization equation to include an approximate expression for peak width due to tails is that the frequency and length have a more powerful effect upon instrument sensitivity than other variables. Increasing either of these parameters allows an increase in axial velocity without infringing the resolution or peak shape. The velocity increase is brought about by increase in the repeller-accelerator voltage which allows a faster rate of charge formations in the ion source.

It would appear from the optimized equation that the resolution could approach infinity ($U \to 0$) and still allow a finite current to be collected because of the constant, .00378. In practice, of course, this could not be true. In applying (A3-22) the resolution cannot be extended too greatly because of the restriction that the base width include a $\Delta q_t$ of at least .000706. These limits occur because of the approximate nature of the expression for tails.

Turning now to Mode 1 and 2 (open ion source) operation, from (61)

$$I_c^+ = \frac{4\, K_1'\, K_2'\, n_s\, V_{ac}\, r_o^2}{V_o} \; (v_z)^2\, (\eta_x)(\eta_y)(\gamma_x)(\gamma_y) \text{ amps} \qquad (61)$$

which immediately reduces to

$$I_c^+ = \frac{C'\,(v_z)^2 \left( U - \left( \frac{.088}{f\ell} \ell n \frac{.048}{\theta} \right) v_z + .00378 \right)^2}{212\, F_1 F_2 F_3 F_4} \qquad (A3\text{-}24)$$

by utilizing the same procedures leading to (A3-20). Now,

$$C' = \frac{4\, K_1'\, K_2'\, n_s\, V_{ac}\, r_o^2}{V_o}$$

Maximizing $I_c^+$ as a function of $v_z$ by the same approach,

$$(v_z) = \frac{1}{2} \frac{(U + .00378)}{\left( \frac{.088}{f\ell} \ell n \frac{.048}{\theta} \right)} \qquad (A3\text{-}25)$$

Inserting in (A3-24)

$$I_c^+ = \frac{C'\,(U + .00378)^4}{212\, F_1 F_2 F_3 F_4\, (4)(4) \left( \frac{.088}{f\ell} \ell n \frac{.048}{\theta} \right)^2}$$

or with combined numerical constants and values for $C'$ and U,

$$I_c^+ (\max)_{1,2} = \frac{0.152\, K_1'\, K_2'\, n_s\, V_{ac}\, (f\ell)^2\, r_o^2}{F_1 F_2 F_3 F_4\, V_o \left( \ell n \frac{.048}{\theta} \right)^2} \left( \frac{q\Delta m}{k_m m} (1 - T/B) + .00378 \right)^4 \text{ amps} \qquad (A3\text{-}26)$$

In this case,

$$(v_z) = \frac{1}{2} \frac{(U + .00378)}{\left(\frac{.088}{f\ell} \ell n \frac{.048}{\theta}\right)} \qquad \text{(A3-27)}$$

$$(\eta_x) = \frac{1}{2 F_4} \left[ \frac{(U + .00378)}{2 (2.6)} \right]^{1/2}$$

$$(\eta_y) = \frac{1}{2 F_2} \left[ \frac{(U + .00378)}{2 (5.1)} \right]^{1/2}$$

$$(\gamma_x) = \frac{1}{2 F_3} \left[ \frac{(U + .00378)}{2 (2.6)} \right]^{1/2}$$

$$(\gamma_y) = \frac{1}{2 F_1} \left[ \frac{(U + .00378)}{2 (5.1)} \right]^{1/2}$$

## APPENDIX 4

## DEFINITIONS

Peak: The presence or nature of an output (ion current) signal at a given mass position.

Scan: To sweep through the mass spectrum of output signals versus mass.

Tail: The pseudonym given the nature or "shape" of the output current as it decreases away from the edge of a peak.

Resolution: The ratio, $M/\Delta M_o$, where M is the atomic mass number at which a specified peak occurs, and $\Delta M_o$ is the width, expressed in atomic mass units, of the peak, measured at a specified fraction of the peak height. For example, the resolution could be 100 for width measured at 10% of peak height.

Crosstalk: The fractional contribution of signal from a unit peak to the adjacent mass positions, in the specified mass range. For example, the crosstalk could be given as $10^{-3}$ or better in the mass range m/e 1 to 100.

Top-to-Base Ratio: The ratio of the top width to the base width of the specified peak, measured at specified fractions of the peak height. For example, the top-to-base ratio may be 0.5 or better measured at 95% and 5% of the peak height.

A Flat-Topped-Peak: A peak falling within a specified fraction of the maximum peak height over a specified fractional range of the peak base width. For example, the peak could be within 5% of the maximum height over a range 0.5 of the base width.

The optimum performance is best described as a peak that is greater than a given fraction of the maximum peak height within a specified region and less than a given set of values at all positions outside that region, i.e., the signal falls within the open region in the following figure.

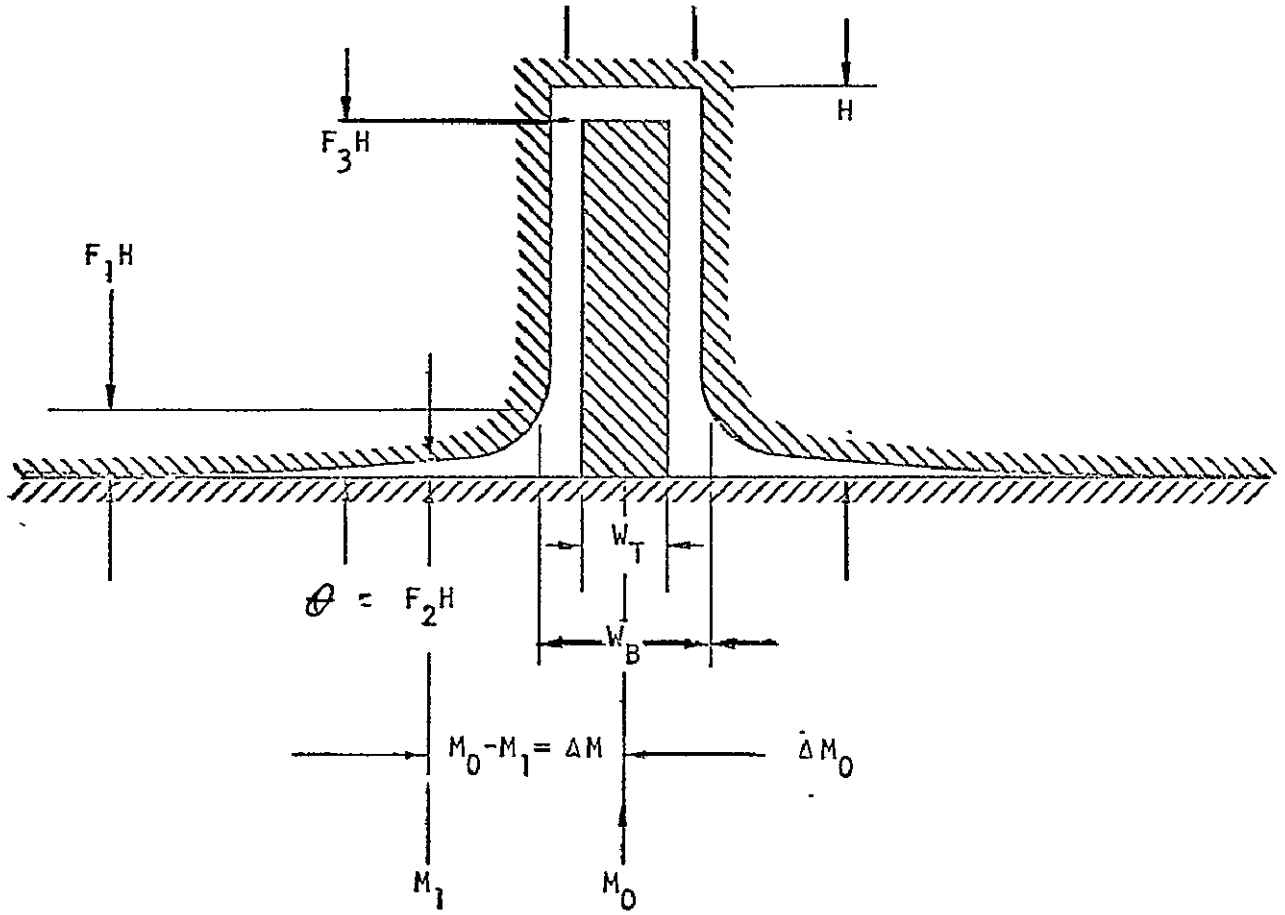


Figure for the Definition of Resolution and Peak Shape

## REFERENCES


1. Paul, W., Reinhard, H.P. and von Zahn, V.; Z Physik, 152, 143 (1958)

2. c.f. Brubaker, W.M.; Neuvieme Colloq. Spectroscopicum Intern., Lyon France 1961 and Brubaker, W.M. and Tuul, J., RSI 35, 1007, 1964.

3. Hall, L.G. and Ruecker, M.R., Proceedings of ASTM Committee E 14 on Mass Spectrometry, Presented Montreal, 1964, Available to Attendees.

4. Brubaker, W.M., "Study of the Introduction of Ions into the Region of Strong Fields within a Quadrupole Mass Spectrometer" Final report for NASA Contract NASW-1298. August 65 through October 67,

5. Final Report for "Specialized Quadrupole Mass Spectrometer" NASA Contract NAS5-3453, August 1967, page 5-18.

6. Perkin-Elmer Study, unpublished.

7. Brubaker, W.M.; J. App. Phys., 26, 1007 (1955).

8. Klemperer; Electron Optics, Cambridge University Press, 1953.

9. See NAS5-3453 Final Report "Summary of Development", August 1967, Appendix.

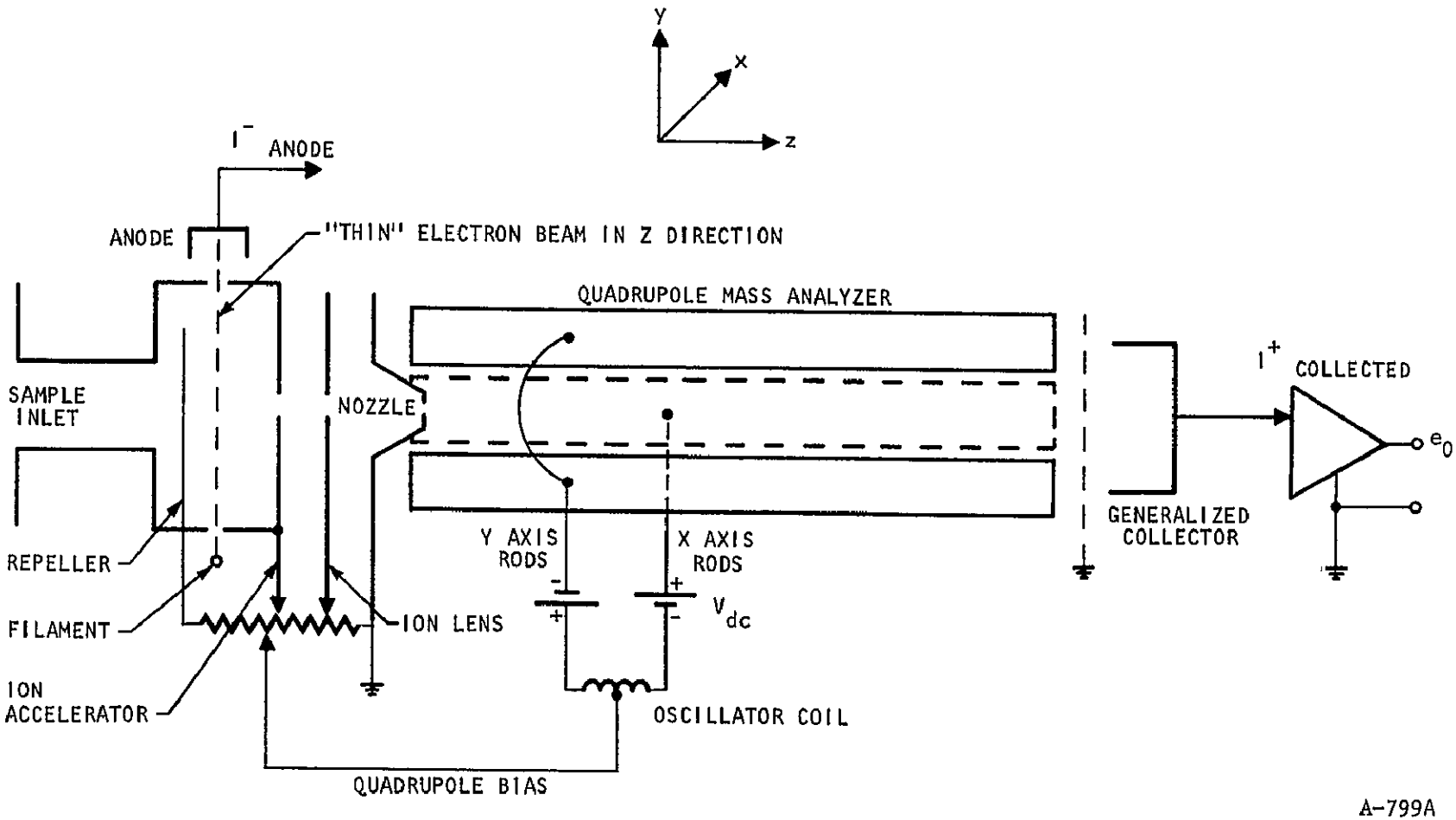


FIGURE 1. General Configuration of the System Optimized

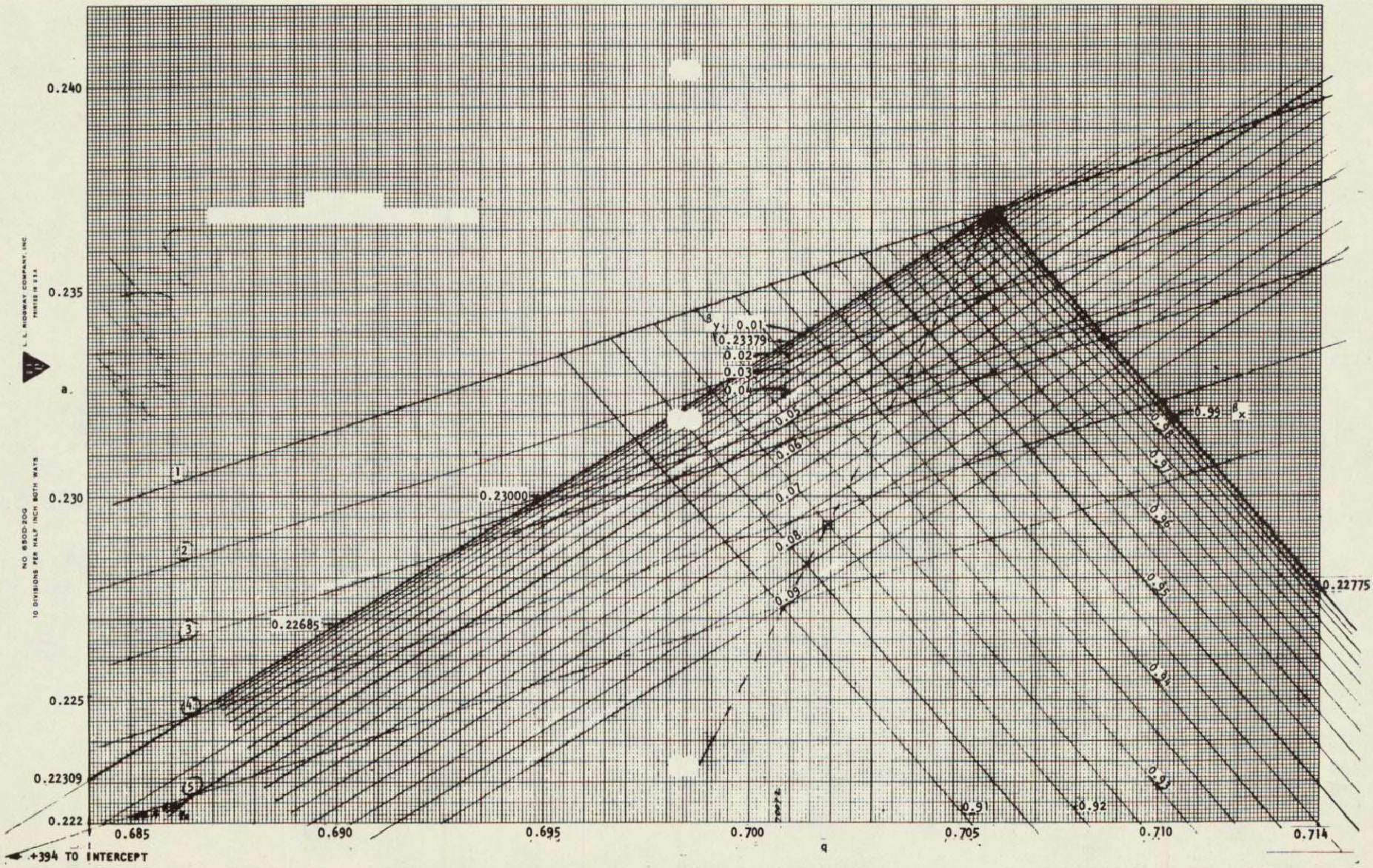


FIGURE 2a. Portion of the Quadrupole Stability Diagram

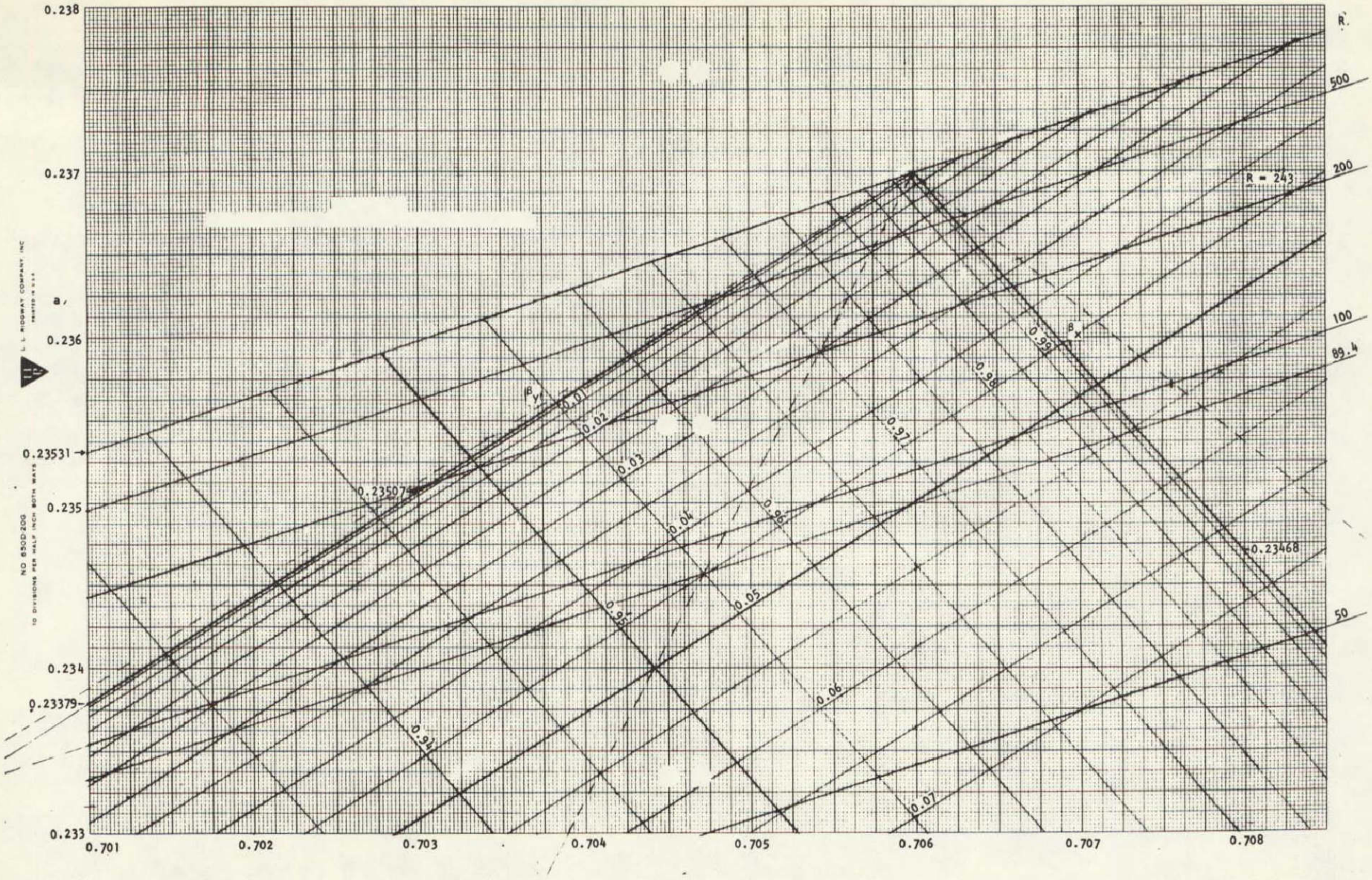


FIGURE 2b. Enlarged Portion of the Quadrupole Stability Diagram

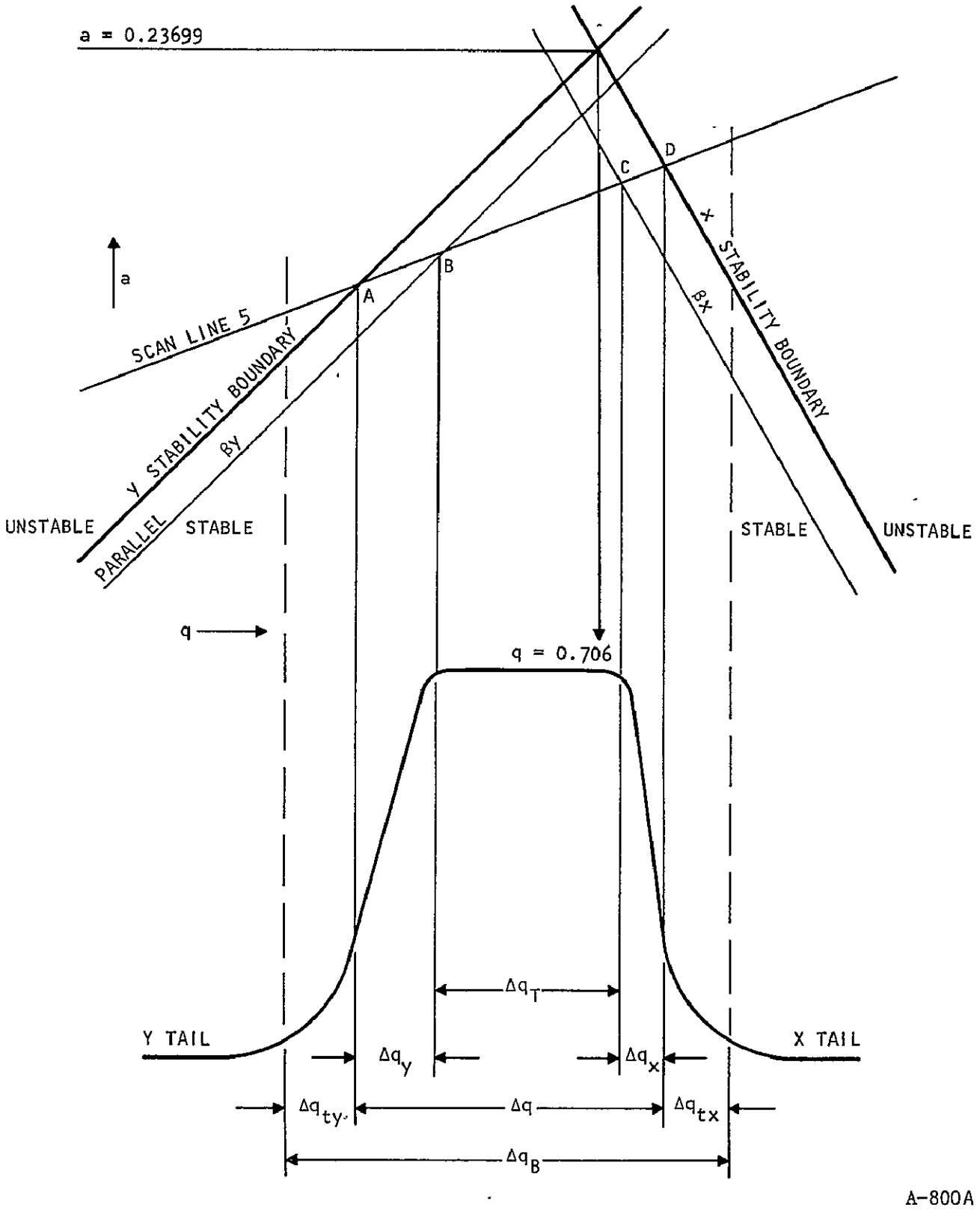


FIGURE 3. Ion Current Transmitted Through Quadrupole as a Function of q

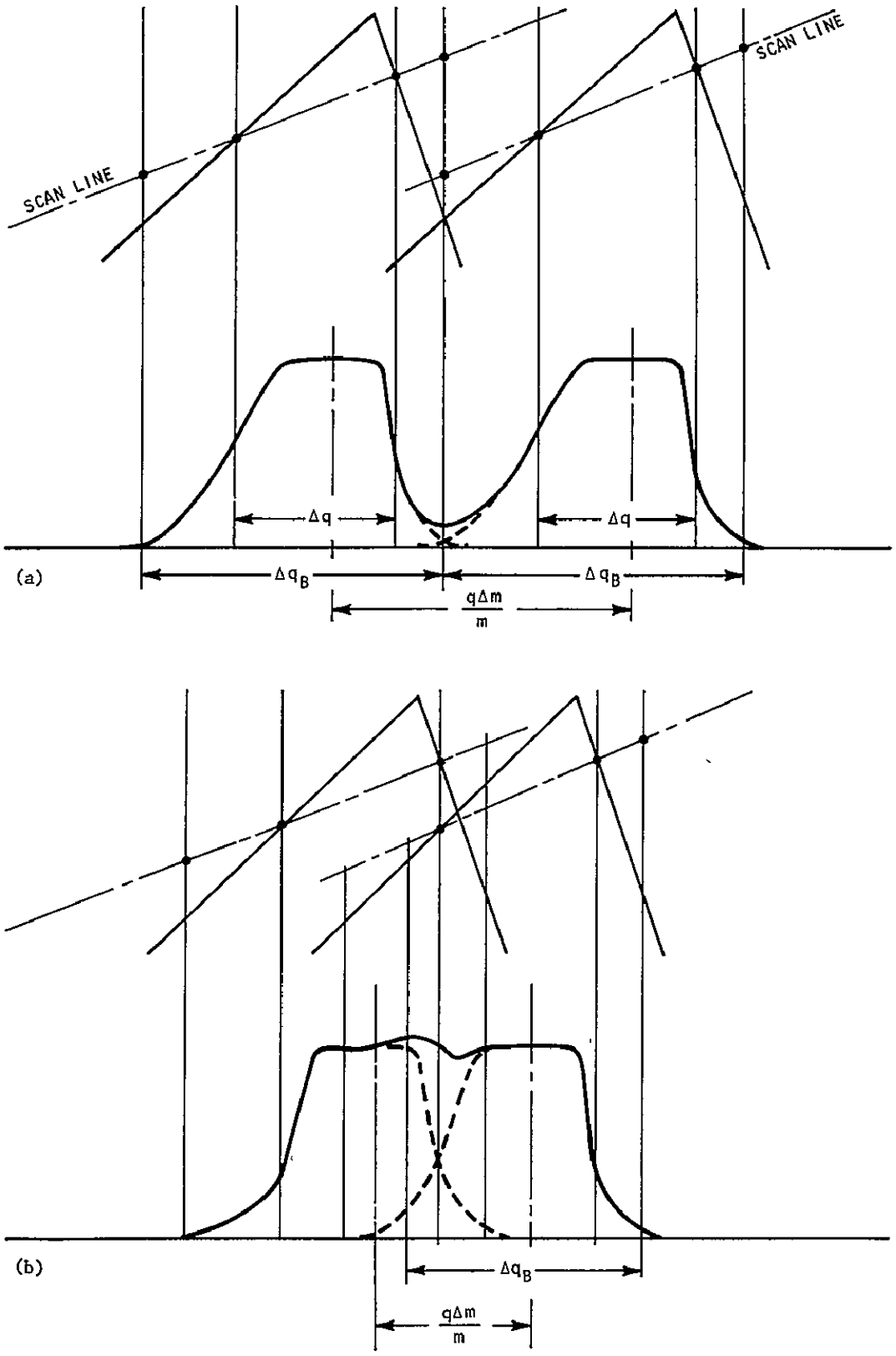


FIGURE 4. · Adjacent Ion Peaks Relative to the Stability Diagram

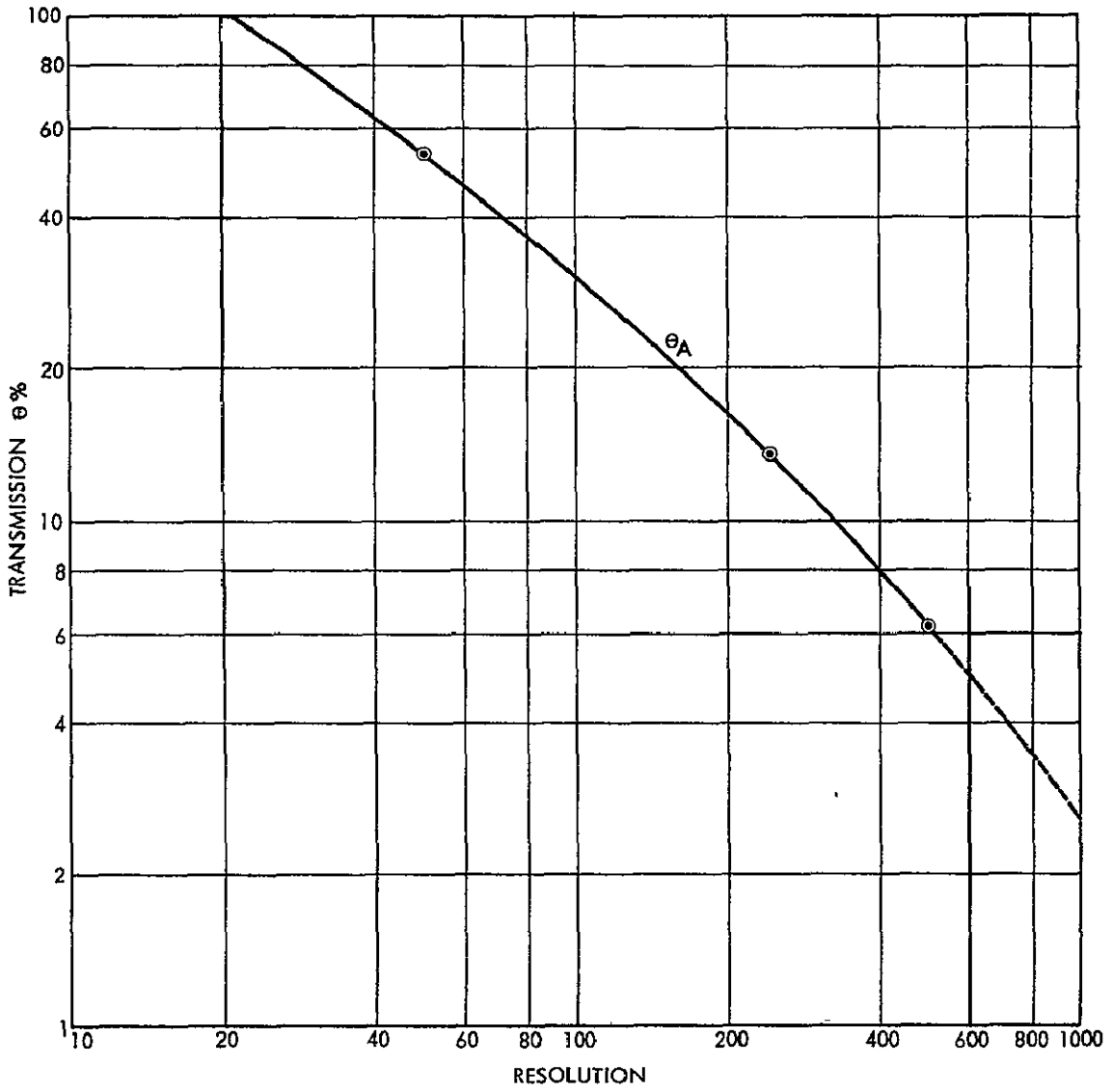


FIGURE 5. Quadrupole Transmission vs Resolution
Uniform Ion Distribution over $\eta_x = \eta_y = .08$

$\gamma_x = \gamma_y = .064$

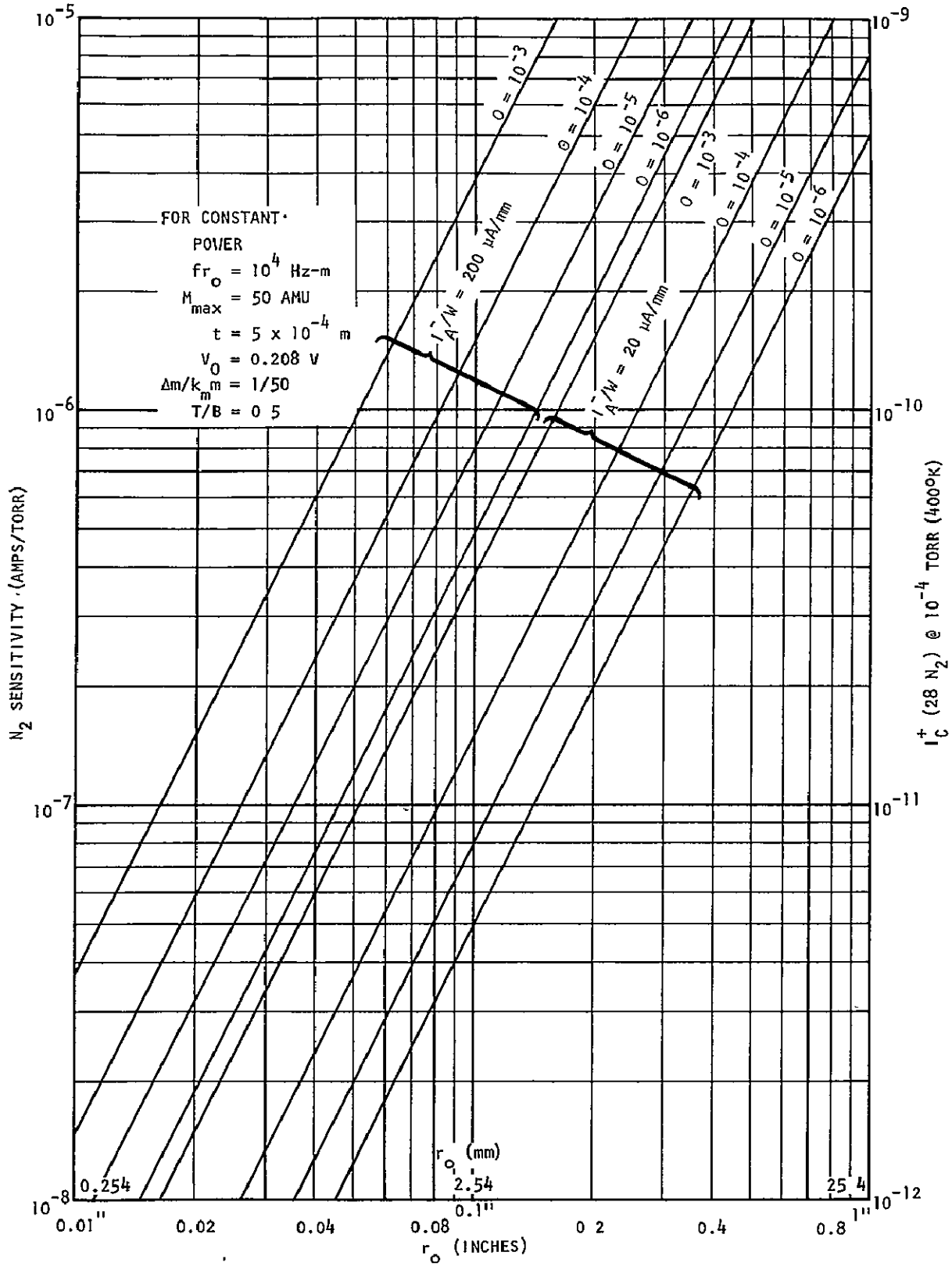


FIGURE 6. $I_c^+$ (max) and Sensitivity vs Size ($r_o$)

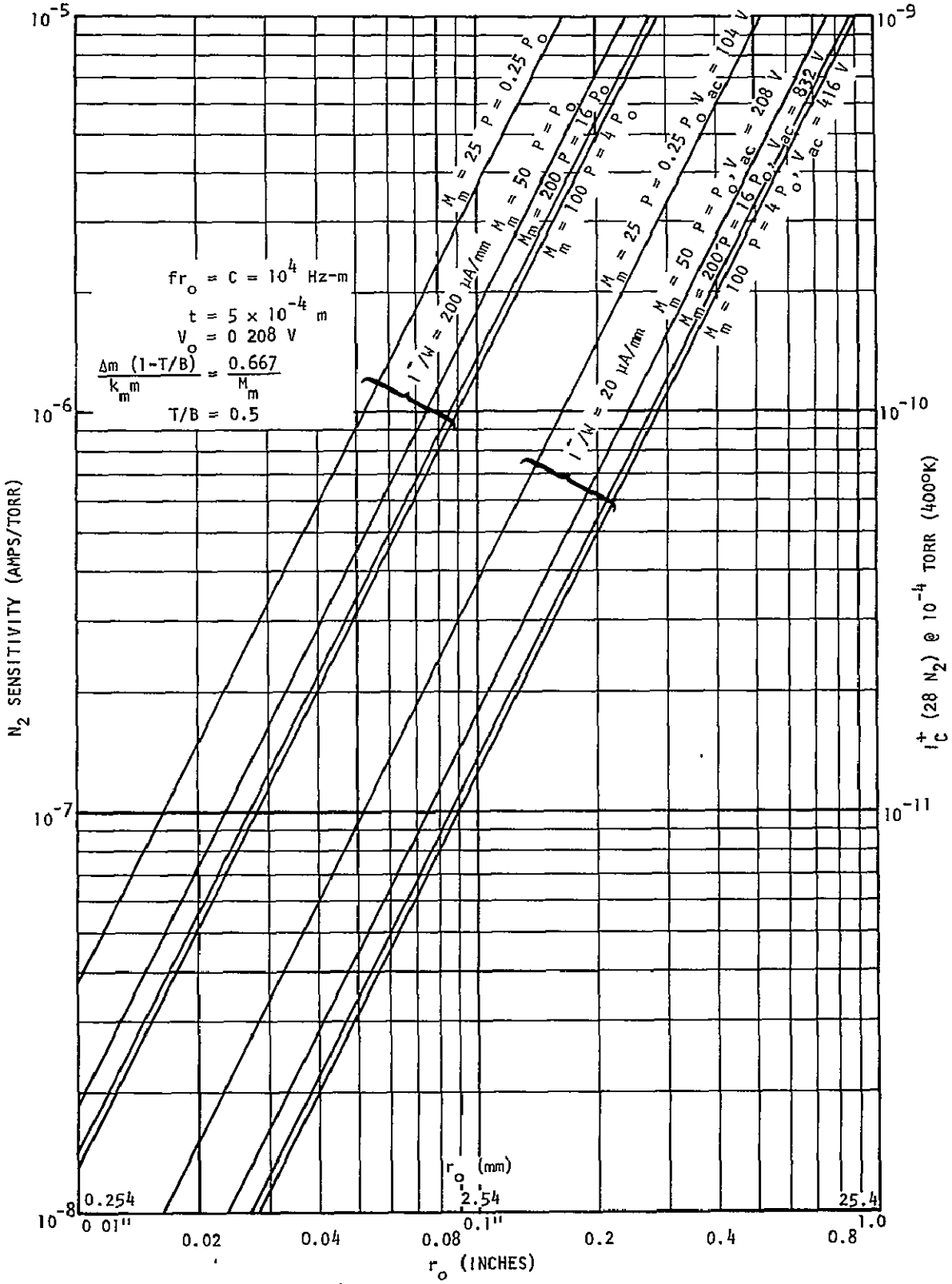


FIGURE 7. $I_c^+$ (max) and Sensitivity vs Size ($r_o$)
With $M_m$, P, $V_{ac}$ as Parameters

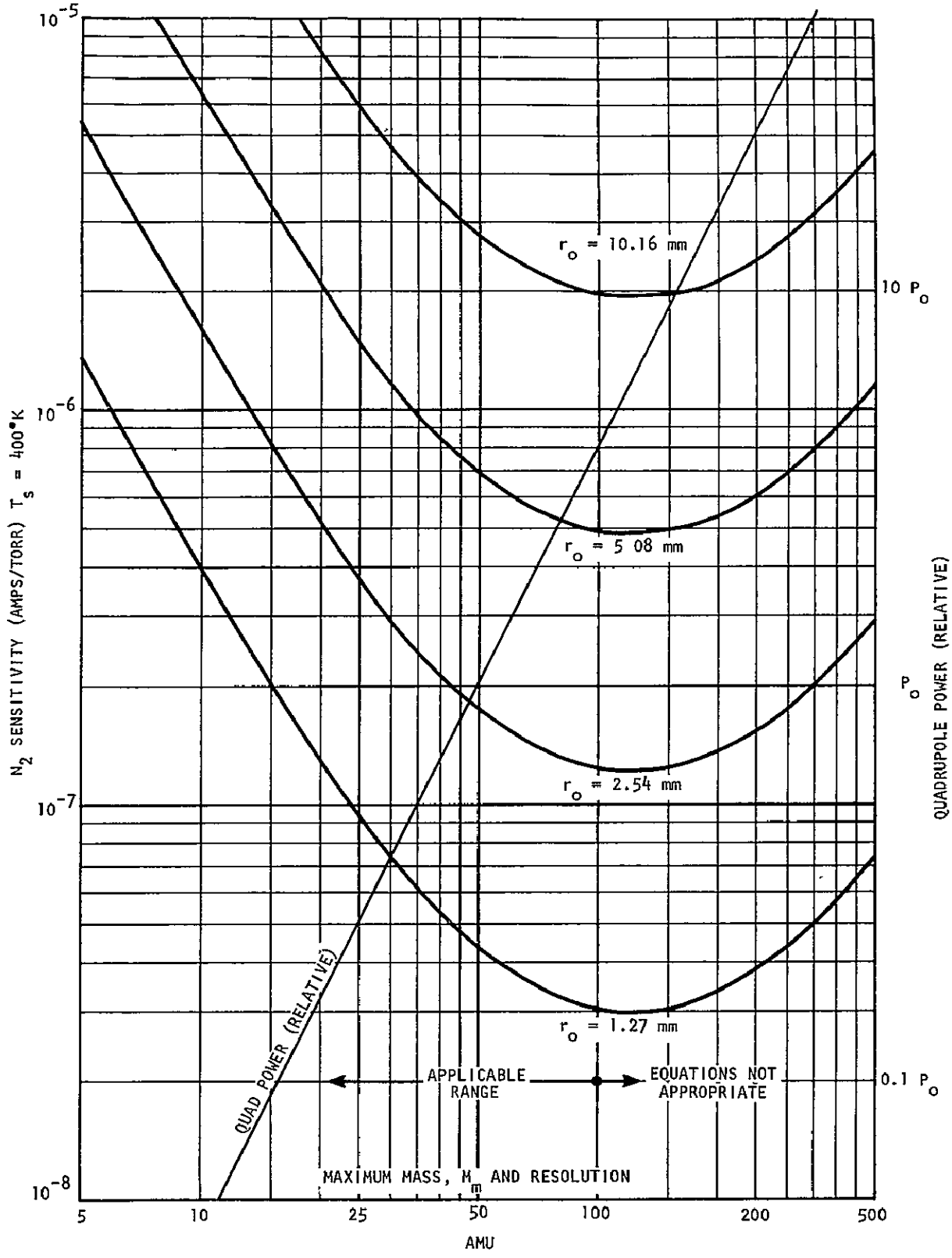


FIGURE 8. Sensitivity and Power vs Maximum Mass Scanned at Unit Resolution

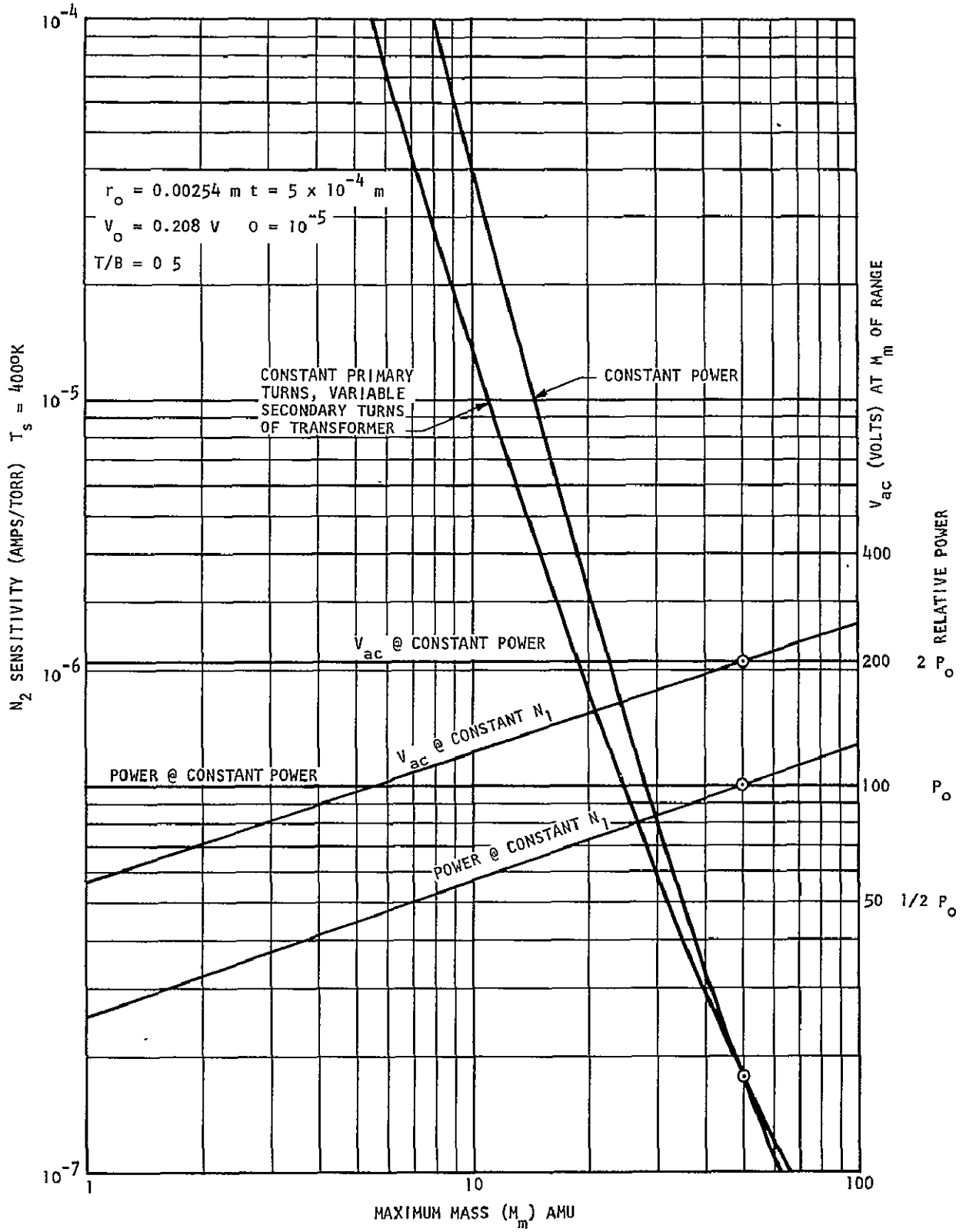


FIGURE 9. Sensitivity vs Maximum Mass of a Set of Mass Ranges

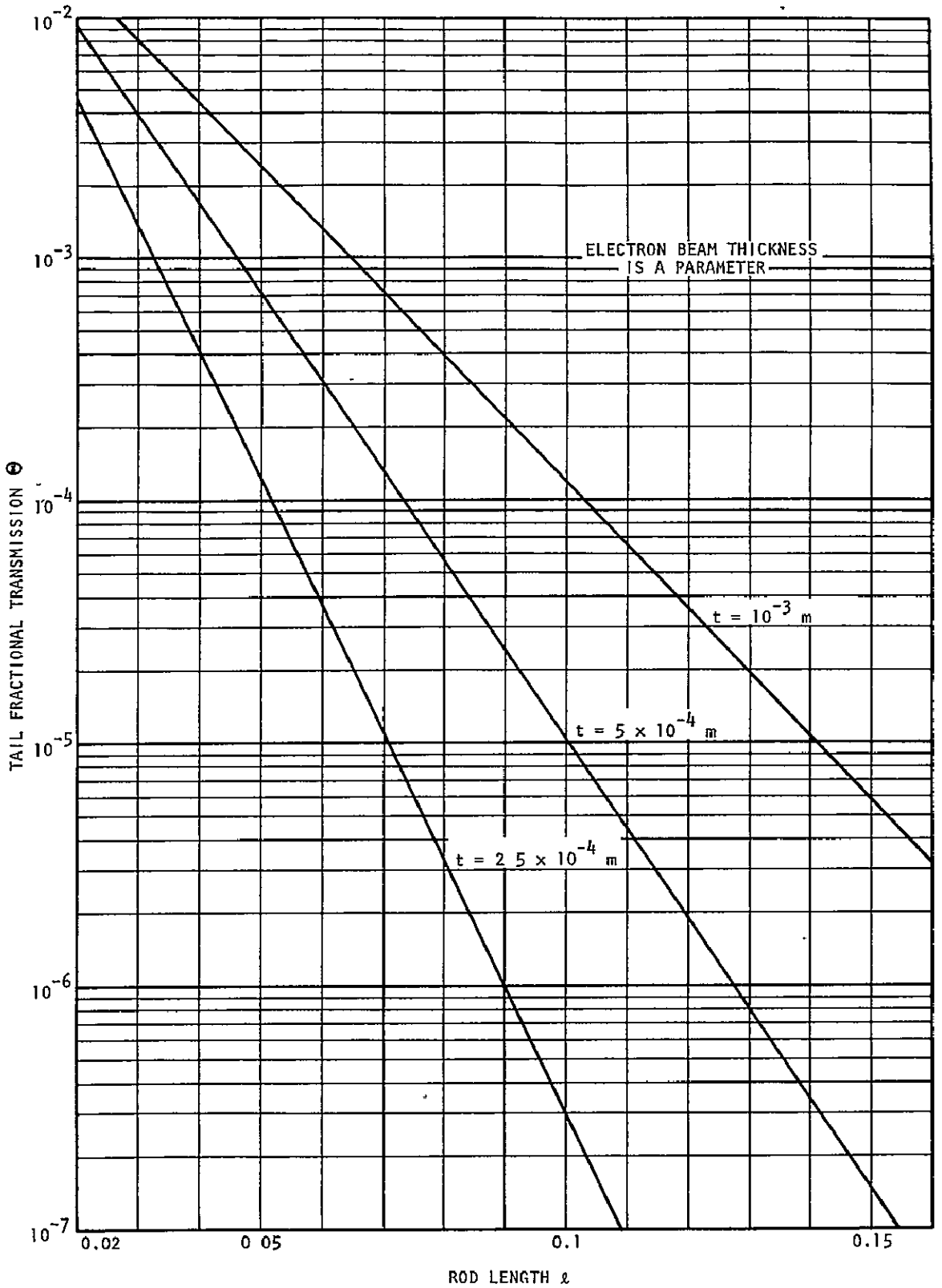


FIGURE 10. Tail Fractional Transmission at the Peak Edge vs Rod Length

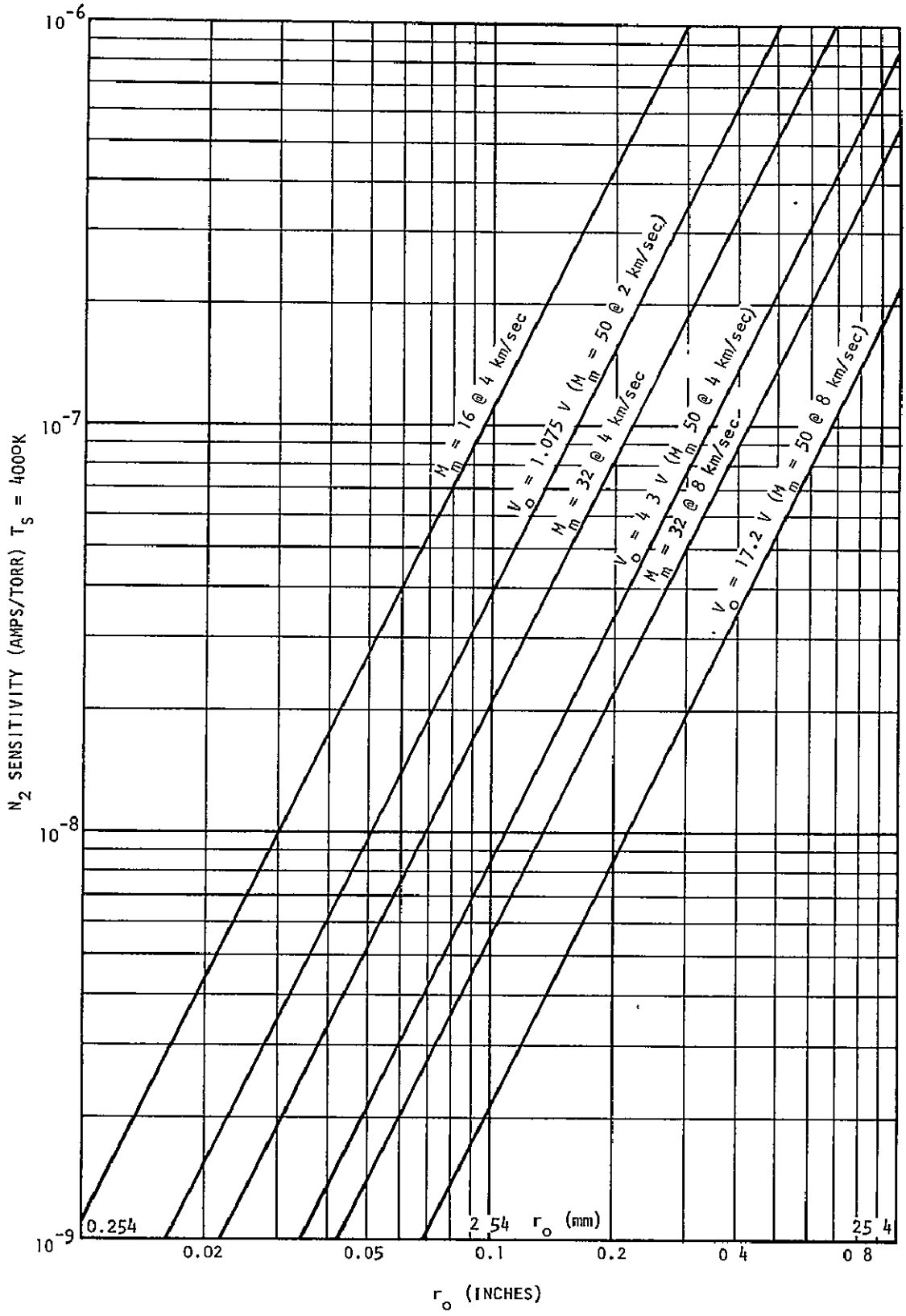


FIGURE 11. Sensitivity vs $r_o$ at Various $V_o$, v and $M_m$

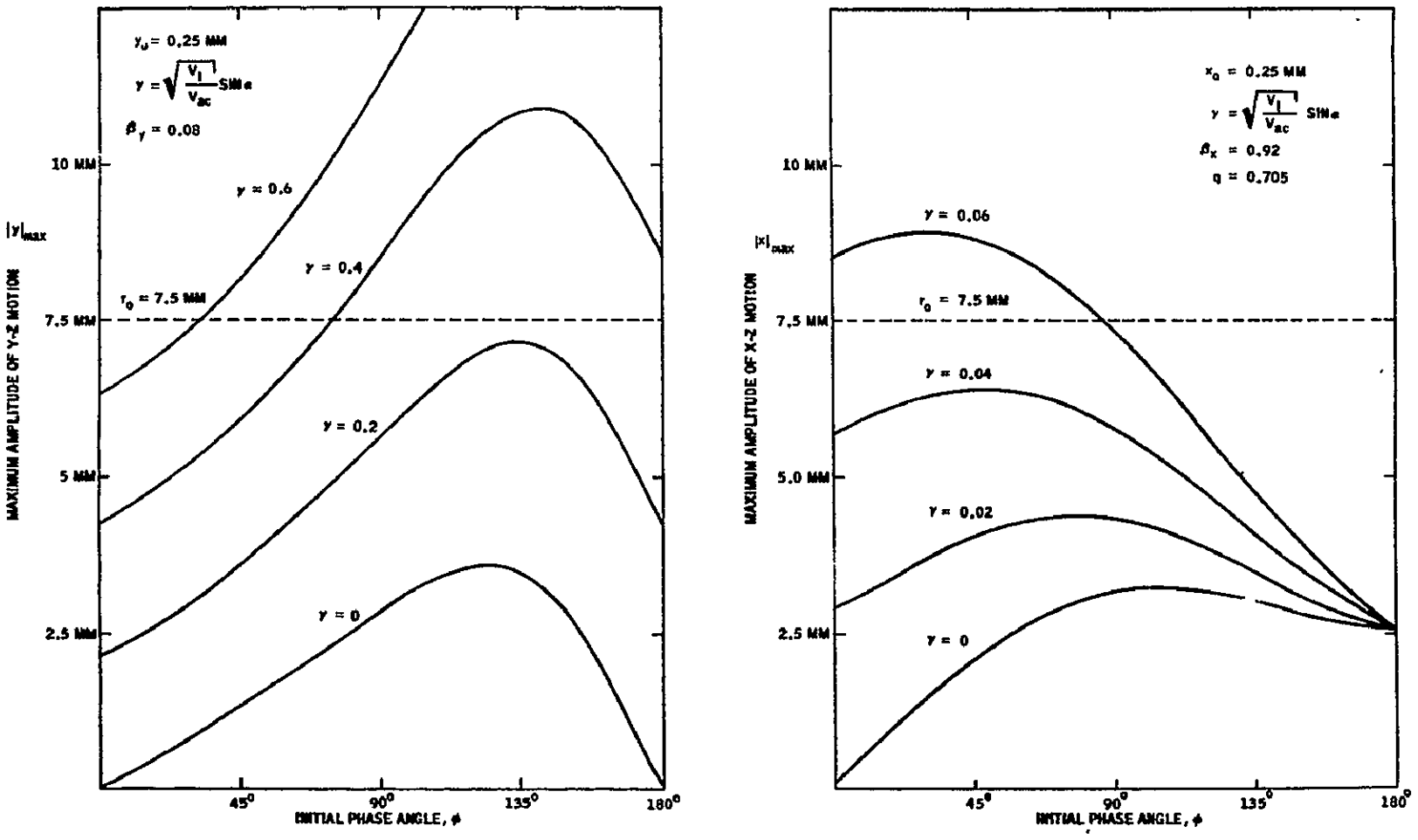


FIGURE 12. Amplitude vs Phase Angle

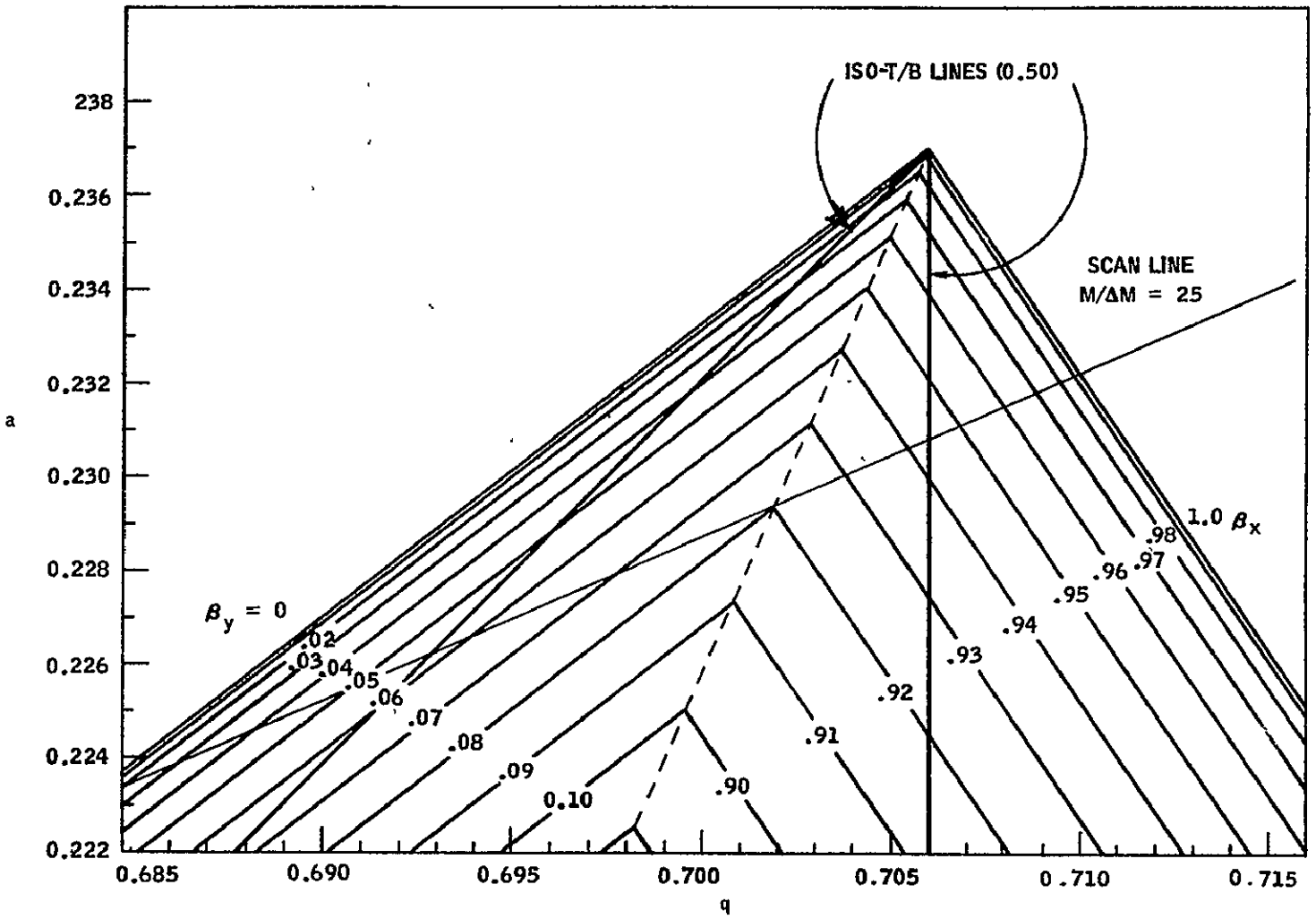


FIGURE 13. Quadrupole Stability Diagram

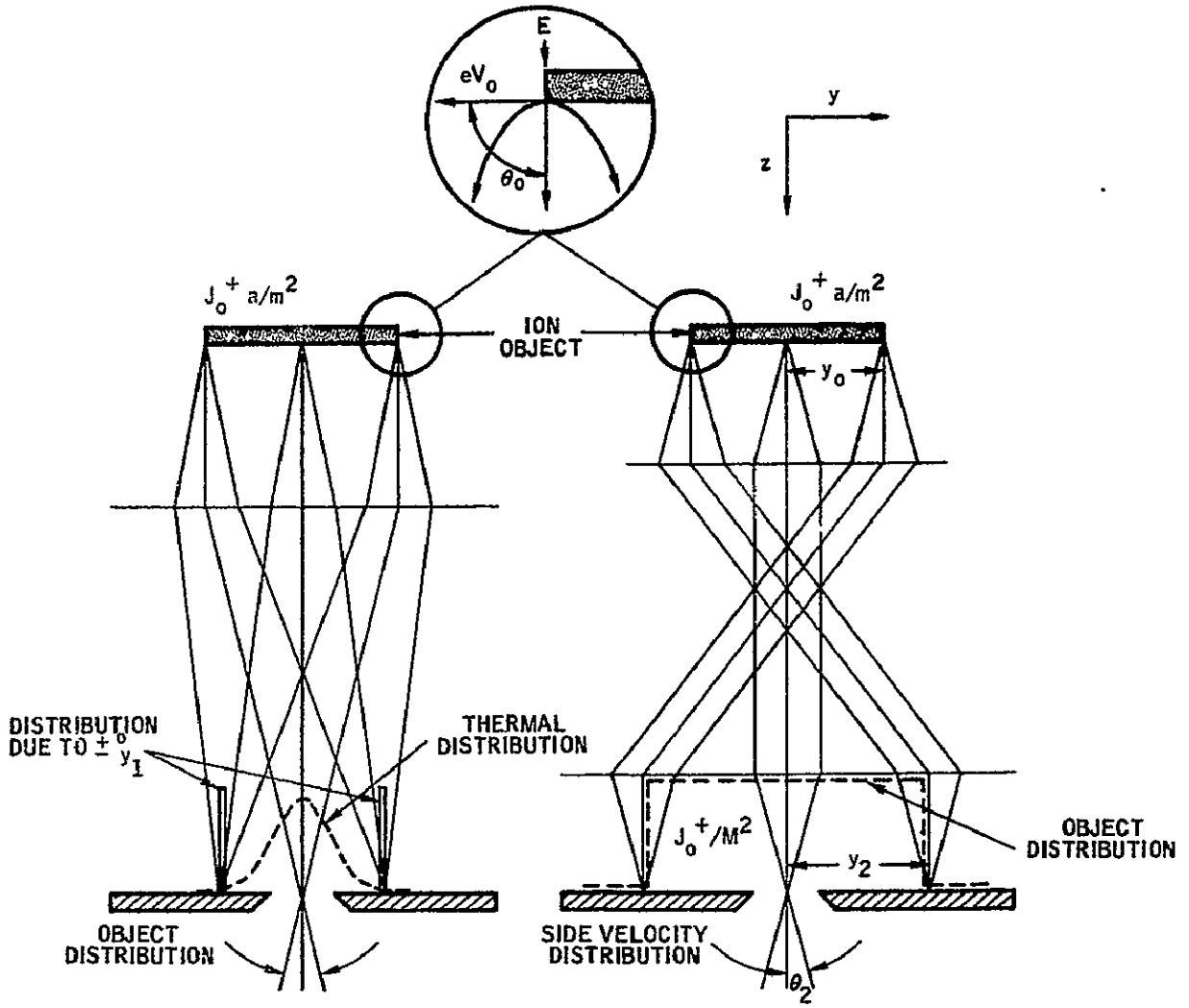


FIGURE 14. Ion Source Focusing

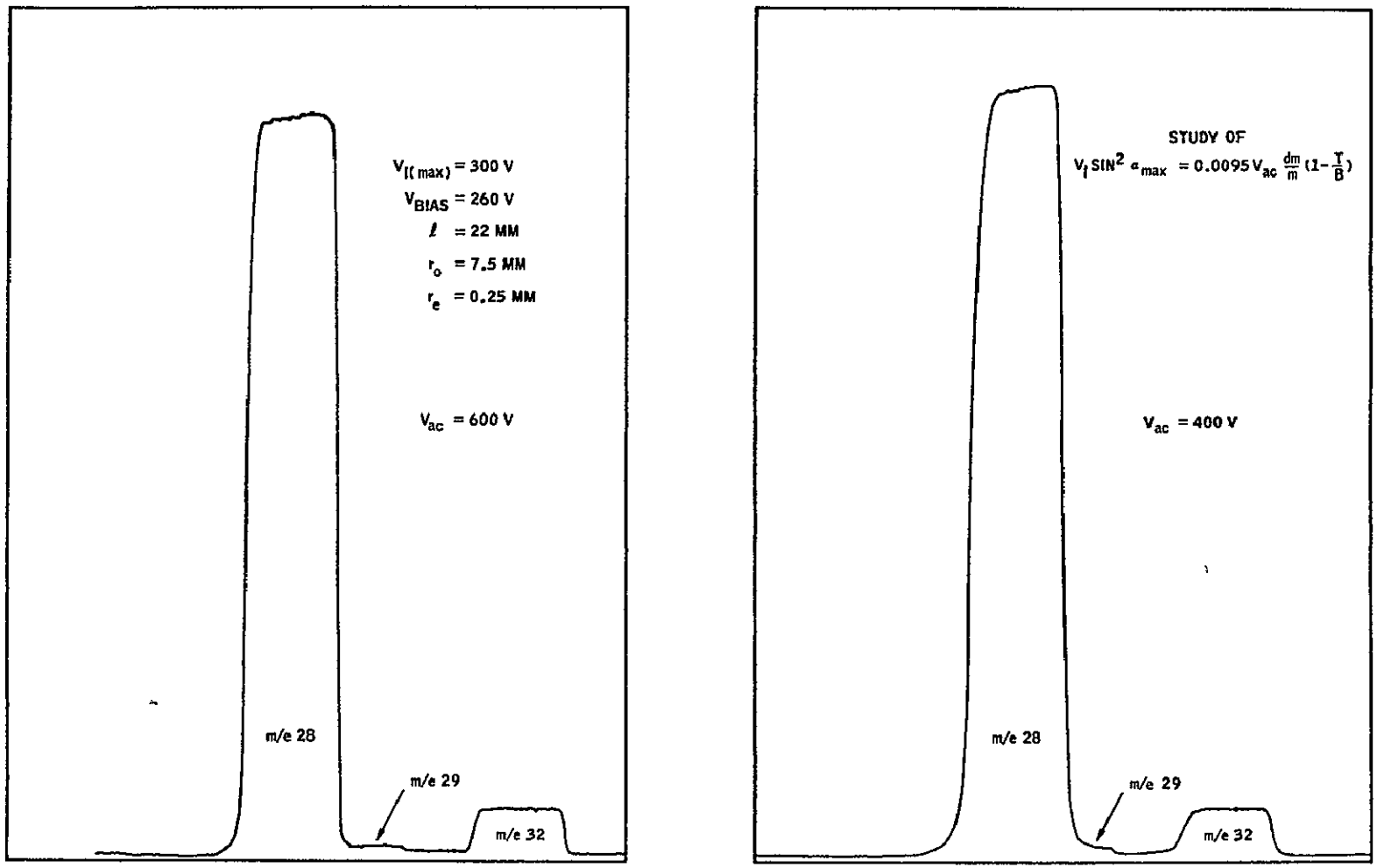


FIGURE 15. Peak Shape

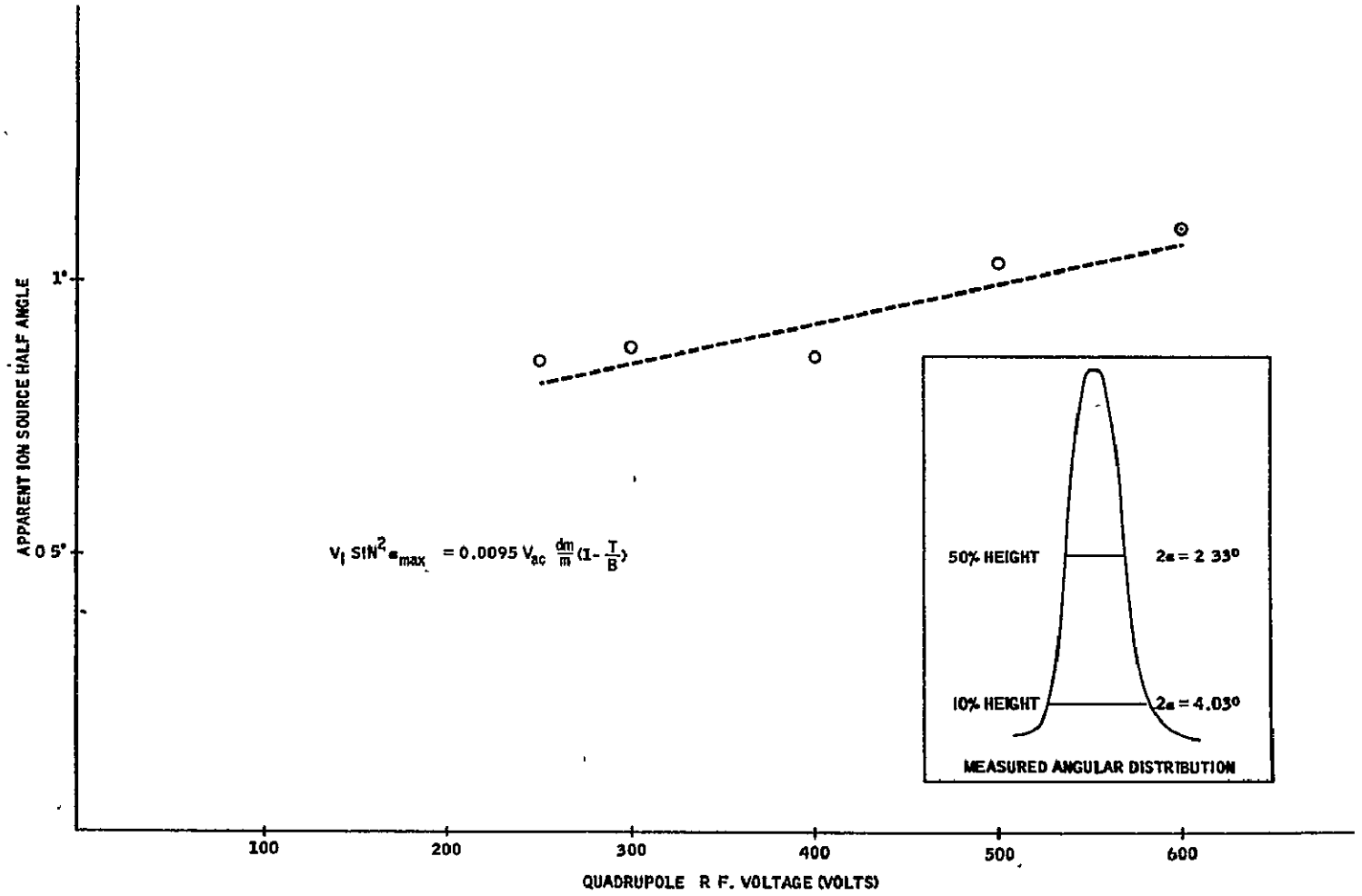


FIGURE 16. Angle vs $V_{ac}$

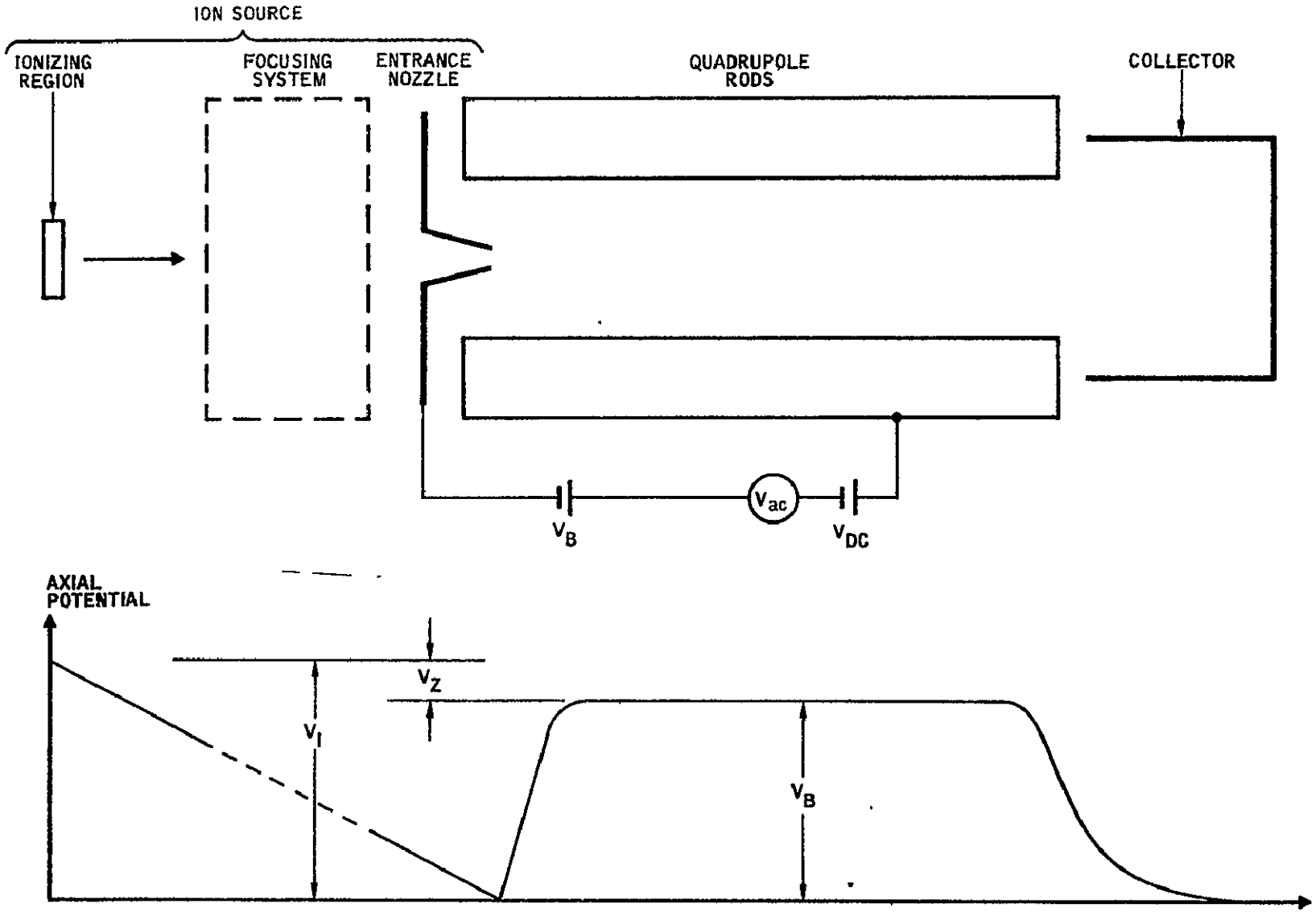


FIGURE 17. Quadrupole Mass Spectrometer Schematic and Axial Potential Distribution

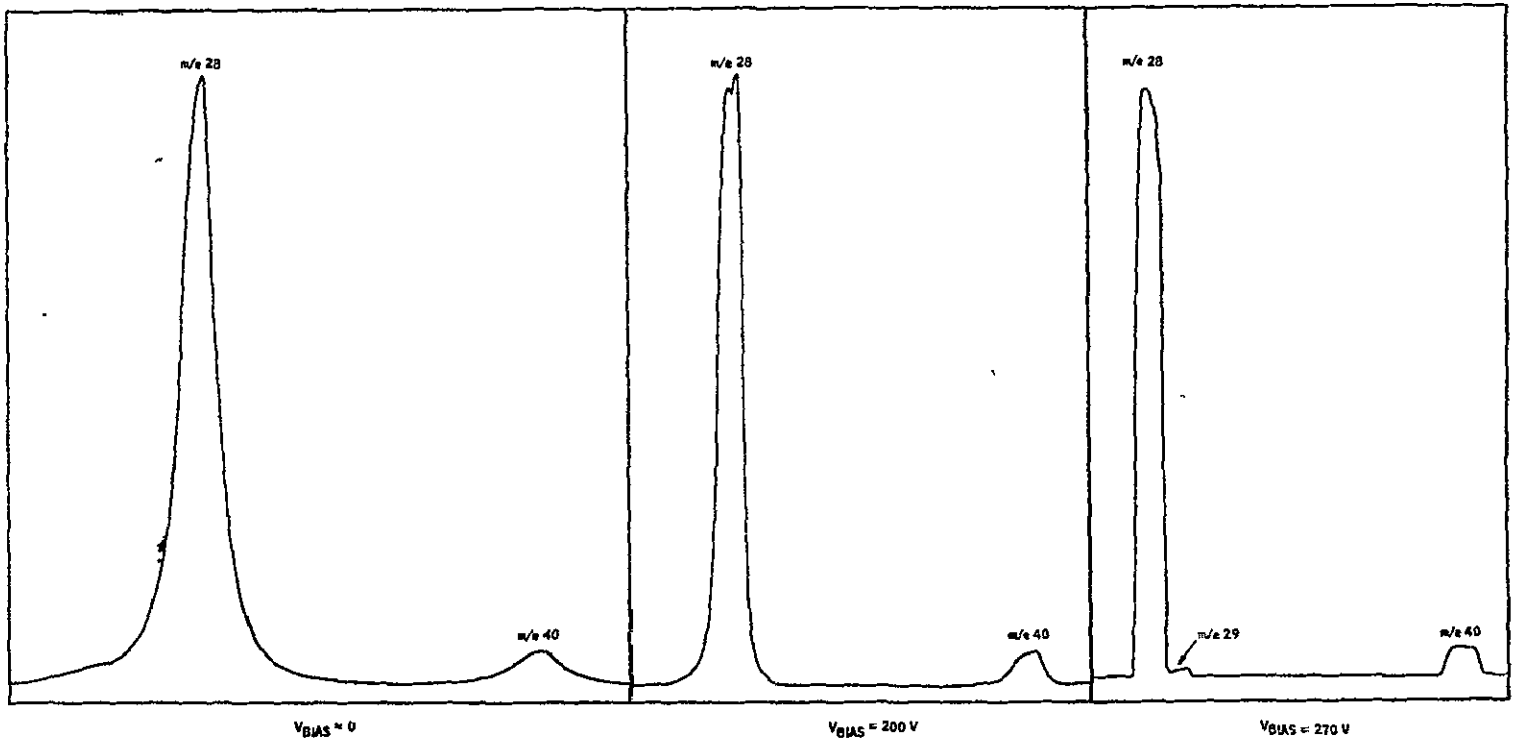


FIGURE 18. Effect of the Quadrupole Bias Voltage on Peak Tails
$\ell$ = 22 CM, $r_o$ = 7.5 MM, $V_{1_{max}}$ = 300 V, and $V_{ac}$ = 400 V

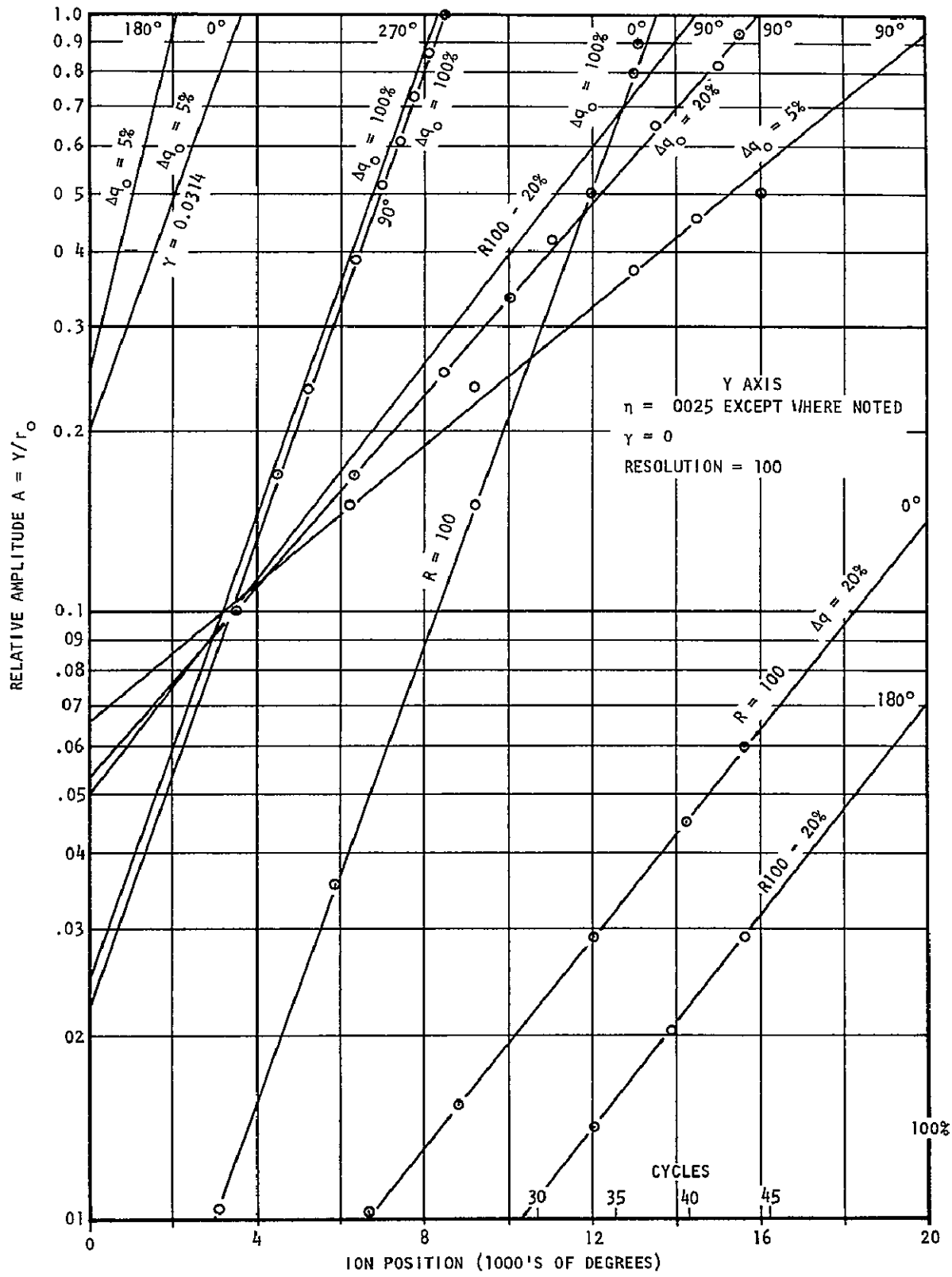


FIGURE 19. Y Axis Quadrupole Ion Amplitude vs Phase Angle of $V_{ac}$ After Entry Into the Quadrupole Field

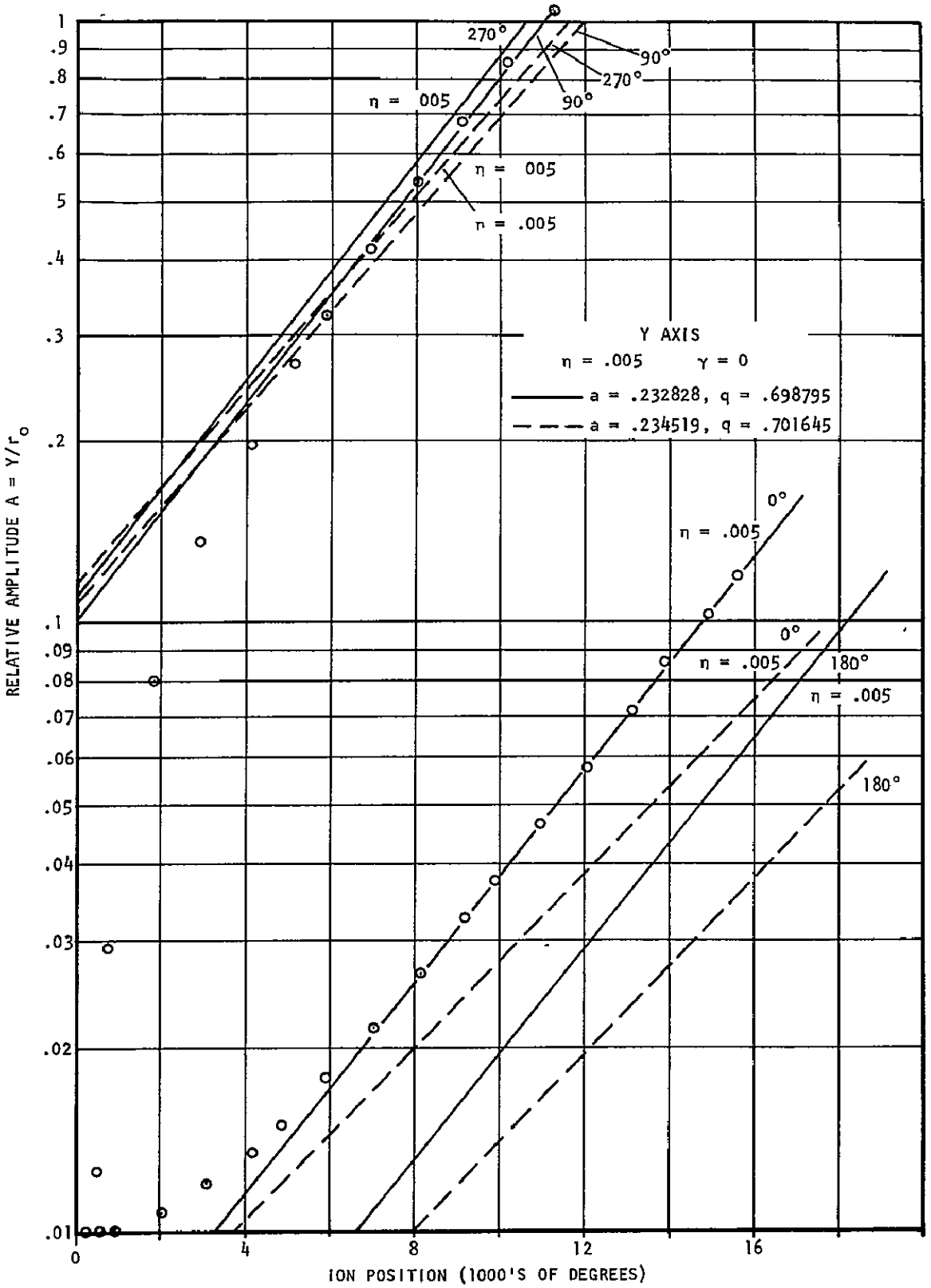


FIGURE 20. Y Axis Quadrupole Ion Amplitude vs Phase Angle of $V_{ac}$ After Entry Into the Quadrupole Field

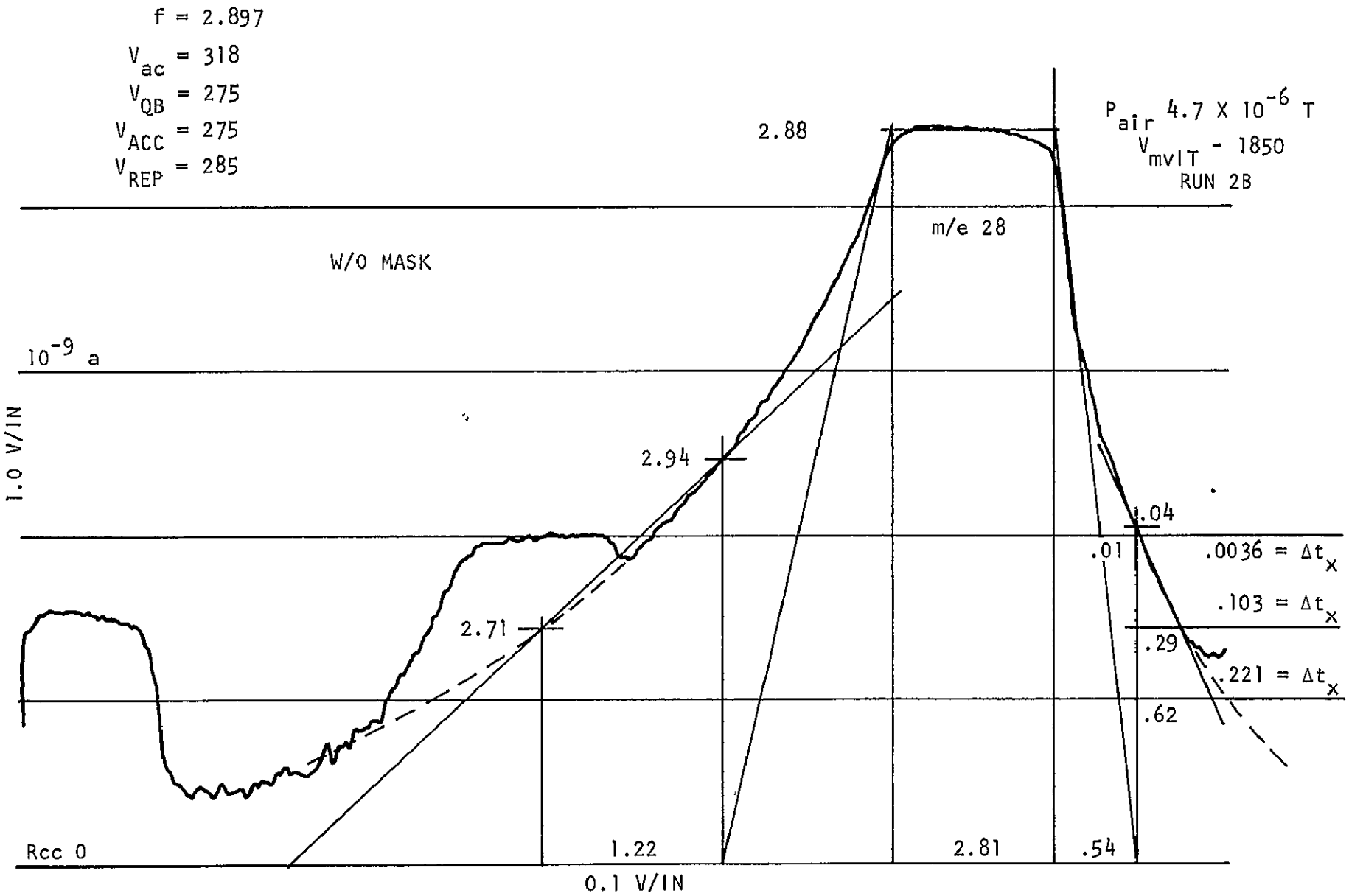


FIGURE 21. Peak Shape Without Mask